

DESIGN OF A WIRELESS PLATFORM FOR WEARABLE AND HOME  
AUTOMATION APPLICATIONS

A THESIS  
IN  
Electrical Engineering

Presented to the Faculty of the University  
of Missouri–Kansas City in partial fulfillment of  
the requirements for the degree

MASTER OF SCIENCE

by  
SHARIKA KRISHNA KUMAR

B. Tech., Cochin University of Science and Technology, India, 2008

Kansas City, Missouri  
2012

© 2012

SHARIKA KRISHNA KUMAR

ALL RIGHTS RESERVED

DESIGN OF A WIRELESS PLATFORM FOR WEARABLE AND HOME  
AUTOMATION APPLICATIONS

Sharika Krishna Kumar, Candidate for the Master of Science Degree  
University of Missouri–Kansas City, 2012

ABSTRACT

In the recent past, a great deal of attention has been given to wireless sensors. Wireless sensors enable a multitude of applications such as environmental monitoring, medical care, disaster response, home automation, urban scale monitoring, gaming etc. These small, low-power, multifunctional sensors includes sensing, data processing and communication components representing a significant improvement over the traditional sensors. The two attractive wireless sensor applications investigated in this thesis are wearable sensors for bio-medical applications and a ZigBee wireless network for home automation applications.

The targeted bio-medical application is bone strain monitoring. The current setup to collect strain data is composed of a data acquisition unit connected to a bench top load instrument. For accurate measurements the lab animals have to be sedated and immobilized in the current setup which is also bulky. A telemetry unit equipped with strain gages

designed for implantable measurement of bone strain was designed to address this problem. The measurements collected by an implantable telemetry unit are of high interest to orthopedic researchers who wish to know the load acting on an orthopedic implant and hence to help guide the rehabilitation outcomes in a patient. This thesis describes two small telemetry units with multiple configurable sensor channels which can be used to sense resistance and voltage. Thus, the designed units can be used in home energy monitoring applications as well. The units have low power consumption and were designed using off-the-shelf components. Their dimensions are 24 mm x 13 mm and 10 mm x 10 mm. The sensor signals are multiplexed, modulated and transmitted to a remote computer by means of a radio transceiver. Besides measuring strain integrated levels the telemetry units can also measure acceleration in 3 axes. Wireless battery charging is another feature that was included in our design which is a key feature for surgically implanted devices. To show that our telemetry units has comparable accuracy and compactness to the current setup, we present the readings from both setups.

A ZigBee wireless sensor network to monitor and control home appliances was designed and successfully tested. A central control unit is the coordinator which sets up the network and configures the ZigBee network parameters. The battery powered sensors are configured as end-devices which periodically report sensor data such as light, temperature, accelerometer and energy consumption values to the coordinator. Any home appliance limited to less than 10 Amps in the ZigBee network can be turned on or off from

the central control unit. With bidirectional communication achieved between the central control unit and the end-device, we were able to achieve a home automation system.

## APPROVAL PAGE

The faculty listed below, appointed by the Dean of the School of Graduate Studies, have examined a thesis titled “Design of a Wireless Platform for Wearable and Home Automation Applications,” presented by Sharika Krishna Kumar, candidate for the Master of Science degree, and hereby certify that in their opinion it is worthy of acceptance.

### Supervisory Committee

Walter D. Leon-Salas, Ph.D., Committee Chair  
Department of Computer Science & Electrical Engineering

Cory Beard, Ph.D.  
Department of Computer Science & Electrical Engineering

Vijay Kumar, Ph.D.  
Department of Computer Science & Electrical Engineering

Yugyung Lee, Ph.D.  
Department of Computer Science & Electrical Engineering

## CONTENTS

ABSTRACT . . . . .	iii
ILLUSTRATIONS . . . . .	x
TABLES . . . . .	xvi
ACKNOWLEDGEMENTS . . . . .	xvii
Chapter	
1 INTRODUCTION . . . . .	1
1.1 Implantable or Wearable Telemetry Sensors . . . . .	1
1.2 Literature Survey . . . . .	3
1.3 Summary of Contributions . . . . .	13
1.4 Plan of Work . . . . .	14
2 BACKGROUND . . . . .	16
2.1 Introduction . . . . .	16
2.2 Sensors . . . . .	17
2.3 Absorption Properties of Tissue Components Causing Wireless RF Attenuation . . . . .	24
2.4 16-Bit Ultra-Low-Power CC430F5137 SOC . . . . .	26
2.5 Inductive Coupling Theory . . . . .	43
2.6 ZigBee Wireless Protocol . . . . .	48
2.7 CC2530 ZNP Mini Kit . . . . .	55

2.8	HB404PWA AC Power/Wattage Meter from Annex Depot Inc. . . . .	63
3	TELEMETRY UNIT ARCHITECTURE . . . . .	67
3.1	Existing Setup . . . . .	67
3.2	915 MHz Telemetry Unit of Dimension 24 mm x 13 mm . . . . .	69
3.3	RFID based Telemetry Unit of Dimension 10 mm x 10 mm . . . . .	85
3.4	User Interface and Base Station . . . . .	94
4	ZigBee Wireless Network for Home Automation . . . . .	96
4.1	Existing Home Automation Technologies . . . . .	96
4.2	Design Goals . . . . .	97
4.3	Hardware . . . . .	100
4.4	Software . . . . .	106
4.5	User Interface . . . . .	115
4.6	Bidirectional Communication . . . . .	116
5	DATA COLLECTION AND RESULTS . . . . .	117
5.1	915 MHz Telemetry Unit of Dimension 24 mm x 13 mm . . . . .	117
5.2	RFID based Telemetry Unit of Dimension 10 mm x 10 mm . . . . .	124
5.3	ZigBee Wireless Network for Home Automation . . . . .	128
6	CONCLUSION AND FUTURE WORK . . . . .	130
A	APPENDIX A . . . . .	132
A.1	Four Layer PCB Layout of the Eight Channel Telemetry Unit . . . . .	132
A.2	Four Layer PCB Layout of the Four Channel Telemetry Unit . . . . .	140

Appendix



REFERENCE LIST . . . . .	147
VITA . . . . .	151

## ILLUSTRATIONS

Figure		Page
1	(a) Longitudinal piezoresistor (b) and (c) Transverse piezoresistor . . . .	20
2	Wheatstone bridge circuits . . . . .	20
3	Serpentine type coil strain sensors . . . . .	23
4	CC430F5137 Chip . . . . .	27
5	Pin Out of CC430F513x series . . . . .	27
6	Functional Block Diagram of a CC430F513x series Micro-controller . . .	28
7	Block Diagram of RF1A radio module based on the CC1101 . . . . .	30
8	CC1101 Based Radio Core Instruction Set: Command Strobes . . . . .	31
9	CC1101 Based Radio Core Interface Interrupts . . . . .	32
10	CC1101 Based Radio Core Interrupt Flags . . . . .	32
11	Data Rate Step Size . . . . .	33
12	Packet Format . . . . .	34
13	Complete Radio-Control State Diagram . . . . .	39
14	Event 0 and Event 1 Relationship . . . . .	42
15	Lines of magnetic flux around a current-carrying conductor and a current-carrying cylindrical coil . . . . .	44
16	The path of the lines of magnetic flux around a short cylindrical coil . . .	46

17	The definition of mutual inductance $M_{21}$ by the coupling of two coil via a partial magnetic flow . . . . .	46
18	Simplified model of the inductively coupled system . . . . .	47
19	A ZigBee Network Cluster Tree of ZigBee Coordinator (black), the Routers (red), and the End Devices (white) . . . . .	49
20	A ZigBee Data Frame . . . . .	52
21	A ZigBee Acknowledgment Frame . . . . .	53
22	A Beacon Data Frame . . . . .	53
23	CC2530 ZNP mini kit . . . . .	55
24	MSP430F2274(CC2530ZNP) Schematic Diagram . . . . .	56
25	The USB programmer listed in the device manager list . . . . .	57
26	Settings for the COM port . . . . .	58
27	The Coordinator Hyper-terminal . . . . .	59
28	IAR Embedded Workbench IDE . . . . .	62
29	ZNP Application interface . . . . .	63
30	HB404PWA AC Power/Wattage Meter from Annex Depot Inc. . . . .	64
31	Back Plate of HB404PWA AC Power/Wattage Meter from Annex Depot Inc. . . . .	64
32	Basic Connection without a current transformer . . . . .	65
33	Basic Connection with a current transformer . . . . .	65
34	Bose ElectroForce 3200 load test instrument connected to the data acquisition system controlled and monitored from a dedicated PC . . . . .	68

35	Block diagram of the telemetry unit . . . . .	73
36	Ramp calibration of the wheatstone bridge by the micro-controller. $V_{SENSOR}$ is the voltage of the branch with the strain gauge. $V_{DAC2}$ is changed by the micro-controller and when the output of the amplifier $V_{OUT}$ is equal to $V_{REF}$ the ramp is stopped. . . . .	78
37	Bose ElectroForce 3200 load test instrument connected to the telemetry unit controlled from a dedicated PC and base station wirelessly monitoring strain data. . . . .	80
38	Top side of the telemetry unit. . . . .	81
39	Bottom side of the telemetry unit. . . . .	81
40	Flow Diagram for 915 MHz Telemetry Unit of Dimension 24 mm x 13 mm	82
41	Flow Diagram of TimerA Interrupt Service Routine . . . . .	83
42	Flow Diagram of Radio Interrupt Service Routine . . . . .	84
43	Block Diagram of an RFID based Telemetry Unit of dimension 10 mm x 10 mm . . . . .	87
44	RFID based telemetry unit vs a penny . . . . .	91
45	Top side of an RFID based telemetry unit . . . . .	93
46	Bottom side of an RFID based telemetry unit . . . . .	93
47	Matlab <sup>®</sup> GUI plotting strain values and accelerometer values . . . . .	94
48	Flow Diagram of Code Executed by the GUI . . . . .	95
49	Data Flow Diagram . . . . .	100

50	Wire-Up in the Back Plate of HB404PWA AC Power/Wattage Meter from Annex Depot Inc. . . . .	103
51	Wire-Up in the Back Plate of HB404PWA AC Power/Wattage Meter with Current Transformer . . . . .	104
52	The Relay Circuit for Controlling ON or OFF Status of an Appliance . . .	105
53	The Whole Wiring Set-Up of the End-Device . . . . .	106
54	Flow Chart of Coordinator Node . . . . .	108
55	Flow Chart of Coordinator Node (continued..)	109
56	Flow Chart of End Device Node . . . . .	111
57	Flow Chart of End Device Node (continued..)	112
58	Flow Chart of End Device Node (continued..)	113
59	Packet Format . . . . .	114
60	Data Collected . . . . .	115
61	Bidirectional Communication Data Flow Diagram . . . . .	116
62	Strain gage glued to the dissected ulna of a mouse . . . . .	117
63	Telemetry unit readings vs StrainSmart <sup>®</sup> readings. . . . .	118
64	Telemetry unit current consumption. . . . .	120
65	Time taken by battery to charge. . . . .	122
66	Un-calibrated Temperature Sensor Data . . . . .	125
67	Accelerometer Values . . . . .	126
68	Data Collected . . . . .	128
69	The Coordinator Hyper-terminal . . . . .	129

70	Four Layer PCB Layout of the eight channeled telemetry unit of dimension 24 mm x 13 mm . . . . .	132
71	Top Layer PCB Layout of the eight channeled telemetry unit of dimension 24 mm x 13 mm . . . . .	133
72	Second Layer PCB Layout of the eight channeled telemetry unit of dimension 24 mm x 13 mm . . . . .	134
73	Third Layer PCB Layout of the eight channeled telemetry unit of dimension 24 mm x 13 mm . . . . .	135
74	Bottom Layer PCB Layout of the eight channeled telemetry unit of dimension 24 mm x 13 mm . . . . .	136
75	Components placed in the top layer of the eight channeled telemetry unit of dimension 24 mm x 13 mm . . . . .	137
76	Radio components placed in the top layer of the eight channeled telemetry unit of dimension 24 mm x 13 mm . . . . .	138
77	Components placed in the bottom layer of the eight channeled telemetry unit of dimension 24 mm x 13 mm . . . . .	139
78	Four Layer PCB Layout of four channeled telemetry unit of the dimension 10 mm x 10 mm . . . . .	140
79	Top Layer PCB Layout of four channeled telemetry unit of the dimension 10 mm x 10 mm . . . . .	141
80	Second Layer PCB Layout of four channeled telemetry unit of the dimension 10 mm x 10 mm . . . . .	142

81	Third Layer PCB Layout of four channeled telemetry unit of the dimension 10 mm x 10 mm . . . . .	143
82	Bottom Layer PCB Layout of four channeled telemetry unit of the dimension 10 mm x 10 mm . . . . .	144
83	Components placed in the Top Layer PCB Layout of the four channeled telemetry unit of dimension 10 mm x 10 mm . . . . .	145
84	Components placed in the Bottom Layer PCB Layout of the four channeled telemetry unit of dimension 10 mm x 10 mm . . . . .	146

## TABLES

Tables		Page
1	Objectives and Goals . . . . .	15
2	Features of the 915 MHz Telemetry Unit of Dimension 24 mm x 13 mm. .	119
3	Cost of a 915 MHz Telemetry Unit . . . . .	123
4	Cost of an RFID based Telemetry Unit . . . . .	127



## ACKNOWLEDGEMENTS

I would like to express my deepest gratitude to my adviser, Dr. Walter D. Leon-Salas, for his excellent guidance, care, patience and providing me with excellent atmosphere for doing research. His passion for research and teaching is truly inspirational, and it is a pleasure working under his leadership. He has invested a lot of time and energy in guiding through my program here at University of Missouri Kansas City.

I would also like to thank my committee members, Dr. Cory Beard, Dr. Vijay Kumar and Dr. Yugyung Lee for their support and interest in my thesis. All the team members of the Toyota project especially Dr. Praveen Rao and Dr. ZhiQiang had motivated me towards the completion of this thesis. I also like to thank Dr. Deep Medhi for guiding me to use and trouble shoot UMKC Latex template.

I would like to thank Moiz Fahad, who as a good friend, was always willing to help and give his best suggestions. It would have been a lonely lab without him. I would also like to thank my friends especially Suvradip Ghosh, Hsuan-Tsung Wang, Mohammad Benyhesan and Feng Shan for their valuable comments and suggestions at various stages of my work.

Finally, and more importantly I wish to thank my husband, Vinoj Pillai for his unconditional support throughout the years I spent in graduate school.

## CHAPTER 1

### INTRODUCTION

#### **1.1 Implantable or Wearable Telemetry Sensors**

An orthopedic fracture is mostly treated by a surgical placement of an implant made of stainless steel and titanium alloys which connects the broken bones to restore the mobility of the patient. The implant design is often application specific, with critical balance between mechanical stability to bear dynamic load due to body movements and sufficient elasticity to give freedom for bone growth. An accurate design, however, requires information about possible range of acting loads and resulting implant and bone deformations. Hence the implant type varies depending upon the fracture as some are pressed to fit so that bone can grow into it while others are cemented into place. Osteoarthritis or degenerative joint disease is the primary driver for orthopedic implants cause cartilage to tear down resulting in painful bone to bone contact. In comparison to diagnosis using X-ray images showing only the callus geometry, monitoring the strain imposed by the implant on the bones is better effective to guide the rehabilitation exercises to increase blood circulation enhancing recovery, as well as to foresee an implant malfunction and to continuously follow up the healing process.

Research [1] highlights the medical relevance of strain monitoring for reducing implant failures by monitoring the bone healing using implants featured with sensors using transcutaneous leads in experimental studies. Due to the simplicity, accuracy and

miniature size of strain gages, they are often chosen as optimum sensors for such an investigation which changes its resistance in accordance to the unidirectional strain applied. Large size of commercial device circuitry, battery-based powering and plastic covered cables made it hazardous to be implanted on a patient under observation as batteries are toxic and no plastic material is absolutely moist proof. Hence understanding the unsuitability of applying transcutaneous leads for general clinical application, the orthopedic implant monitoring research methodologies further drifted towards a telemetric approach [2], with major design concerns being low power consumption, minimizing the dimensions, usage of an inductive power supply as well as long term sensor stability and safe encapsulation.

The history of telemetric measurements on orthopedic implants begins with Rydell (1966), who used a battery-powered hip prosthesis with wired strain gages and tested on two patients. His results enlightened much information about hip loading in those times. Another battery-powered multichannel instrument to measure pressure distribution on prosthetic head of a hip joint implant built by Carlson (1974) was implanted on a single patient in-vitro. Brown et al. (1984) came up with an inductively powering 50 mm (diameter) x 20 mm (height) cylindrical telemetry with 14 strain gages to determine artificial hip joint implant deformations. The large size of the circuitry and usage of toxic batteries and plastic materials to seal wires were remarked as major drawbacks in most of these early designs.

## 1.2 Literature Survey

In the past decade, a plethora of wireless sensors related research have been carried out with a deeper impact on many aspects of science as they change the scientific observation from a passive process to active process. Research in biomedical applications of smart sensors has been galvanized in recent years due to advances in smart sensor technology coupled with demand in numerous applications in comparison to the weak traditional patient data collection methods. A brief literature survey of previously published research work is presented.

A telemetric version of transcutaneous system [3] using strain gage technique proved to be better reliable and convenient. In that implementation a wireless inductive link was used in place of a battery due to high power drain of the strain gage sensors. Usage of high resistive strain gages along with hybrid fabrication technology could reduce the power consumption to an acceptable level as well. A custom design chip of size 4.47 mm x 2.86 mm, integrating an instrumentation amplifier, a voltage-to-PPM converter and a data transmitter mounted on a ceramic hybrid circuit of 19 mm x 13 mm was fabricated helped to reduce it to an implantable size. A rectangular shaped RF antenna of 12.5 mm x 8.5 mm printed on a Teflon glass carrier was used for transmission of the data at a frequency of 220 MHz using on-off keyed amplitude modulation only. This coil formed a loosely coupled transformer, connected in parallel to a high-Q capacitor creating a tank circuit resonating at driver frequency hence increasing the power transfer efficiency. This methodology helped to achieve the *in vivo* strain sensing mechanical behavior of the implant was proved valuable by extensive medical researches.

The orthopedic applications further demanded multiple strain gage requiring multichannel capabilities in the telemeter, such as three-channel telemetry circuit for determining the spatial hip joint forces transmitted by prosthesis [4]. This telemetric design approach had three main goals:

- Minimal power demand for minimal inductive supply
- Least number of components for small feasible device
- Ensuring stable long term measurements without zero drifts

To achieve these goals strain is measured as a combination of two usual concepts: matrix method and current difference method. The combination of these two methods avoids the power consuming amplifiers allowing reading a single strain gage without Wheatstone bridge of higher power demand. Exploiting the current difference concept, the telemetry is low energy and remains insensitive to changes in the supply voltage. At a supply voltage of 4.2V the circuit consumes only 6mW. The zero point was stable for years due to the lack of long term drift problems encountered while using operational amplifiers in earlier designs. The design uses a pulse spacing modulation with transmitter sending RF pulses at 150 MHz. The circuit was fabricated in thick-film hybrid technology with bonded chips and resistors and has a final size of 6.9 mm x 15 mm. An enclosure made from a high permeable material, Mega perm 40L, houses the circuit to a size of 25 mm (length), 2 mm (thick) and 10 mm (diameter) cylinder. Two electrical lead wires connecting the antenna to the telemetry inside the ceramic implant head is made of sapphire and are gold soldered to a ferrule and a wire, both made from niobium eliminating the toxic plastic usage.

Surgeons use implanted micro devices such as microelectrodes for electrical and chemical recording for diagnosis and treatments. These bio-medical signals are mostly very weak electrical signals which are acquired via wires connected through skin. However, studies show that there are physical changes in animal neurological structures when movement is restricted, and also animals recover faster from brain injuries in a locomotion-allowing environment [5]. The smallest battery powered active telemetry device was still large for cranial implantation. A very promising alternative is RF power harvesting through inductive coupling offering a two way link of power gathering and data transmission. The concept is same as that of RFID, which uses inductive coupling to read an encoded identification sequence stored in the tag memory and then report the value to the interrogator. The first biological application was with RFID tag implanted in animals read by appropriate hardware to keep track of livestock. Later the same technology started being used with sensors rather than with static memories.

The generic design for power harvesting and telemetry in CMOS for implanted devices [6] could achieve data rates as high as 10kbs with bit error rates (BERs) below  $3 \times 10^{-5}$  over 25 mm distance using modified Miller encoding. This power harvesting microchip was fabricated in  $0.5\mu\text{m}$  CMOS technology and supplies 1.7 mA at 3.3 V, over a distance up to 25 mm between coils. The chip has dual voltage regulators that can be used to supply both digital and analog sources encoding. Any need for a physical connection was removed by allowing power as well as data transmission back to the module. The device was designed to provide power, control signals, and a data link as well as various clocks and reference voltages for any accompanying sensor to function. A transponder

coil of 1 cm radius was chosen as a trade-off between maximizing the coupling coefficient and size constraints. This was used to receive power from the reader coil with a 2.5 cm radius coil chosen for maximum magnetic field. The reader coil has 17 turns and the implanted coil had 9 turns depending upon the designed inductance values. A generic quad PMOS transistor rectifier was used along with an external RC filter to remove voltage ripples to obtain a stable voltage supply. A data acquisition card sampling at 50 kHz was used to sample the envelope of the voltage output of the current sensor on the transmitter to detect transmitted data. The effect of human tissue was experimented by bringing water with colloids between the two coils. A slight increase in decrease in the signal to noise ratio of the data stream with increasing thickness of the colloidal solution was identified. The two major drawbacks of this design were that a minimum 7 V is required at the reader coil limiting the range of operation of the sensor. In the design of the voltage regulator, the pass transistor does not switch on completely and this reduces the current supplied to the circuit.

An implantable in-vivo 9-channel telemetry system integrating all active components on a custom-made BiCMOS chip [7] with a high sampling rate of about 124 Hz enables recording of fast load changes and force peaks. The advantages of this system were nearly-linear force conversion, independent channel programming, an additional synchronization channel, an increased supply voltage range, less power consumption, and smaller dimensions. The BiCMOS chip integrated a 9-channel multiplexer, programmable memory, pulse interval modulator and a radio frequency transmitter which when interfaced with appropriate sensors could measure temperature, supply voltage and other 6 load

components. A microcontroller regulated the alternating magnetic field produced by a power oscillator and pulse synchronize to interval modulated data stream while the sensor signals are multiplexed, modulated and transmitted to the external device. The system had drawbacks such as the inductive power supply with air-coupled coils at a distance of several cm had a very low efficiency and hence a relatively large induction coil cable-connected to the external device is required. The RF transmission range of data was limited to 50 cm. The discussed method used ASK (Amplitude Shift Keying) modulation which hindered the commercialization as a product due to existing FCC regulations. This was tested on 3 patients with shoulder endoprotheses.

A 0.5-mW passive telemetry IC for biomedical applications [8] powered by an external RF source at 27/40 MHz, realized wireless communication through absorption modulation. The system has been integrated in a 2  $\mu\text{m}$  40-V BiCMOS technology comprising a low-offset amplifier, a low-pass notch filter, an A/D converter, a voltage doubler/rectifier, as well as a low power voltage regulator. The core area is 3600  $\mu\text{m}$  x 4350  $\mu\text{m}$ . The switched-capacitor amplifier implemented featured 45  $\mu\text{V}$  offset and an integrated noise of 21  $\mu\text{V}$  for a 30 Hz bandwidth while the power consumption was less than 30  $\mu\text{W}$ . At a rate of 1 k Baud the digitized sensor data is transmitted as PPM-AM signals with low duty-cycle. The system was well suited for long-term monitoring of biomedical signals as the entire system, including the 1.6 k  $\Omega$  bridge sensor, consumes only 520 $\mu\text{W}$ . By using the concept described, efficient reduction of the power consumption was possible while keeping the dynamic range required. The biocompatibility of the system is



better as the radiated power can be extremely low. Without increasing the power consumption of the entire system significantly, applications with multichannel transponders are now possible. With a transmitted power of 11 mW at 27 MHz, the received power was 2 mW. The overall functionality of the monitoring system including the telemetry link was verified by connecting the transponder to a single-loop, 150-nH antenna of 5-cm diameter.

An implantable telemetry platform system for in vivo monitoring of physiological parameters [9] describes a microcontroller-based multichannel telemetry system can digitize and transmit up to three analog signals coming from different sensors. An ASK modulation is used at a carrier frequency of 433.92 MHz with signal data rate as 13 kbps per channel. The usage of a microcontroller gave attractive performance such as transmission error detection, low power consumption by using sleep mode as well as threshold monitoring. As the overall size is less than  $1\text{cm}^2$ , it was well suited for minimally invasive diagnostic tests. The electromagnetic waves generated by any transmission circuits gets absorbed by human body, thus a suitable frequency of 433.92 MHz was designed to avoid energy attenuation in human tissues. Sensor inputs are 3:1 multiplexed into 10 bit ADC producing 2 bytes per sample (25KSamples per second) digital information which is fed into the microcontroller is 128-byte ROM. The microcontroller selects the input channel, does the error checking, encodes the information and transfers them into transmission unit (size 1.8 cm x 0.8 cm). The maximum transmission power is 5.62 mW, the power density has been 30 mW and sensitivity of 14 mV/kPa at a supply voltage of 3 V. The data acquisition takes place if the flux density is larger than 2 mT hence conserving

power. The receiver module has a size of 38 mm x 12 mm x 5.5 mm. It connects to a PC with a GUI being developed using Labview 7 Express software.

A European Consortium was created under the Brite-Euram Program of the Commission of the European Communities to develop new smart orthopedic implants [10], sensitive to deformation, equipped with a sensing cell to monitor the mechanical characteristics of the system called bone-callus-implant. Their project named IMPACT proposed 4 different implants targeting to increase the effectiveness of present implant designs, by taking the opportunities offered by new technologies. Their monitoring concept was centered with a 5 k $\Omega$  strain gage put on a Wheatstone bridge configuration, connected to a differential amplifier yielding a signal proportional to implant strain which was converted into a low duty pulse signal and transmitted through 5 mW Colpitts transmitter running at 180 MHz. To prevent high transmitter output drain, a pulsed on-off transmission mode with low duty cycle is chosen in their design. A circular power coil 20 mm (diameter) and 6 mm (length) connected to a parallel capacitor was tuned onto the frequency of applied magnetic field for a higher link efficiency. For constant DC voltage independent of coupling variations due to patient movements, a voltage regulator was added. An internal coil with a hybrid substrate of 18 mm diameter could transfer power up to 20 mW, at a regulated output of 4V. Mechanical characterization of these implants were performed and confirmed through dynamic compression, static compression and static bending tests on nail plates as well as corrosion susceptibility tests at critical interfaces to ensure safety of the patient. This technique of monitoring was made as a user friendly marketable product and is now fully accepted in the Orthopaedic Department at Hospital Erasme, Brussels

used on a routine basis by the surgeons and physiotherapists in accordance to STACA (Science and Technology Acquisition Corps Advisor) prototype guiding the surgeon to position the sensing cell close to bone fracture.

The bestselling book written by futurist Michio Kaku *visions: How Science will revolutionize the 21st Century and beyond* (Oxford University Press, 1999), describes wearable technologies that will silently monitor, detect irregularities, heart rhythm and alert emergency personnel in the event of a heart attack. A body area sensor network enables human-centric sensing for a variety of applications such as fitness, healthcare, and entertainment further promising applications formerly depicted only in science fiction such as motion captured video games. To achieve social acceptance, body area sensor network nodes must be extremely noninvasive, and should have fewer and smaller nodes relative to a conventional wireless sensor networks. Smaller nodes means smaller batteries, creating strict tradeoffs between the energy consumed by storage, processing, and communication resources(packaging and placement) and the fidelity, throughput, and latency required by applications. The economic concerns demanding mass production created design tradeoffs between application- specific optimizations and general-purpose programmability. The ability to selectively process and deliver information at fidelity levels and rates appropriate to the destination of data, call for the ability to aggregate hierarchical information and integrate body area sensor network systems into the existing information technology infrastructure. Identification of challenges and realization of opportunities [11] is a critical need for collaboration between technologists and domain

experts who can help define the specifications and requirements for body area sensor network systems and applications.

Considering the biomedical application of implantable wireless sensors, the attenuation due to biological tissue absorption is an important concern. To ensure adequate wireless data or supply transfer in spite of the biological tissue attenuation, the power transfer should be optimized. Due to the presence of biological tissue of various layers there exist a possibility of a frequency selective attenuation of RF signal. The frequency choice for RF transmission and its power are the two factors that needs to be considered while designing a wireless data or supply transfer. Since the wireless medical implants keeps increasing in complexity and hence providing advanced functionality, higher communication data rate will be a requirement. IEEE 802.15.6 defines the standards for body area networks (BAN) which has emerged as the key technology for health monitoring of a patient in real time and to diagnose other threatening diseases.

Home automation can be described as the introduction of technology within a home environment to improve the life quality of its occupants by providing services such as multimedia entertainment, tele-health and energy conservation. A rapid introduction of network enabled with digital technology in the home environment was seen in recent past. This increased the connectivity between devices within the home environment. Smart home using wireless communication also replaces the messy wired system which was difficult to setup. With rapid expansion of Internet, the potential for the monitoring and for remote controlling of such network enabled devices was possible.

The oldest standard identified was the X10 industry standard developed in 1975

[30] which was about the communication between the electronic devices. Through the home power lines this could provide limited control over household devices. A Java based home automation system [31] where an embedded board connected physically all the home automation devices and by integrating with a personal computer (PC) based web server could provide remote access to the system. Built-in network security featured a secure solution by incorporating the use of Java. However, the system requires an expensive and intrusive wiring installation as well as a high end PC.

A Bluetooth based home automation system was introduced in [32] which includes a primary controller and multiple Bluetooth sub-controllers. Each home device was connected physically to a Bluetooth sub-controller. By wireless communication all sub-controllers sends information to the primary controller. Hence each home device has a dedicated Bluetooth module. Since these Bluetooth modules are expensive, they are sometimes shared among several devices. This design reduces physical wiring and thus the intrusiveness of installation. The sharing of the Bluetooth module has the drawback of an access delay. Hence each dedicated wireless module has to be made more cheaper.

An alternative approach of a phone based remote controller for home automation is presented in [33]. All communications happen over a fixed telephone line rather than over the Internet. This system could be accessed by using any telephone which can supports dual tone multiple frequency(DTMF). The disadvantages of this system are that there was no graphical user interface for the user and hence users have to remember an access code and also they have to remember the sequence of buttons to press for the controlling connected devices.

### 1.3 Summary of Contributions

This thesis is part of a research effort that aims at developing two multi-channel telemetry circuit which can be used in implantable applications. The main contributions of this work in bio-medical applications such as bone strain monitoring are as follows:

- A new telemetry unit including off-the-shelf components is proposed to do bone strain monitoring.
- A comparison between telemetry units and with the existing setup to depict the accuracy and compactness.
- *In-vivo* test results of our telemetry unit opening possibilities as an implantable sensor.

The Smart Grid, as an Energy Internet promises the transformation of the behavior of individuals as well as communities towards more greener and efficient use of electric power. Currently in many communities, there is a lack of social awareness and the Smart Grid that we propose will have potential to improve social justice. The objectives of Smart Grid in social justice are to realize a smart grid enabled smart life for both unrepresented and majority groups. Technologically, smart devices do not by themselves guarantee socially smart life, but the design we propose in this thesis will allow all communities to gain the advantage of the ability to make smarter energy choices. Due to the increasing demands to realize socially-aware energy saving to reduce cost, the goal of this project is to develop smart energy solutions for smart life particularly targeted for under-represented communities that can realize

- Non-intrusive monitoring of energy consumption and behavior at multiple scales
- Autonomous energy saving mechanisms that are transparent to general users
- Intelligent prediction of energy costs and expenditures
- Evaluation of personalized experiences
- Discovering cost saving opportunities for community facilities

The objectives are summarized in table.1 as well. This thesis describes only the hardware design and implementation details of a ZigBee wireless sensor network for home automation.

#### **1.4 Plan of Work**

The main underlying principles involved for implantable telemetry sensor circuits and for ZigBee wireless sensor networks for home automation are described in chapter 2. Chapter 3 will focus on the two different architectures of the RF powered telemetric circuit for orthopedic implants. Design techniques and implementation are described in this chapter. Chapter 4 describes the system design and wire up details of a ZigBee wireless sensor network designed for home automation. Chapter 5 will includes all the results collected. Summary and conclusions drawn from the results, future work are discussed in chapter 6.

Table 1: Objectives and Goals

Objective	Goal	Deliverables
Data Collection	Infrastructure setup and instrumentation of the environment for data collection	The Green Zones in Flarsheim Hall at UMKC
Non-intrusive monitoring of energy consumption and behavior at multiple scales	Continuous energy monitoring based on the cloud-based storage	IBM cloud-based storage for the Green Zones data
1. Autonomous energy saving mechanisms that are transparent to general users 2. Intelligent prediction of energy costs and expenditures	Data mining and decision making for Intelligent prediction of energy costs and expenditures	A prototype of the Semantic Framework used for autonomous energy saving and intelligent prediction of energy costs and expenditures
1. Evaluation of personalized experiences for smart grid-enabled life at both residence and community levels 2. Discovering cost saving opportunities for community facilities	Continuous energy reporting and evaluation for smarter energy saving at individual facilities (households) and at the community level	LCD screen-based reporting and mobile apps for checking energy usage and controlling the devices in the Green Zones



## CHAPTER 2

### BACKGROUND

#### **2.1 Introduction**

Wireless sensors are small, low-power and includes sensing, data processing and communication components. Two attractive wireless sensor applications investigated in this thesis are wearable sensors for bio-medical applications and a ZigBee wireless network for home automation applications. The targeted bio-medical application is bone strain monitoring. An implantable telemetry unit for bone strain measurement has been designed to address the problems of the existing set up. This thesis describes a small telemetry unit with multiple configurable sensor channels which can be used to sense resistance and voltage. The unit has low power consumption and was designed using off-the-shelf components. The sensor signals are multiplexed, modulated and transmitted to a remote computer by means of an integrated radio transceiver. Wireless battery charging is another feature that was included in this design which is a key feature for surgically implanted devices. Alternatively, a telemetry unit with RFID interface was designed and tested. A ZigBee wireless sensor network to monitor and control home appliances was designed and successfully tested. This chapter focuses on the underlying principles used in the implementation of system design for two applications of interest.

## 2.2 Sensors

An implantable telemetry unit for bone strain measurement has been designed to address the problems of the existing set up. This thesis describes a small telemetry unit with multiple configurable sensor channels which can be used to sense resistance and voltage. Resistance and voltage variant sensors are attached to the telemetry unit to measure the desired sensed information. The most common sensing principle for micro machined sensors is Piezoresistivity. First discovered by Lord Kelvin in 1856, the piezoresistive effect is the change of resistance in an electrical resistor when it experiences a strain and deformation. This effect provides a direct simple energy-signal transduction mechanism between the mechanical and electrical domains. Today, it is widely used in MEMS field for a variety of sensing applications including accelerometers, pressure sensors, gyro rotation, rate sensors, tactile sensors, flow sensors, and chemical/biological sensors. A brief detail on the underlying principle of MEMS especially strain gages used for bone strain measurement is discussed in this section.

The resistance value of a resistor with the length  $l$  and the cross-sectional area  $A$  is given by

$$R = \rho \frac{l}{A} \quad (2.1)$$

It could be seen that the bulk resistivity( $\rho$ ) and the dimensions determine the resistance. Hence the resistance value may change with applied strain due to two important ways. Firstly the dimensions including length and cross section changes with strain. Secondly the resistivity of certain materials changes as a function of strain. The magnitude

of resistance change stemming from the second principle is much greater than what is achievable from the first one.

Piezoresistors by definition change their resistivity with applied strain. Metal resistors who change their resistance in response to strain by shape deformation are called strain gauges. Silicon is considered as a true piezoresistor as the resistivity of silicon semiconductor changes as a function of strain. Hence both semiconductor piezoresistors and metal strain gauges are considered.

The fact that the resistivity of semiconductor silicon may change under applied strain is fascinating. The resistivity of a semiconductor material depends on the mobility of charge carriers. The resistivity of semiconductor depends upon the mobility of the carriers. The formulae for mobility is

$$\mu = \frac{q\bar{t}}{m^*} \quad (2.2)$$

where  $q$  is the charge per unit charge carrier,  $\bar{t}$  the mean free time between carrier collision events, and  $m^*$  the effective mass of a carrier in the crystal lattice. Both the mean free time and the effective mass are related to the average atomic spacing in a semiconductor lattice, which is subject to changes under applied physical strain and deformation.

### 2.2.1 Strain Gage

In a piezoelectric resistor the change in resistance is linearly related to the applied strain, according to

$$\frac{\Delta R}{R} = G \frac{\Delta L}{L} \quad (2.3)$$

The proportional constant  $G$  in the above equation is called the gauge factor of a piezoresistor. We can rearrange the terms in this equation to arrive at an explicit expression for  $G$

$$G = \frac{\frac{\Delta R}{R}}{\frac{\Delta L}{L}} = \frac{\Delta R}{\varepsilon R} \quad (2.4)$$

The resistance of a resistor is customarily measured along its longitudinal axis. External strain applied may contain three primary vector components, one along the longitudinal axis of a resistor and two arranged  $90^\circ$  to the longitudinal axis and each other. The behavior of a piezoresistive element towards longitudinal and transverse strain components is different. The change of measured resistance under the longitudinal stress component is called longitudinal piezoresistivity and change of measured resistance to the longitudinal strain is called the longitudinal gauge factor. On the other hand, the change of resistance under transverse strain components is called transverse piezoresistivity. The relative change of measured resistance to the transverse strain is called the transverse gauge factor.

Longitudinal and transverse piezoresistor configurations and external force loading directions are presented in Fig. 1

Resistance changes are often read using the Wheatstone bridge circuit configuration. A basic Wheatstone bridge consists of four resistors connected in a loop as shown

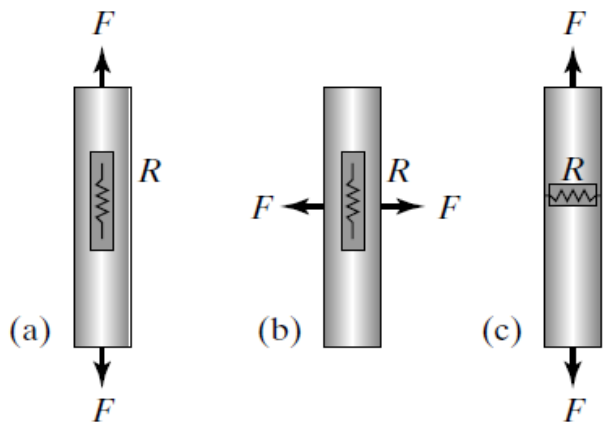


Figure 1: (a) Longitudinal piezoresistor (b) and (c) Transverse piezoresistor

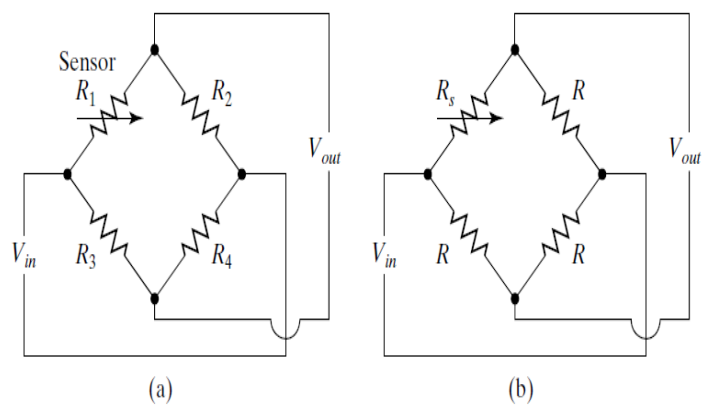


Figure 2: Wheatstone bridge circuits

in Fig. 2. An input voltage is applied across two junctions that are separated by two resistors while the voltage drop across the other two junctions forms the output. One or more resistors in the loop may be sensing resistors, whose resistances change with the intended variables while other resistors are made insensitive to strains. The output voltage is related to the input voltage according to the following relationship

$$V_{out} = \left( \frac{R_2}{R_1 + R_2} - \frac{R_4}{R_3 + R_4} \right) \times V_{in} \quad (2.5)$$

In many practical applications, all four resistors share an identical nominal resistance value,  $R$  with variable resistor,  $R_s$  as

$$R_s = R + \Delta R \quad (2.6)$$

Hence the output voltage would change linearly to input voltage as

$$V_{out} = \left( \frac{-\Delta R}{2\Delta R + R} \right) \times V_{in} \quad (2.7)$$

Commercially available metal strain gauges are often in the form of metal-clad plastic patches that can be glued to surfaces of mechanical members of interest. Resistors are etched into the metal cladding layer. Shown in Fig. 3 is a typical strain gauge pattern which has a zigzagged conductor path is commonly used to effectively increase the length of the resistor and the amount of total resistance under a given area. Some of the criteria that are applied when selecting a metal strain gauge include accuracy; long-term stability; cyclic endurance; range of operational temperature; ease of installation; tolerable amounts of elongation; and stability in a harsh environment. To satisfy these

requirements, commercial metal strain gauges are often not made of pure metal thin films but of tailored metal alloys. The size of device is very small for a micro machined sensor hence it is impractical to bond or attach discrete strain gauges to devices, instead strain gauges are fabricated on mechanical beams and membranes using monolithic integration processes.

Metal resistors are generally deposited (by evaporation or sputtering) and patterned. Elemental metal thin films can be used as strain gauges in MEMS, with their gauge factors ranging from 0.8 to 3.0. The sources and procedures for depositing elemental metal films are readily available. Strain gauges made of thin-film metals do not compare favorably with semiconductor strain gauges in terms of piezoresistive gauge factors. However, metal thin films provide sufficient performance for many applications. Using metal instead of a semiconductor eliminates the need for doping and lengthy process steps. Also, metal resistors can be deposited and processed under temperatures much lower than what would be needed for doping semiconductors. Metal can generally sustain a much greater elongation before fracture. As such, metal resistors can be placed on polymer materials for polymer MEMS devices (e.g., tactile sensors) and provide improved mechanical robustness compared with silicon counterparts.

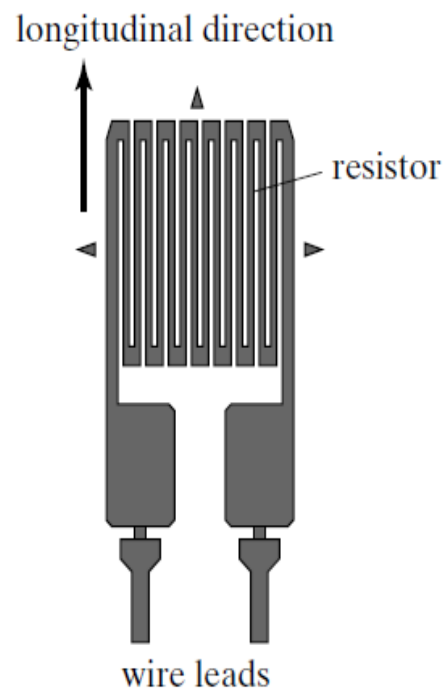


Figure 3: Serpentine type coil strain sensors



## 2.3 Absorption Properties of Tissue Components Causing Wireless RF Attenuation

The probability of photon absorption in tissue per unit path length is given by the absorption coefficient  $\mu_a$ . The absorption coefficient varies in different components as well as with frequency changes. The photon absorption in tissue is described by molar extinction coefficient  $\varepsilon$ . The few different includes of the animal tissue causing absorption of RF signals are discussed below.

### 2.3.1 Blood

The two different types of hemoglobin that blood consists are oxyhemoglobin  $HbO_2$  which is bound to oxygen and deoxyhemoglobin  $Hb$  which is unbound to oxygen. These two different types of hemoglobin exhibit different absorption spectra that are normally represented in terms of molar extinction coefficients. The concentrations of oxyhemoglobin and deoxyhemoglobin changes the absorption spectra of tissues.

### 2.3.2 Water

In the range of visible light, water is nearly transparent but over the near-infrared region it becomes absorbing. The concentration of water is high in human tissue hence water is a critical component. The absorption spectrum of water in the range from 250 to 1000 nm.

Other less significant tissue components with contributions to the total absorption spectrum of tissue are melanin and fat.

### 2.3.3 Melanin

Melanin exists in the human epidermal layer of skin which is responsible for protecting from harmful UV radiation. Melanin is produced when melanocytes are stimulated by solar radiation. In some biological tissues Melanin is one of the major absorbers of light. The molar extinction coefficient spectra corresponding to two different types of melanin such as eumelanin which is black-brown and pheomelanin which is red-yellow varies.

### 2.3.4 Fat

Around 10-40% of the tissue consists of fat. The absorption increases as the amount of fat increases.

## 2.4 16-Bit Ultra-Low-Power CC430F5137 SOC

This thesis describes an implantable telemetry unit for bone strain measurement designed with multiple configurable sensor channels which can be used to sense resistance and voltage. The unit has low power consumption and was designed using off-the-shelf components. The sensor signals are multiplexed, modulated and transmitted to a remote computer by means of an integrated radio transceiver. This telemetry unit is mainly designed around a 16-Bit Ultra-Low-Power CC430F5137 SOC. The ultra-low-power micro-controller system-on-chip from the Texas Instruments CC430 family with integrated RF transceiver cores includes several devices having different sets of peripherals intended for a wide range of applications. To achieve extended battery life in portable measurement applications, the architecture is optimized by combining with five low-power modes. The device features the powerful MSP430 16-bit RISC CPU, constant generators contributing to maximum code efficiency and 16-bit registers.

Between the micro-controller core, its peripherals, software, and RF transceiver the CC430 family provides a tight integration hence making it true easy to use system-on-chip as well as improving performance. Typical applications of these micro-controllers includes wireless digital and analog sensor systems, metering (AMR/AMI), thermostats, smart grid wireless networks etc.

The CC430F513x series are configurations of micro-controller system-on-chip which combines MSP430 CPUXV2CC1101 with sub-1-GHz RF transceiver. These micro-controllers have upto 32 kB of programmable flash memory, two 16-bit timers, 4 kB of RAM, six external inputs, inbuilt temperature and battery sensors, 12-bit A/D converters.

A universal serial communication interfaces (USCI), DMA, real-time clock module with alarm capabilities, comparator and 30 Input-output pins are other features of this series. Fig. 4 shows the image of a CC430F513x chip. The pin-outs of a CC430F513x series micro-controller is shown in Fig. 5. The functional block diagram of CC430F513x series micro-controllers is shown in Fig. 6.



Figure 4: CC430F5137 Chip

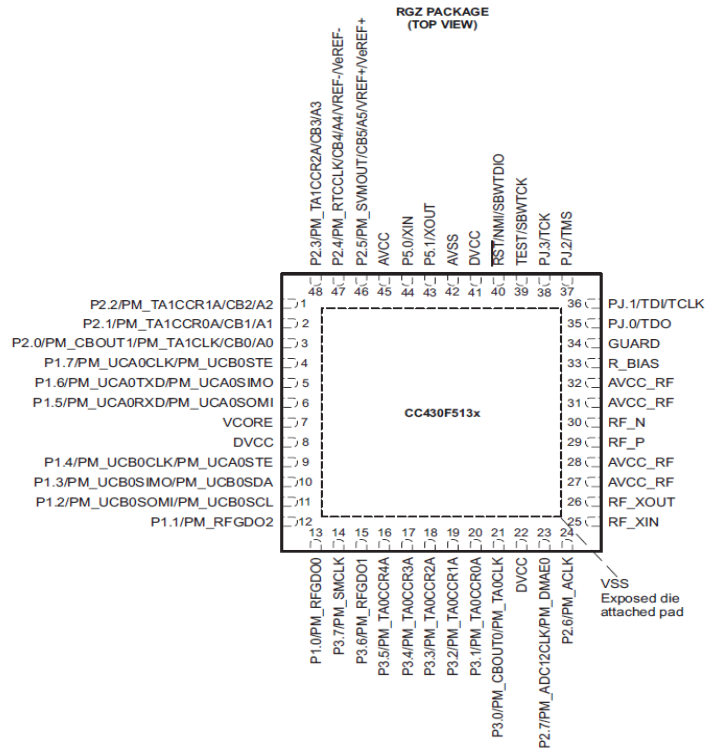


Figure 5: Pin Out of CC430F513x series

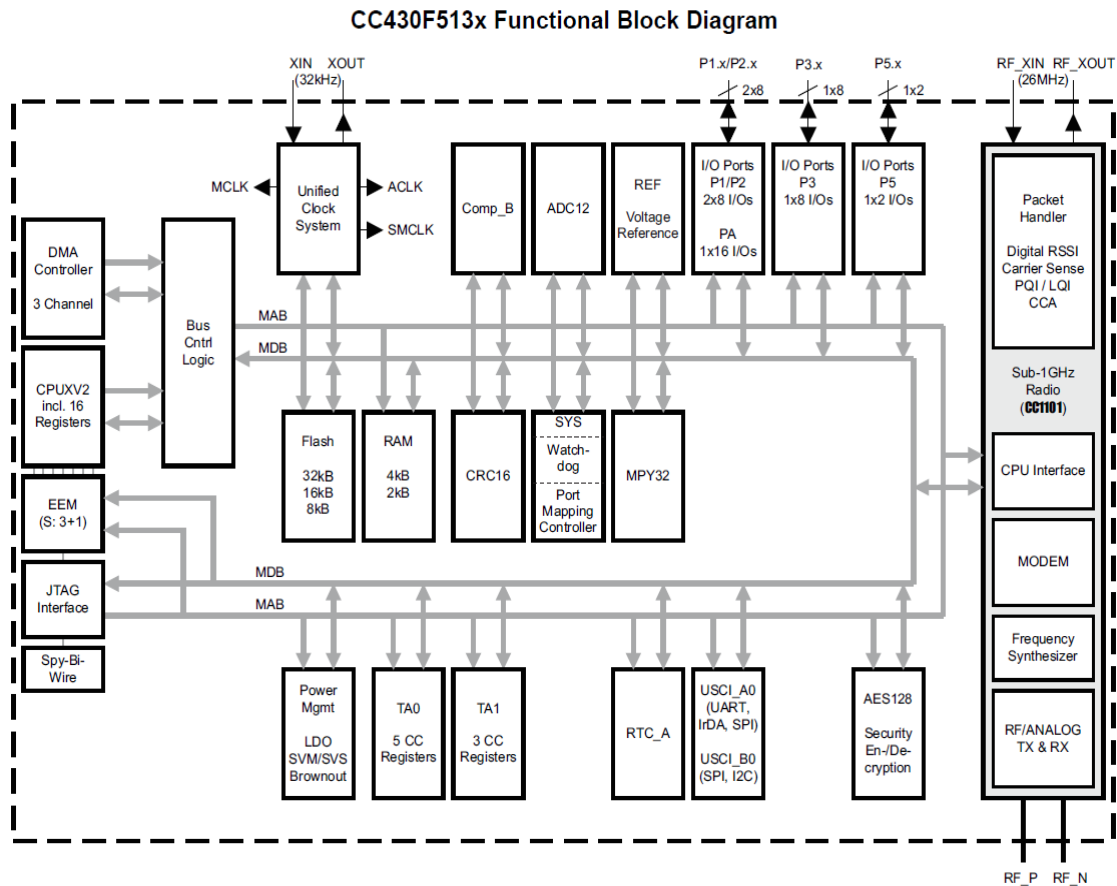


Figure 6: Functional Block Diagram of a CC430F513x series Micro-controller

### 2.4.1 CC1101 - Based Radio Module

The CC1101 sub-1-GHz radio core is integrated with the MSP430 by the RF1A radio module. The radio core based on CC1101 features a low intermediate frequency (IF) receiver. The the low-noise amplifier (LNA) amplifies the received radio frequency (RF) signal and down-converted in quadrature (I and Q) to the IF. At IF, the quadrature-phase or in-phase (I/Q) signals are being digitized by the ADCs. Fine channel filtering, Automatic gain control (AGC) and demodulation bit/packet synchronization is performed

digitally. The transmitter operates on direct synthesis of the RF frequency. The frequency synthesizer consists of a on-chip LC voltage-controlled oscillator (VCO) and a 90° phase shifter for generating the I and Q local oscillator (LO) signals to the down-conversion mixers in receive mode. The reference frequency for the synthesizer is generated by a crystal oscillator with a 26-MHz crystal which clocks the ADC and the digital part. The digital baseband supports channel configuration, packet handling, and data buffering.

The CC1101-based radio module features frequency bands of 300 MHz to 348 MHz, 389 MHz to 464 MHz, and 779 MHz to 928 MHz. The data rate can be programmed from 0.8 kBaud to 500 kBaud. The radio module exhibits a high sensitivity as high as -110 dBm at 1.2 kBaud at 868 MHz with 1 % packet error rate. The modulation schemes supported by the radio module are 2-FSK, 2-GFSK, MSK, OOK and flexible ASK shaping. The flexible support offered for packet oriented systems such as on-chip support for sync word detection, flexible packet length, address check and automatic CRC handling. The received signal strength digital indicator (RSSI) output and support for automatic clear channel assessment (CCA) before transmitting (for listen-before-talk systems) are two other interesting features of the radio module. A simplified block diagram of the RF1A radio module based on the CC1101 is shown in Fig. 7.

#### **2.4.1.1 Radio-Core Operation**

To communicate with the CC1101-based radio core the available command strobes are tabulated in Fig. 8. The nomenclature used is as follows:

- $i:[\dots]$  is the value to be written into the radio interface instruction register

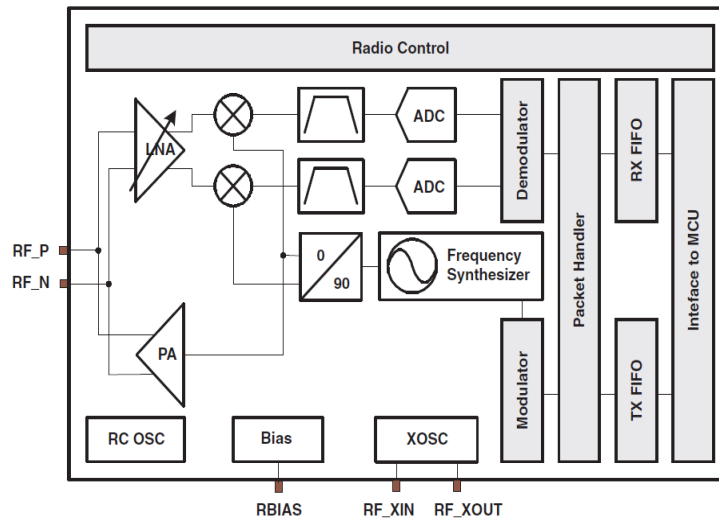


Figure 7: Block Diagram of RF1A radio module based on the CC1101

- $s:[...]$  is the value to be returned to the radio interface status register after the instruction was transferred to the radio core.

The most significant bit shown as 'x' in the command strobes in Fig. 8 means that it can be set as 1 to receive a status byte indicating the number of bytes available in the RX FIFO or it can be also set to 0 to receive a status byte indicating the number of bytes available in the TX FIFO.

A number of interrupt flags to control the data-flow between the radio core and the CPU is provided by the radio interface provides. The interrupt flags are listed in Fig. 9. Interrupt signals to the radio interface are provided by the radio core. The radio core interrupt flags are prioritized. The radio interface interrupts and radio core interrupt flags are combined to source a single interrupt vector .

Instruction Mnemonic	Inputs	Outputs	Description
SRES	i:[x011 0000]	n/a	Command strobe: reset radio core Nothing returned. Accordingly STATIFG is not set.
SFSTXON	i:[x011 0001]	s:[ssss ssss]	Command strobe: enable and calibrate frequency synthesizer (if MCSM0.FS_AUTOLOCAL = 1). If in RX (with CCA), go to a wait state where only the synthesizer is running (for quick RX/TX turnaround). Returns status byte with bytes available in TX FIFO when x=0 and with bytes available in RX FIFO when x=1.
SXOFF	i:[x011 0010]	s:[ssss ssss]	Command strobe: radio core to enter SLEEP state Returns status byte with bytes available in TX FIFO when x=0 and with bytes available in RX FIFO when x=1.
SCAL	i:[x011 0011]	s:[ssss ssss]	Command strobe: calibrate frequency synthesizer and turn it off. SCAL can be strobed from IDLE mode without setting manual calibration mode (MCSM0.FS_AUTOLOCAL = 0). Returns status byte with bytes available in TX FIFO when x=0 and with bytes available in RX FIFO when x=1.
SRX	i:[x011 0100]	s:[ssss ssss]	Command strobe: enable RX. Perform calibration first if coming from IDLE and MCSM0.FS_AUTOLOCAL = 1. If in RX state and CCA is enabled, only go to TX if channel is clear. Returns status byte with bytes available in TX FIFO when x=0 and with bytes available in RX FIFO when x=1.
STX	i:[x011 0101]	s:[ssss ssss]	Command strobe: enable TX if in IDLE state and perform calibration first if MCSM0.FS_AUTOLOCAL = 1. Returns status byte with bytes available in TX FIFO when x=0 and with bytes available in RX FIFO when x=1.
SIDLE	i:[x011 0110]	s:[ssss ssss]	Command strobe: exit RX/TX, turn off frequency synthesizer, and exit WOR mode, if applicable. Returns status byte with bytes available in TX FIFO when x=0 and with bytes available in RX FIFO when x=1.
SWOR	i:[x011 1000]	s:[ssss ssss]	Command strobe: start automatic RX polling sequence (Wake-on-Radio, WOR) as described in . Returns status byte with bytes available in TX FIFO when x=0 and with bytes available in RX FIFO when x=1.
SPWD	i:[x011 1001]	s:[ssss ssss]	Command strobe: radio core to enter SLEEP state Returns status byte with bytes available in TX FIFO when x=0 and with bytes available in RX FIFO when x=1.
SFRX	i:[x011 1010]	s:[ssss ssss]	Command strobe: flush the RX FIFO buffer. Only issue SFRX in IDLE or RX_OVERFLOW states. Returns status byte with bytes available in TX FIFO when x=0 and with bytes available in RX FIFO when x=1.
SFTX	i:[x011 1011]	s:[ssss ssss]	Command strobe: flush the TX FIFO buffer. Only issue SFTX in IDLE or TX_UNDERFLOW states. Returns status byte with bytes available in TX FIFO when x=0 and with bytes available in RX FIFO when x=1.
SWORRST	i:[x011 1100]	s:[ssss ssss]	Command strobe: reset WOR timer to Event1 value. Returns status byte with bytes available in TX FIFO when x=0 and with bytes available in RX FIFO when x=1.
SNOP	i:[x011 1101]	s:[ssss ssss]	Command strobe: no operation. Can be used to read the radio core status byte Returns status byte with bytes available in TX FIFO when x=0 and with bytes available in RX FIFO when x=1.

Figure 8: CC1101 Based Radio Core Instruction Set: Command Strokes

The interrupt vector register RF1AIV is used to determine which radio core interrupt flag requested an interrupt. Fig. 10 tabulates the radio interface interrupts used in CC1101 based radio core.



Interrupt Flag	Interrupt Condition
RFINSTRIFG	The radio core is ready to accept the next instruction; i.e., the previous instruction was completely processed and all required data was provided.
RFDINIFG	The radio core is ready to accept additional data.
RFSTATIFG	The radio core updated the status accessible via the RF1ASTAT registers. If the instruction was provided as a word via RF1AINSTRW, the flag is set after the first data byte is also available.
RFDOUTIFG	Data was provided by the radio core and can be read via the RF1ADOUT registers. If the corresponding parameters were provided as 16-bit data, the flag is set only after 16-bit data is available. With the auto-read feature, the flag is set after the selected amount of data is available. With each read access of the RF1ADOUT registers, the flag is cleared; if there is still data available after the read access, the RFDOUTIFG is set again.
RFERRIFG	An error occurred interfacing to the radio core. The error condition can be encoded using the error flags. The error interrupt flag is set as long as one of the error flags (OPERR, OUTERR, OPOVERR, or LVERR) is set. It is cleared automatically when all error flags are cleared.

Figure 9: CC1101 Based Radio Core Interface Interrupts

Interrupt Flag	Interrupt Condition
RFIFG0	Based on GDO0 signal - programmable using IOCFG0 (0x02) register of radio core.
RFIFG1	Based on GDO1 signal - programmable using IOCFG1 (0x01) register of radio core.
RFIFG2	Based on GDO2 signal - programmable using IOCFG2 (0x00) register of radio core.
RFIFG3	Positive edge: RX FIFO filled or above the RX FIFO threshold. Negative edge: RX FIFO drained below RX FIFO threshold. (Equal to GDOx_CFG=0)
RFIFG4	Positive edge: RX FIFO filled or above the RX FIFO threshold or end of packet is reached. Negative edge: RX FIFO empty. (Equal to GDOx_CFG=1)
RFIFG5	Positive edge: TX FIFO filled or above the TX FIFO threshold. Negative edge: TX FIFO below TX FIFO threshold. (Equal to GDOx_CFG=2)
RFIFG6	Positive edge: TX FIFO full. Negative edge: TX FIFO below TX FIFO threshold. (Equal to GDOx_CFG=3)
RFIFG7	Positive edge: RX FIFO overflowed. Negative edge: RX FIFO flushed. (Equal to GDOx_CFG=4)
RFIFG8	Positive edge: TX FIFO underflowed. Negative edge: TX FIFO flushed. (Equal to GDOx_CFG=5)
RFIFG9	Positive edge: Sync word sent or received. Negative edge: End of packet or in RX when optional address check fails or RX FIFO overflows or in TX when TX FIFO underflows. (Equal to GDOx_CFG=6)
RFIFG10	Positive edge: Packet received with CRC OK. Negative edge: First byte read from RX FIFO. (Equal to GDOx_CFG=7)
RFIFG11	Positive edge: Preamble quality reached (PQI) is above programmed PQT value. Negative edge: (LPW) (Equal to GDOx_CFG=8)
RFIFG12	Positive edge: Clear channel assessment when RSSI level is below threshold (dependent on the current CCA_MODE setting). Negative edge: RSSI level is above threshold. (Equal to GDOx_CFG=9)
RFIFG13	Positive edge: Carrier sense. RSSI level is above threshold. Negative edge: RSSI level is below threshold. (Equal to GDOx_CFG=14)
RFIFG14	Positive edge: WOR event 0 Negative edge: WOR event 0 + 1 ACLK. (Equal to GDOx_CFG=36)
RFIFG15	Positive edge: WOR event 1 Negative edge: RF oscillator stable or next WOR event0 triggered. (Equal to GDOx_CFG=37)

Figure 10: CC1101 Based Radio Core Interrupt Flags

### 2.4.1.2 Data Rate Programming

The transmitting data rate used is programmed by the MDMCFG3.DRATE\_M and the MDMCFG4.DRATE\_E configuration registers. The data rate is given by equation 2.8.

The programmed data rate hence depends on the crystal frequency.

$$R_{DATA} = \frac{(256 + DRATE\_M) \times 2^{DRATE\_E}}{2^{28}} \times f_{XOSC} \quad (2.8)$$

If DRATE\_M is rounded to the nearest integer and becomes 256, DRATE\_E is incremented with DRATE\_M = 0. With the minimum step the data rate can be changed from 0.8 kBaud to 500 kBaud as shown in Fig. 11.

DATA RATE (kBaud)			DATA RATE STEP SIZE (kBaud)
MINIMUM	TYPICAL	MAXIMUM	
0.8	1.2 / 2.4	3.17	0.0062
3.17	4.8	6.35	0.0124
6.35	9.6	12.7	0.0248
12.7	19.6	25.4	0.0496
25.4	38.4	50.8	0.0992
50.8	76.8	101.6	0.1984
101.6	153.6	203.1	0.3967
203.1	250	406.3	0.7935

Figure 11: Data Rate Step Size

### 2.4.1.3 Packet Format

The data packet format consists of the following items as shown in Fig. 12:

- Preamble
- Optional length byte
- Synchronization word
- Payload
- Optional address byte
- Optional 2-byte CRC

The preamble pattern is a sequence of n alternating ones and zeros (10101010). The MDMCFG1.NUM\_PREAMBLE value is programmed with minimum length of the

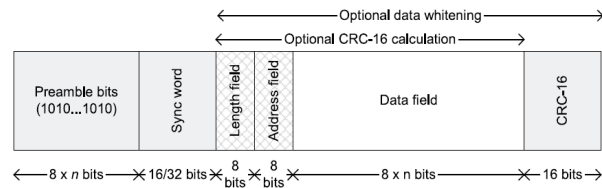


Figure 12: Packet Format

preamble. The modulator starts transmitting the preamble once TX is enabled. The modulator sends the sync word and then data if available from the TX FIFO after the programmed number of preamble bytes has been transmitted. Until the first byte is written to the TX FIFO the modulator continues to send preamble bytes if the TX FIFO is empty. The modulator later sends the sync word and the data bytes. Set in the SYNC1 and SYNC0 registers the synchronization word is a two-byte value which provides byte synchronization for the incoming packet. The radio supports constant packet length protocols and variable length protocols. For packets up to 255 bytes variable or fixed packet length mode is used. Infinite packet length mode should be used for longer packets.

Fixed packet length mode is selected by setting `PKTCTRL0.LENGTH_CONFIG = 0`. The `PKTLEN` register sets the desired packet length. In variable packet length mode, by setting `PKTCTRL0.LENGTH_CONFIG = 1`, the first byte after the sync word configures the packet length. Excluding the length byte and the optional CRC the packet length is the payload data. To set the maximum packet length allowed in RX the `PKTLEN` register is used. Any packet which was received with a length byte value greater than `PKTLEN` is discarded. By setting `PKTCTRL0.LENGTH_CONFIG = 2`, the packet length is configured as infinite, hence until turned off manually the transmission and reception continues. This can also be used to support packet formats having different length than

other than natively supported. One byte of payload data is the minimum packet length supported which excludes the optional length byte and CRC.

#### **2.4.1.4 Packet Handling**

For packet oriented radio protocols the radio has built-in hardware support. In transmit mode, the packet handler adds the following elements to the packet assembled in the TX FIFO:

- A CRC checksum computed over the data field.
- A 2-byte synchronization (sync) word. Can also be duplicated to give a 4-byte sync word which is recommended.
- A programmable number of preamble bytes

In receive mode, the packet handler deconstructs the data packet by the following:

- CRC computation and CRC check
- Sync word detection
- Preamble detection
- Packet length check against the maximum programmable length
- Dewhitening
- One byte address check

#### **2.4.1.5 Modulation Formats**

The frequency, amplitude and phase shift modulation formats are supported by the radio. In the MDMCFG2.MOD\_FORMAT register the desired modulation format is set. The data stream can also be Manchester coded by the modulator and decoded by the demodulator optionally by setting MDMCFG2.MANCHESTER\_EN = 1.

#### **2.4.1.6 Modulation Formats - Frequency Shift Keying**

The radio can use a Gaussian shaped 2-FSK (2-GFSK). A 2-GFSK modulated signal is produced by shaping a 2-FSK signal with Gaussian filter of  $BT = 0.5$ . Improved adjacent channel power (ACP) and occupied bandwidth is achieved by using this spectrum-shaping feature improves. With abrupt frequency shifting in 2-FSK systems, the spectrum is inherently broad. The spectrum can be made significantly narrower by making the frequency shift smoother. Thus, in the same bandwidth using 2-GFSK higher data rates can be transmitted.

When 2-FSK/2-GFSK modulation is used, the expected frequency deviation of incoming signals in RX specified in the DEVIATN register should be the same as the TX deviation for demodulation for reliably and robustness. The frequency deviation is programmed using in the DEVIATN register with the DEVIATION\_M and DEVIATION\_E values.

#### **2.4.1.7 Modulation Formats - Minimum Shift Keying**

The complete transmission including preamble, sync word, and payload is MSK modulated when MSK is used. With constant transition time phase shifts are performed. Modifying DEVIATN.DEVIATION\_M setting the fraction of a symbol period used to change the phase can be changed which is equivalent to symbol shape change. When we use MSK the DEVIATN register setting has no effect in RX. Manchester encoding and decoding should be disabled by setting MDMCFG2.MANCHESTER\_EN = 0.

#### **2.4.1.8 Modulation Formats - Amplitude Modulation**

Two different forms of amplitude modulation supported by the radio are amplitude shift keying and on off keying. OOK modulation simple turns on or off modulation. By programming of the modulation depth that is the difference between 1 and 0 and pulse amplitude shaping, ASK is performed. More bandwidth constrained output spectrum is produced by pulse shaping. When using OOK or ASK, the DEVIATN register setting has no effect in neither TX nor RX. Guidelines in [27] must be followed on how to find optimum OOK or ASK settings from the preferred settings.

#### **2.4.1.9 Received Signal Qualifiers**

To increase the likelihood for a valid sync word detection the following radio qualifiers are used:

- RSSI
- Carrier Sense

- Sync Word Qualifier
- Clear Channel Assessment
- Link Quality Indicator
- Preamble Quality Threshold

#### **2.4.1.10 Received Signal Qualifiers - Received Signal Strength Indicator (RSSI)**

The RSSI value is an estimate of the signal power level in the chosen channel. This value is based on the current gain setting in the RX chain and the measured signal level in the channel. In RX mode, the RSSI value can be read continuously from the RSSI status register until the demodulator detects a sync word (when sync word detection is enabled). At that point the RSSI readout value is frozen until the next time the radio enters the RX state.

If PKTCTRL1.APPEND\_STATUS is enabled the last RSSI value of the packet is automatically added to the first byte appended after the payload.

#### **2.4.1.11 Radio Control**

To switch between different operational states the radio has a built-in state machine. By internal events such as TX FIFO underflow or by using command strobes the change of state is done. The complete radio control state diagram is shown in Fig. 13. The state numbers readable in the MARCSTATE status register are the numbers referred in the figure.



Figure 13: Complete Radio-Control State Diagram

### 2.4.1.12 Radio Control - Active Modes

Receive and transmit are the two active modes that the radio has. By using the SRX and STX command strobes these modes can be directly activated by the CPU. The frequency synthesizer must be regularly calibrated. There is three automatic calibration options and one manual calibration option (by using the SCAL strobe) that are controlled by the MCSM0.FS\_AUTOCL settings:



- Calibrate while going from either RX or TX to IDLE automatically
- Calibrate while going from IDLE to either RX or TX (or FSTXON)
- Calibrate every fourth time while going from either RX or TX to IDLE automatically

By issuing an SIDLE strobe if the radio goes from TX or RX to IDLE, there is no calibration performed. A constant number of crystal oscillator cycles are taken for calibration. If RX is activated, the radio goes into receive mode until the RX termination timer expires or a packet is successfully received. By using PQT, maximum sync word length, CS and sync word qualifier mode the possibility of a false sync word detection is reduced. The radio controller goes to the state indicated by the MCSM1.RXOFF\_MODE setting after a packet is successfully received. The possible destinations are:

- TX: Start sending preamble
- RX: Start search for a new packet
- IDLE
- FSTXON: Frequency synthesizer on and ready at the TX frequency (Activate TX with STX)

Similarly, the radio remains in the TX state when TX is active until the current packet has been successfully transmitted. As indicated by the MCSM1.TXOFF\_MODE setting later the the state changes . The possible destinations remains same as for RX.

By using the command strobes the CPU can manually change the state from TX to RX and vice versa. If the SRX strobe is used while radio controller is currently in transmit, after the current transmission is ended the transition to RX is done.

The STX or SFSTXON command strobes are used if the radio controller is in RX. The radio remains in RX if the channel is not clear. The conditions for clear channel assessment is controlled by MCSM1.CCA\_MODE setting. To force the radio controller to go to the IDLE state the SIDLE command strobe can always be used.

#### **2.4.1.13 Radio Control - Wake On radio (WOR) Timer**

To wake up the radio core periodically to listen for incoming packets, the Wake on Radio (WOR) timer functionality can be used. The radio core goes to the SLEEP state when the SWOR strobe command is sent. With WORCTRL.ACLK\_PD = 0 the WOR timer function can be enabled. This should be done before the SWOR strobe otherwise the SWOR strobe clears it automatically and the WOR timer starts. The WOR timer has two events that is Event 0 and Event 1. After a programmed timeout Event 1 follows Event 0. The interrupt signals are generated WOR timer on Event 0 and Event 1 by setting the RFIFG14 and RFIFG15 registers respectively. The time between two consecutive Event 0 is programmed changing WOREVT1.EVENT0 and WOREVT0.EVENT0, and WORCTRL.WOR\_RES. The equation is:

$$t_{Event0} = EVENT0 \times 2^{5 \times WOR\_RES} \frac{1}{f_{ACLK}} \quad (2.9)$$

By changing the WORCTRL.EVENT1, the Event 1 timeout is programmed. Fig. 14

shows the timing relationship between Event 0 timeout and Event 1 timeout.

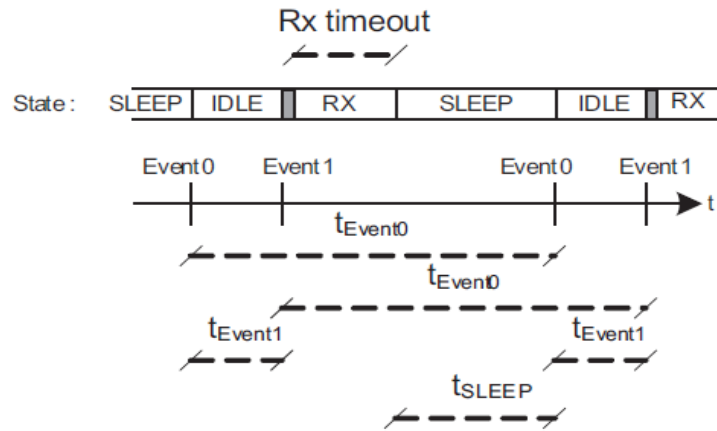


Figure 14: Event 0 and Event 1 Relationship

When  $f_{ACLK} = 32.768$  kHz, then the time from entering the SLEEP state to the next Event 0 must be larger than 11.72 ms. If  $t_{SLEEP}$  is less than 11.72 ms, then there is a chance that the consecutive Event 0 will occur  $128 \times \frac{1}{f_{ACLK}}$  seconds too early. If the WOR feature is used along with low-power mode LPM3 the average power consumption of the micro-controller can be reduced.

#### 2.4.1.14 Using Radio with Low-Power Modes

In LPM0 to LPM2 the radio works seamlessly. By setting the PMMHPMRE bit in the PMMCTL0 register of the PMM module as 1 the radio operation in LPM3 or LPM4 is enabled. While the radio is active, the PMM thus provides sufficient current. The current consumption will drop to the usual LPM3 numbers when the radio goes into SLEEP state. Whereas while the radio is active the current consumption of respective radio state can be seen. When the radio needs a transition from SLEEP state to an active state until the radio

is active the CPU must not go into a low power mode. If the WOR feature is used along with low-power mode LPM3 the average power consumption of the micro-controller can be reduced.

## 2.5 Inductive Coupling Theory

An alternative telemetry unit with RFID interface was designed based on inductive coupling theory. Inductive coupling theory is the underlying principle for wireless power charging which is an important feature for our implantable telemetry device. The working of inductive coupling theory is detailed in this section. This RFID based design enables a smaller telemetry unit of dimensions 10 mm x 10 mm. However, the drawback of the RFID interface is its limited communication range.

### 2.5.1 Magnetic field strength H

Every moving charges (electrons in wires or in a vacuum), i.e. flow of current, is associated with a magnetic field Fig. 15 in accordance to the shape of the conductor.

The generic equation 2.10 for the magnetic field strength H is independent of material properties of space and hence could be used for different types of conductor.

$$\sum I = \oint \vec{H} d\vec{s} \quad (2.10)$$

The magnetic field strength H for a short cylindrical coil antenna shown in Fig. 16 similar to the type used in the antennas of inductively coupled RFID systems is given as equation 2.11.

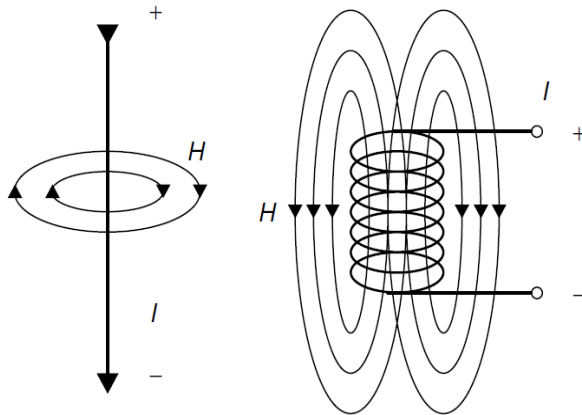


Figure 15: Lines of magnetic flux around a current-carrying conductor and a current-carrying cylindrical coil

$$H = \frac{INr^2}{2\sqrt{r^2 + x^2}} \quad (2.11)$$

Where  $N$  is the number of windings,  $R$  is the circle radius  $r$  and  $x$  is the distance from the center of the coil in the  $x$  direction. It could be inferred from equation 2.11 that as the distance  $x$  increases the magnetic field strength  $H$  decreases.

In electromagnetism and electronics, inductance  $L$  is the ability of an inductor to store energy in a magnetic field expressed as the ratio of the interlinked flux  $\psi$  to enclosed current  $I$  in an area  $A$ . Self-inductance is defined as the induction of a voltage in a current-carrying wire when the current in the wire itself is changing. In the case of self-inductance, the magnetic field created by a changing current in the circuit itself induces a voltage in the same circuit. Therefore, the voltage is self-induced. The changing magnetic field created by one circuit (the primary) can induce a changing voltage and/or current in a second circuit (the secondary). The mutual inductance,  $M$ , of two circuits describes the

size of the voltage in the secondary induced by changes in the current of the primary.

Consider two conductor loop1 (area A1) and loop2 (area A2) placed relatively close to one another. If a current  $I_1$  flows through loop1 with a total flux of  $\psi(I_1)$ , then loop2 is exposed to a proportion of magnetic flux  $\Psi(I_1)$  generated in loop1. The two circuits are now connected by this partial flux or coupling flux. The coupling flux  $\psi_{21}$  depends on the relative position of the coils, geometric dimensions of each conductor loops and magnetic properties of the medium. The mutual inductance  $M_{21}$ , inductance induced in loop2 due to inductance of loop1 is the basic principle behind most inductively coupled passive RFID systems.

### 2.5.2 Coupling Coefficient

One primary coil is driven by a RF amplifier to create an electromagnetic field while the second coil captures a portion of this field creating an induced current in itself on the implanted device. The coupling factor,  $k$  represents the proportion of energy captured by the secondary coil ranging from 0.01 to 0.1 expressed empirically for the case of air coupling assuming the two coils are parallel and center aligned as the following:

$$k = \frac{r_{implant}^2 r_{reader}^2}{\sqrt{r_{implant} r_{reader}} \left( \sqrt{x^2 + r_{reader}^2} \right)^3} \quad (2.12)$$

Where the radius of the reader coil is  $r_{reader}$ ,  $r_{implant}$  is the radius of the implant coil and  $x$  is the distance between the coils.

The concept of power transfer is same as that in transformer but the two coils are weakly coupled here.

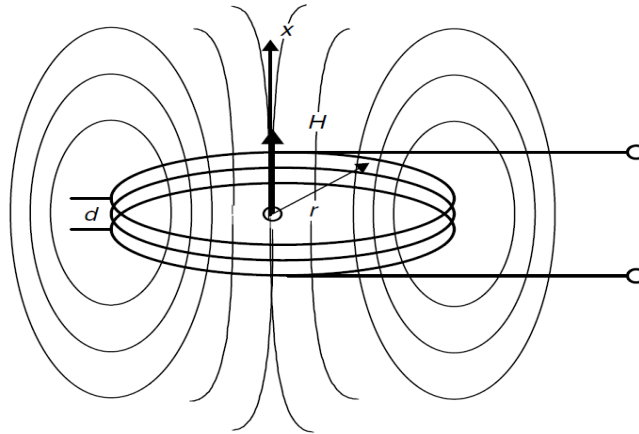


Figure 16: The path of the lines of magnetic flux around a short cylindrical coil

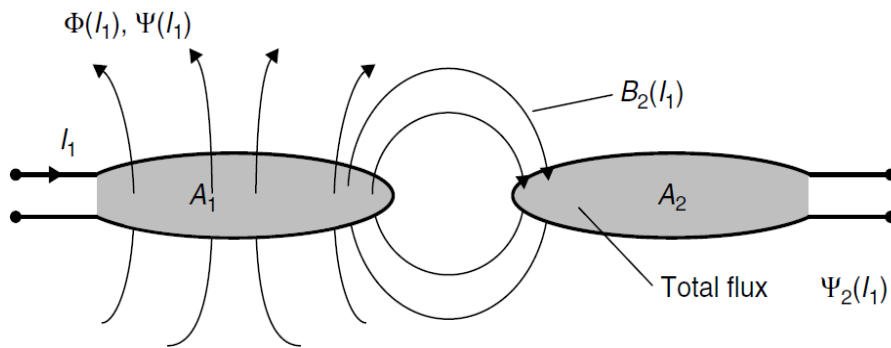


Figure 17: The definition of mutual inductance  $M_{21}$  by the coupling of two coil via a partial magnetic flow

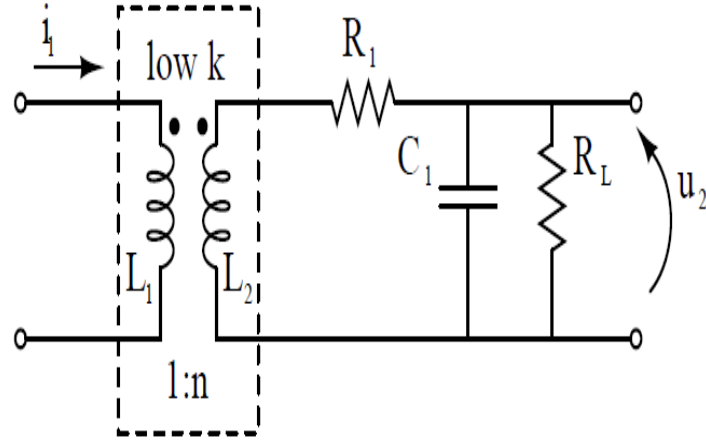


Figure 18: Simplified model of the inductively coupled system

$R_1$  represents the parasitic resistance in the coil,  $C_1$  is the tuning capacitance used to raise the coil voltage, and  $R_L$  is the load on the system and two discrete coils  $L_1$  and  $L_2$ . For an increased induced current  $i_2$  in the secondary coil a low  $k$  value is desired. Following equation shows the relation.

$$i_2 = \frac{i_1}{k \sqrt{\frac{L_2}{L_1}}} \quad (2.13)$$

Using the impedance equation of the inductor at a known frequency, the voltage,  $uT$  induced across the  $L_2$  component of the transformer induced by the current  $i_1$  is

$$uT = i\omega k \sqrt{L_1 L_2} i_1 \quad (2.14)$$

The basic equation for the voltage across the load,  $u_2$  is given by



$$u_2 = \frac{\omega k \sqrt{L_1 L_2} i_1}{\sqrt{\left(1 - \omega^2 L_2 C_1 + \frac{R_1}{R_L}\right)^2 + \left(\frac{\omega L_2}{R_L} + \omega R_1 C_1\right)^2}} \quad (2.15)$$

Where A is the linear gain factor defined by the system parameters. Therefore by changing the current through the primary coil of the system the voltage on the implanted coil could be adjusted for a fixed coupling factor.

## 2.6 ZigBee Wireless Protocol

For home automation applications, compared to other wireless protocols ZigBee was selected as a best fit. A ZigBee wireless sensor network to monitor and control home appliances was designed and successfully tested. A ZigBee system consists of one central control unit and multiple end-devices. The ZigBee wireless protocol standards such as the architecture and the packet formats used for communication are discussed in this section.

With battery-powered devices, a multi-hop network built is called a ZigBee network. Two devices wishing to exchange data within a ZigBee network depends on other intermediate devices. Hence each device in the network does the following tasks:

1. Perform specific networking functions
2. Configure certain parameters to specific values

Device type determines the set of networking functions performed by a device and hence decides the role of the device in the network. A stack profile sets the parameters that is to be configured to specific values.

### 2.6.1 Device Types

A ZigBee network has three logical device types:

1. Coordinator
2. Router
3. End-device

A ZigBee network consists of one Coordinator node, multiple Routers and multiple End-device nodes. Around a coordinator or a router the end devices are arranged in a star network helping the network to be low-cost. The routers and coordinators are arranged in a mesh network. Altogether the ZigBee network is of a cluster tree architecture as shown in Fig. 19.

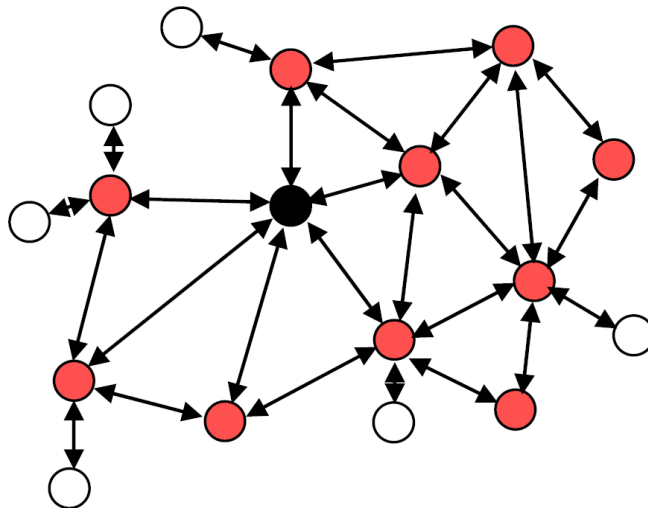


Figure 19: A ZigBee Network Cluster Tree of ZigBee Coordinator (black), the Routers (red), and the End Devices (white)

### **2.6.1.1 Coordinator**

The coordinator device starts a ZigBee network. It is always the first device on a ZigBee network. The coordinator scans the RF environment for existing networks, then chooses a channel and a network identifier or PAN ID. Thus the coordinator starts the network. Optionally the coordinator node is used to assist setting up of security and application-level bindings in the network. The main role of the Coordinator is starting up and configuring the network. Once this is done, the Coordinator behaves just like a Router node or can even be absent in the network later on. The network continues to operate regardless of the presence of the coordinator due to the distributed nature of the ZigBee network.

### **2.6.1.2 Router**

The main functions of a Router are:

- Allowing other devices to join the network
- Multi-hop routing
- Assisting in communication for its child battery-powered end devices

Routers are designed to be active all the time.

### **2.6.1.3 End-device**

There is no responsibility with the end-device to maintain the network infrastructure, hence it can wake up or sleep any time. Thus they are battery powered with low

memory requirements.

## 2.6.2 ZigBee Protocol Definition

Zigbee is a low cost, low power wireless connectivity focusing on low data rate and low duty cycle connectivity. Extremely low power consumption and modest bandwidth requirements but low latency are other features of ZigBee. Built based on IEEE 802.15.4 standard the Zigbee defines the Physical (PHY), Medium Access Control (MAC), Data Link (DLL) Network (NWK), Application (APL) layers. Operating bands used in ZigBee are 2.4 GHz or 915 MHz or 868 MHz due to their propagation characteristics. Zigbee features a coverage range of 10 to 75 m and a data throughput of 10 kbps to 115 kbps. Zigbee uses half-sine filtered Offset Quadrature Phase Shift Keying (OQPSK) and Direct Sequence Spread Spectrum (DSSS) coding and modulation as defined by the IEEE 802.15.4. It utilize the Carrier Sense Multiple Access (CSMA) before transmitting for listening to a clear channel to avoid collisions. Whenever there is an unacknowledged transmission, back off and retry procedures are followed. ZigBee also supports 4 AES-128 enables encryption for security.

The IEEE 802.15.4 standard specifies 27 channels:

- 868.3 MHz: 1 channel of 20 kbps
- 2.4 GHz: 16 channels of 250 kbps each
- 902-928 MHz: 10 channels of 40 kbps each

ZigBee devices supports two types of addresses:

- A 64-bit IEEE address or MAC address or Extended address(set by the manufacturer thus is globally unique address maintained and allocated by the IEEE)
- A 16-bit network address or logical address or short address(only unique within a network and assigned when a device joins the network)

All ZigBee devices use 64-bit IEEE addresses by default. However devices can be configured to use a 16-bit address only to reduce the communication overhead. Hence 120 bits are added to each transmitted packet by the physical and MAC layers.

The communications frame is kept as simple as possible but still robust to work on a noisy channel. There are four frame structures such as one for data, one for acknowledgement, one for peer entity control transfers and one for beacons. The data frame is shown in Fig. 20.

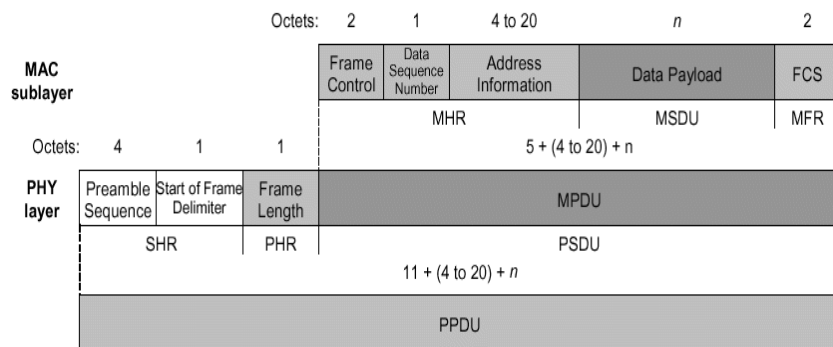


Figure 20: A ZigBee Data Frame

A Packet receipt is acknowledged by a 88-bit ACK frame shown in Fig. 21 sent while a 'quiet time' immediately after packet transmission. This setup is ideal for sensors that report their data occasionally and require no communication from the coordinator.

When data comes to the sensor, the sensor immediately sends out a message and waits for acknowledgement. The sensor later keeps trying until it succeeds. The transceiver is only occasionally awake, and only for brief moments. The drawback of this approach is in noisy environments where latency will be a problem and the sensors keep on re-transmitting.

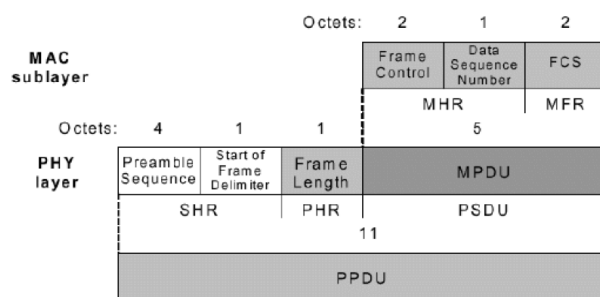


Figure 21: A ZigBee Acknowledgment Frame

A node must always be listening to receive information, which consumes power. Thus the ZigBee standard defines a beacon network, where the coordinator periodically sends out a beacon frame as shown in Fig. 22.

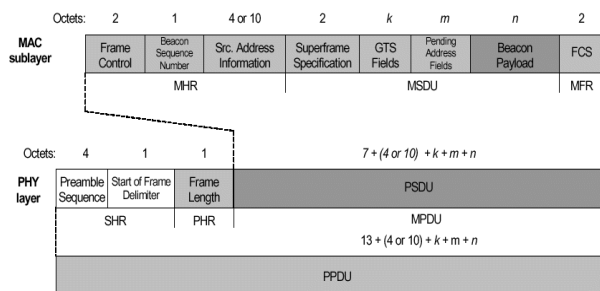


Figure 22: A Beacon Data Frame

This beacon specifies guaranteed time slots (GTSs), defines the boundaries of a

communications period and identifies nodes that the coordinator wishes to send information. To listen to the beacon the nodes wake up periodically and communicate during their assigned GTS. Thus there are minimum packet collisions and two-way communication is achieved even though the node transceivers are only intermittently powered. The standard however allows only a portion of the time in between the beacons to be assigned as GTSs. Thus new nodes can join the network on the fly just by announcing their presence during the unassigned period known as the Contention Access Period (CAP).

Establishing a network, configuring a new device, leaving or joining a network, assigning an addresses to a new device, providing security, synchronization and routing are handled by the network layer. A variant of the AODV algorithm for routing with table driven optimization.

Both the MAC layer and the network layer handles encryption. Single-hop transmissions are handled by the MAC layer even though secure multihop messaging needs participation of upper layer. In slightly different ways both use the AES algorithm.

For the MAC layer each key is associated with a single security suite. The MAC frame header has a bit indicating if the packet is encrypted or not. The network layer uses the same key for different suites while specifying which one to apply to a particular packet. To prevent replay attacks both levels allows appending of a Message Integrity Code (MIC) which is calculated and combined with frame and sequence counts to form a nonce.

Finally, the application interface layer provides binding and discovery services allowing devices to learn about other devices that may be accessible and what data or

functionality they provide. Later the nodes are matched together based on their needs and services. The layer also do message forwarding between these bound devices.

## 2.7 CC2530 ZNP Mini Kit

A ZigBee wireless sensor network to monitor and control home appliances was designed and successfully tested. A ZigBee system consists of one central control unit and multiple end-devices. The central control unit or coordinator is connected to a PC which sets up the network and keeps polling for data packets from all active end-devices. Each end-device is battery powered and is connected to a home appliance. The end-device periodically reports to the coordinator the energy consumption of the connected appliance as well as light in lux, temperature in Fahrenheit and acceleration in 3 axes. The whole ZigBee wireless sensor network was designed around the CC2530 ZNP Mini Kit which is discussed in the section. Fig. 23 depicts the CC2530ZDK-ZNP-MINI kit from Texas Instruments.



Figure 23: CC2530 ZNP mini kit



## 2.7.1 Hardware Setup

The ZigBee Network Processor development kit gives a simple introduction to ZigBee wireless networks. The hardware includes an MSP430F2274 microcontroller that controls the ZigBee device and a CC2530 ZigBee device preprogrammed with ZigBee software. The MSP430F2274 microcontroller has an inbuilt temperature sensor. This controller is further interfaced with a light sensor, accelerometer, LED's and input-output ports as shown in the schematic diagram in Fig. 24. The target board connected to the USB stick programmer is programmed with a coordinator application. The coordinator sets up the ZigBee network and configures the ZigBee network parameters which is the central control unit of the network. A ZigBee system can only have one coordinator.

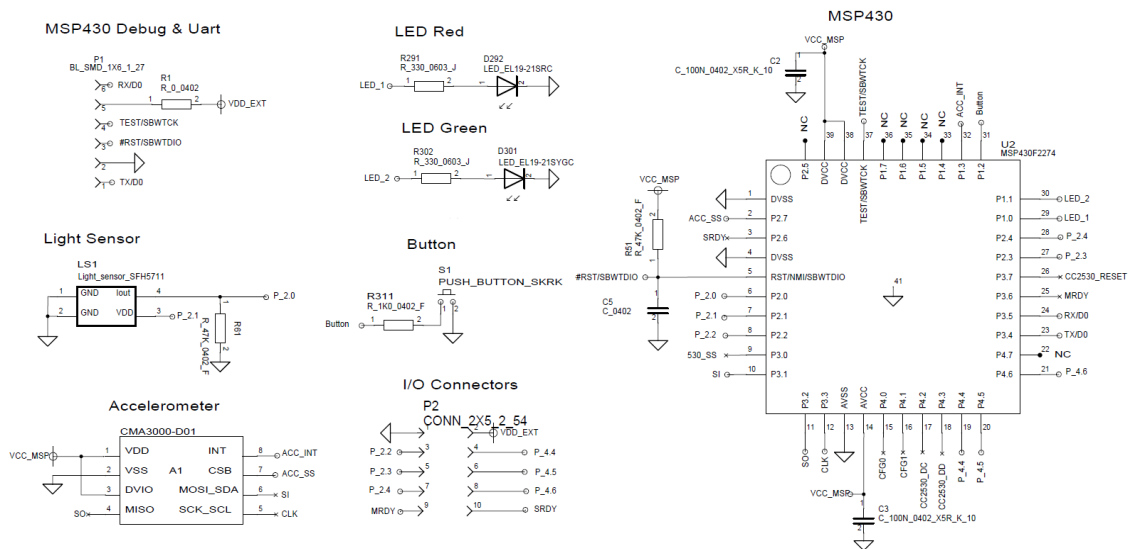


Figure 24: MSP430F2274(CC2530ZNP) Schematic Diagram

The battery powered sensors are end-devices that periodically report their key sensor data such as temperature, light and movement sensor data(accelerometer) to the

coordinator. These devices can also be programmed as routers that are typically used to extend the ZigBee network by routing messages from other end-devices. The hardware for coordinator, router and end-device are identical. Each target board can be programmed as coordinator or router or end-device.

The drivers for the programmer was downloaded and installed from [21]. On connecting the USB programmer to the USB port on a PC installed with these drivers, the device will be automatically detected as shown in Fig. 25. The driver can be found at the default location C:/Texas Instruments/CC2530ZNP Mini Kit/Drivers if not found automatically.

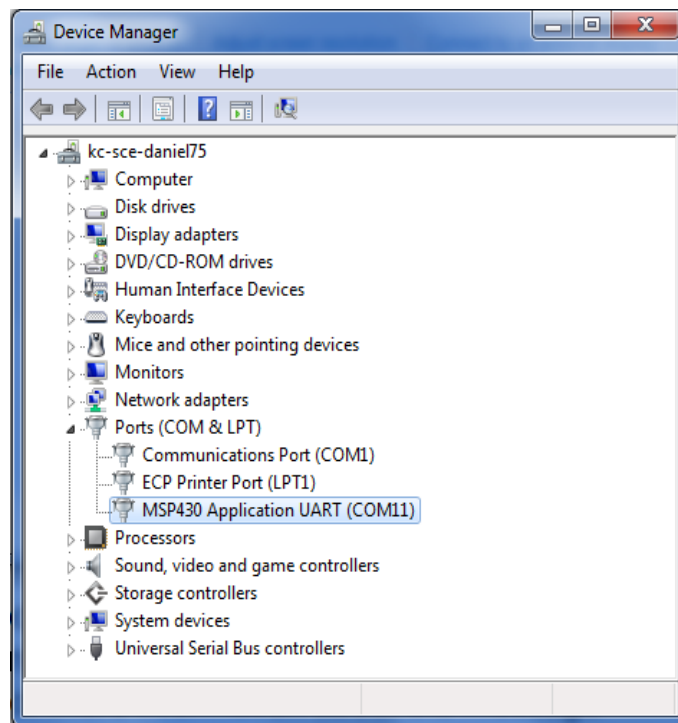


Figure 25: The USB programmer listed in the device manager list

This USB stick serves both as a debugger or programmer and as virtual serial port

interface. This means that the USB stick should be connected to the coordinator target board during normal operation . The USB stick can also be used to debug and program the end-device target boards using the IAR Embedded Workbench.

Using a virtual USB serial port the ZigBee coordinator on the USB stick connects to the PC. Through a terminal program the serial port interface can be accessed. The Windows default terminal interface can be found on the Windows Start menu/Accessories/Communication/Hyperterminal. On starting HyperTerminal, with a name given to the connection, the COM port used by the USB stick is selected. In accordance to the program the the COM port properties are selected. Default properties are no flow control, 1 stop bit, 9600 baud, no parity, 8 data bits as shown in Fig. 26. The information about the ZNP and the device is displayed on the connected Hyperterminal. The coordinator is ready now to connect to other devices on the network. If the end-devices are connected and active, the received end-device messages are displayed on this coordinator HyperTerminal as shown in Fig. 69.

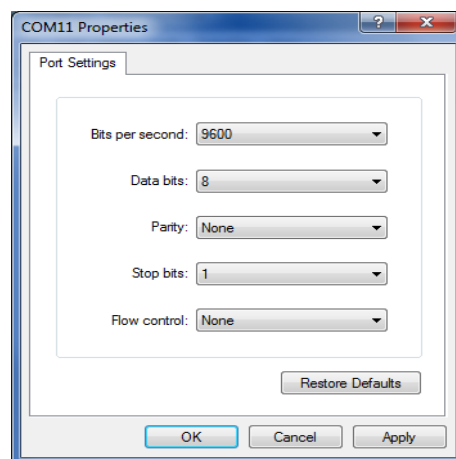


Figure 26: Settings for the COM port

```

COM 11 - HyperTerminal
File Edit View Call Transfer Help
*****
Basic Communications Example - COORDINATOR - using AFZDO
Initializing the ZNP Success
Setting StartupOptions Success
Reset the ZNP Success
Setting Zigbee Device Type Success
Enabling Callbacks Success
Registering Application Success
Starting the Application Success
Rx: 01 45 C0 09
On Network!
ZNP Configuration Parameters
ZCD_NV_PANID          FFFF

ZCD_NV_CHANLIST      00 08 00 00
ZCD_NV_SECURITY_MODE 00
ZCD_NV_PRECFGKEYS_ENABLE 00
Device Information Properties (MSB first)
Device State:        DEV_ZB_COORD (9)
MAC Address:          00 12 4B 00 01 CA 8B 9A
Short Address:        0000
Parent Short Address: 0000
Parent MAC Address:   00 00 00 00 00 00 00
Device Channel:       11
PAN ID:               AF51
Extended PAN ID:      00 12 4B 00 01 CA 8B 9A
Rx: 0D 45 C1 DF 22 DF 22 04 E9 64 01 00 4B 12 00 00
Rx: 1F 44 81 00 00 77 00 DF 22 D7 D7 00 05 00 D0 B7 00 00 00 0E 00 03 00 48 01 F
4 03 69 00 06 00 30 FF F3
Rx: 1F 44 81 00 00 77 00 DF 22 D7 D7 00 2F 00 AA F6 00 00 00 0E 00 03 00 4A 01 F
4 00 01 00 06 00 30 FF F3
Rx: 1F 44 81 00 00 77 00 DF 22 D7 D7 00 3D 00 B7 27 01 00 00 0E 00 03 00 49 01 F
4 00 01 00 06 00 30 FF F3
Rx: 1F 44 81 00 00 77 00 DF 22 D7 D7 00 1E 00 CD 58 01 00 00 0E 00 03 00 49 01 F
4 00 01 00 06 00 30 FF F3
Rx: 1F 44 81 00 00 77 00 DF 22 D7 D7 00 35 00 DF 89 01 00 00 0E 00 03 00 4B 01 9
0 00 01 00 06 00 30 FF F3
-
Connected 0:01:29 Auto detect 9600 8-N-1 SCROLL CAPS NUM Capture Print echo

```

Figure 27: The Coordinator Hyper-terminal

On inserting the batteries in one or more end-devices and by making sure that the jumper is connected to power the end-device is activated. On activation the end-device is programmed to send information packets to the coordinator. This message includes network information as well as sensor data. The message is send periodically as programmed into the end-device. A RX-message from the end-device will appear in the coordinator terminal. A green LED interfaced is programmed to blink while an end-device is sending

a message. The LED will remain on indicating that the end device lost connection with the coordinator.

### 2.7.2 Software

Along with the CC2530ZDK-ZNP-MINI kit, Texas Instruments provides ZNP library methods. The execution flow of the programs for the coordinator and end-device are discussed here. The Coordinator displays messages that arrive from the end-device. This time, the coordinator checks if an info message is received, and if so it displays the parsed message. To send a message from coordinator to the end-device we should know the short address (or long address) of the device which you wish to send the message to. This is out of the scope of the Zigbee protocol and is typically set during network commissioning or using binding. However all end-devices receives a broadcast message from the coordinator. To receive messages the application waits for SRDY to be asserted. Once this happens, it polls for pending message and then if there is a pending message it displays the header information and payload. Once this information is displayed the controller is again waiting for the next message.

The generic ZNP startup sequence for coordinator programming is as follows:

1. Initialize the hardware
2. Reset the ZNP
3. Set Startup Options (STARTOPT\_CLEAR\_CONFIG + STARTOPT\_CLEAR\_STATE)
  - upon reset this will restore the ZNP to a blank configuration

4. Set the Zigbee Device Type as COORDINATOR, ROUTER, or END\_DEVICE
5. Turn on callbacks
6. Register the application
7. Start the application
8. LED indication that the device has started successfully.

The ZigBee end-device periodically send sensor data on start up with a sleep in between transmissions. The accelerometer is configured such that the ZigBee end-device can send message upon motion interrupt. The SPI port has to be initialized every time we wish to use it since it is shared between the Accelerometer and the ZNP.

Each packet has a message header, which includes sender's MAC Address, device-type information, protocol version, flags and sequence numbers. The study about the message format was done referring [27]. The software was written and developed using IAR Embedded Workbench for MSP430 as shown in Fig. 28. A free kickstart edition with 4 Kbyte code size limitation is available from [25]. However if the code size is above 4Kbyte optimization options can be used to make the code more compact. To flash the program into the target board, the USB stick with the target board was plugged into the USB port and the 'Download and Debug' from the project menu was used. Further information on how to use the IAR Embedded workbench for compiling and debugging was referred from the user guide [26].

The CC2530ZNP-Mini Kit is the updated version of the EZ430-RF2480. It uses the Zigbee Network Processor (ZNP) firmware on the CC2530 system on chip(SoC). The

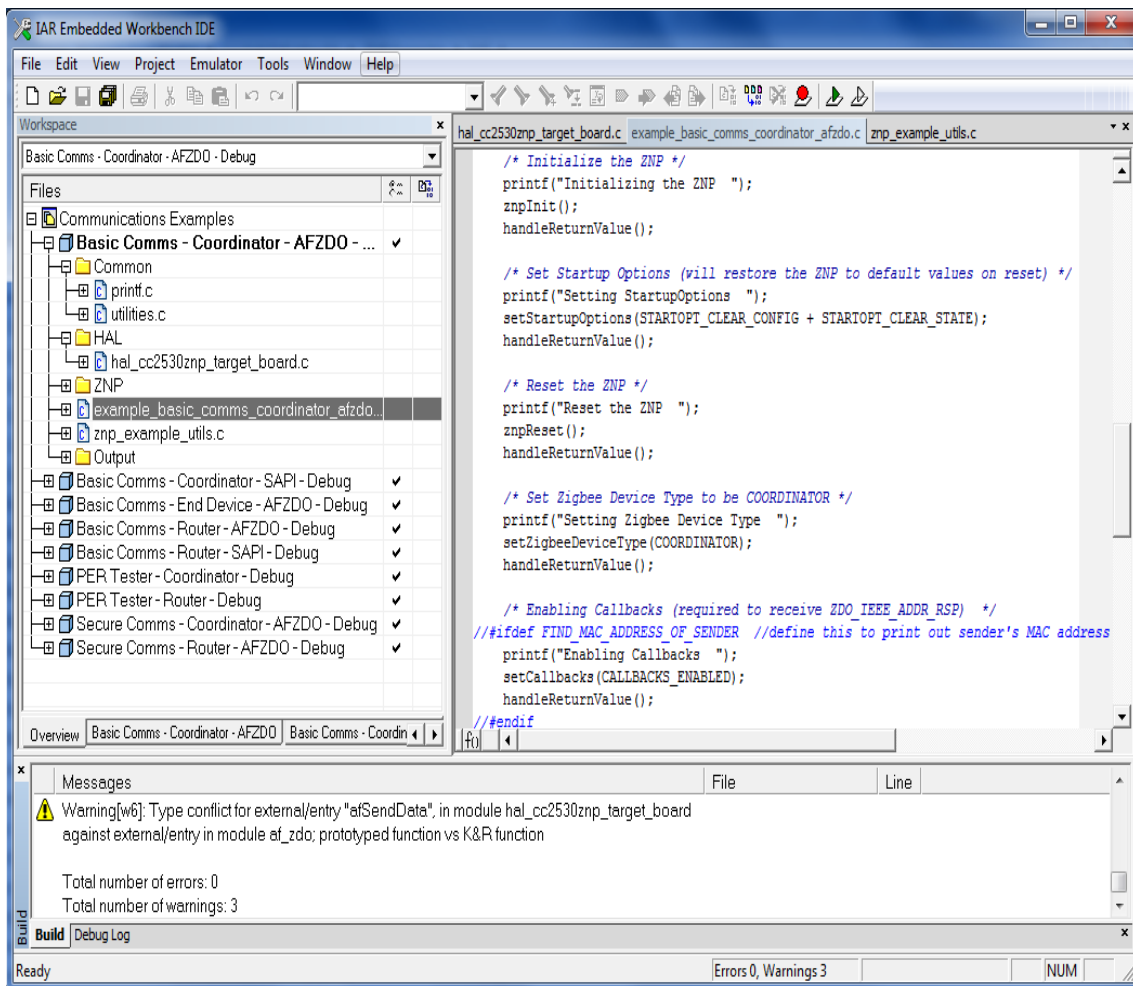


Figure 28: IAR Embedded Workbench IDE

zigbee stack can be separated from the applications processor using CC2530ZNP which enables a faster time to market. Hence ZNP gave an easy way to add ZigBee connectivity to existing systems. All protocol handling of the ZigBee communication is done by a ZigBee processor which allows the existing applications to add a serial interface to a ZigBee processor.

Fig. 29 shows how an application processor can be connected to CC2530 SoC

based ZNP to obtain ZigBee connectivity. The Application Processor describes the MCU or a Processor which is running the application code, that is using the CC2530-ZNP API via the UART or SPI or USB interface to communicate with the ZNP, that runs the full Z-Stack and provides the ZigBee connectivity with its own IEEE 802.15.4 radio

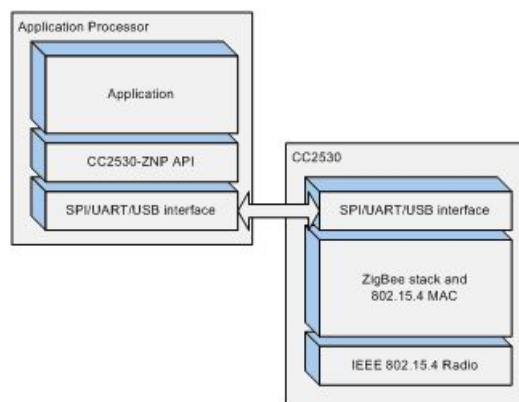


Figure 29: ZNP Application interface

## 2.8 HB404PWA AC Power/Wattage Meter from Annex Depot Inc.

To measure energy consumption of any home appliance in a ZigBee home automation system, we used a HB404PWA AC Power/Wattage Meter from Annex Depot Inc shown in Fig. 30. The meter has an AC voltage input range of 0 to 400V with a 0 to 20 mA analog data output. Among the available products in the market, this device was chosen because it offered a 0 to 20 mA analog data output, which could be routed into appropriate analog port if the CC430 micro-controller.

The load current  $I_1$ ,  $I_2$  (series input). Without an external current transformer, it supports 5A max (see Fig. 32). To measure over 5A, an external current transformer





Figure 30: HB404PWA AC Power/Wattage Meter from Annex Depot Inc.

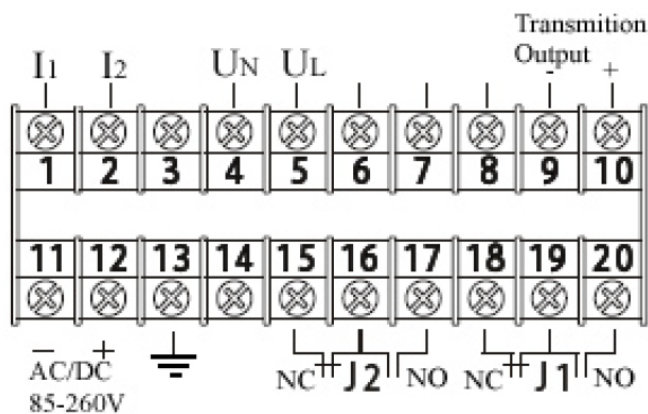



Figure 31: Back Plate of HB404PWA AC Power/Wattage Meter from Annex Depot Inc.

is required. Since most home appliances consumer more than 5A an external current transformer was used. I1 and I2 also serves as input for the current transformer as shown in Fig. 33. The load voltage input is UN,UL. If '-' sign happen, either reverse the I2 or Un and I1, the issue will be taken care by UL.

The 9th and 10th pin in the back plate gives the ground and analog measurement of the energy consumed by any device via the HB404PWA power meter. To change the operating range of the HB404PWA AC Power/Wattage meter, press  to enter the

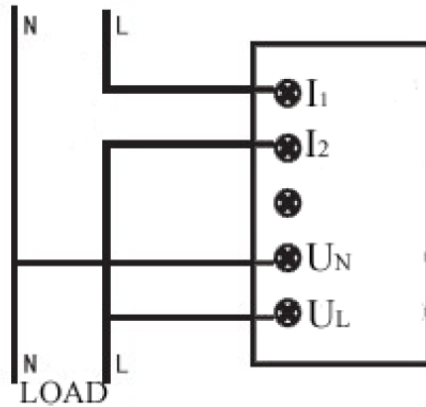


Figure 32: Basic Connection without a current transformer

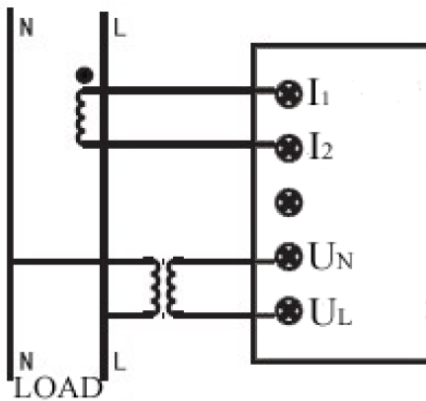


Figure 33: Basic Connection with a current transformer

programming stage. Use  $\otimes$ ,  $\otimes$  and  $\otimes$  to enter password. The password for analogy output setup is 0042. There are three parameters that may be changed to get the output range of your choice that are listed below:

1. Transmission mode(obty): Output selection either in 0 - 20 mA, 4 - 20 mA, or 4 - 20 mA
2. Transmission lower limit(obL): output is either in 0 mA or 4 mA

3. Transmission upper limit(obH): output is 20 mA(or 10 mA ).

The resolution varies depends on the obH setting. To set value use  $\Delta$  and  $\nabla$ .

Once you fix on a value press  $\textcircled{\text{SET}}$  to confirm and save.

## CHAPTER 3

### TELEMETRY UNIT ARCHITECTURE

#### 3.1 Existing Setup

The Bose ElectroForce 3200 load test instrument that we currently use features a maximum force of 225 N (450 N optional) with the versatility of static to 200 Hz frequency response. However, only a force of 3N at 3 Hz was used for our measurements. This table-top configuration is adaptable to a variety of bio-medical research and engineered materials test applications, including creep under dynamic loading, torsion testing and special environments (hot/cold chambers). Fig. 34 depicts the existing setup using Bose ElectroForce 3200 system whose settings can be modified using WinTest<sup>®</sup> software to apply forces of different frequencies and magnitude. The strain values are normally collected using the Vishay Micro-Measurement 7000 data acquisition system through StrainSmart<sup>®</sup> software. WinTest<sup>®</sup> and StrainSmart<sup>®</sup> software's run on a dedicated PC connected to the setup. A Vishay EA-06-015DJ-120 strain gage of nominal resistance of 120<sup>®</sup> and gage factor(GF) of  $2.07 \pm 2\%$  is used. The strain gage is glued to the surgically removed bone of a mouse or bone of a sedated mouse. To measure the bone strain *in-vivo* the subject has to be sedated and the strain gage sensors has to be glued on to the bone with transcutaneous leads connected to the data acquisition unit. These bio-medical signals are mostly very weak electrical signals which are acquired via wires

connected through skin. This limits the scope of experimental studies to immobilized animals. However for orthopedic researchers, measurement of bone strain while a subject is in motion is much essential. As no plastic is absolutely moist proof, thus using transcutaneous leads for general clinical purposes is not recommended. The current set up as a whole is not portable and is moreover very bulky. Hence the subject has to be brought near to the fixed current setup in order to take measurements. Due to all the above reasons, there is a requirement of small implantable device for recording strain on a non restricted subject.

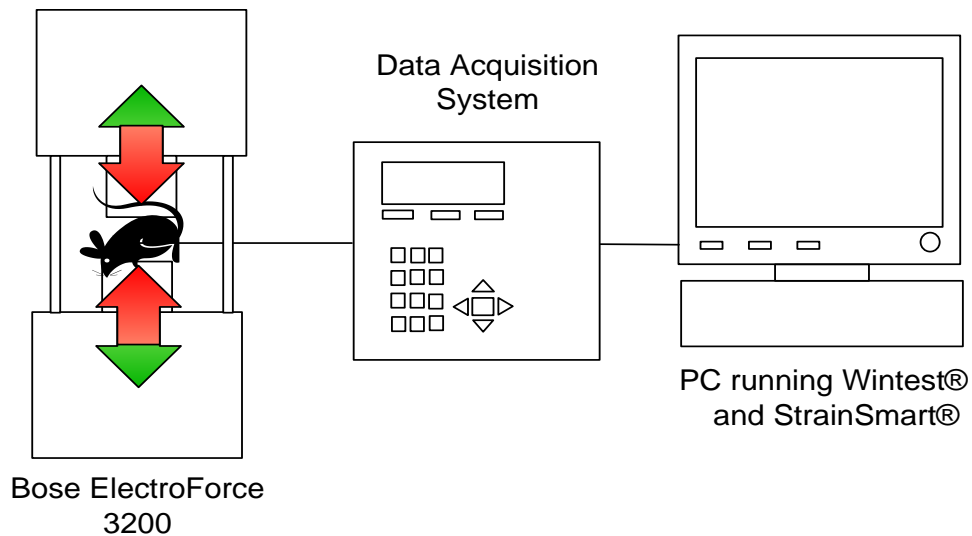


Figure 34: Bose ElectroForce 3200 load test instrument connected to the data acquisition system controlled and monitored from a dedicated PC

### **3.2 915 MHz Telemetry Unit of Dimension 24 mm x 13 mm**

In the current set-up the for *in-vivo* measurement of bone strain the animal has to be sedated and immobilized. However, studies show that there are physical changes in animal neurological structures when movement is restricted, and also animals recover faster from brain injuries in a locomotion-allowing environment. Hence bone strain measurement on a mobilized animal is essential for experimental studies. Thus, there is a requirement for an implantable device which facilitates unrestricted movement and hence enhancing experimental research.

To measure bone strain in animals in motion, the implantable sensors used must be very compact and tiny so that it can be implanted in the animal under observation. The functionality of the existing set up has to be made implantable and hence should be made more compact and smaller. To measure the bone strain *in-vivo* the subject has to be sedated and the strain gage sensors has to be glued on to the bone with transcutaneous leads connected to the data acquisition unit in the existing set up. These signals are mostly very weak electrical signals which are acquired via wires connected through skin. To eliminates transcutaneous leads through the skin, the bone strain measuring device must operate wirelessly. An implantable telemetry unit for bone strain measurement has been designed to address all these problems.

#### **3.2.1 Design Objectives**

An implantable or wearable telemetry unit was designed to overcome the drawbacks of the existing system. The telemetry unit must however be of smallest size possible

so that the telemetry unit can go implanted even in small animals. To design a telemetry unit of smallest size, the unit has to be designed with minimal off-the-shelf components. The key feature of the telemetry unit must be preserved with minimal off-the-shelf component usage which was a challenging goal. The more advanced features possible for a telemetry unit like more number of sensor channels had to be trade-off-ed to keep the telemetry unit small.

Further to reduce the overall size of the telemetry unit each of the off-the-shelf component of smallest available size was chosen. The PCB placement and routing was another important design goal to keep the telemetry unit compact. An efficient placement and routing allows the designer the feasibility to accommodate more components.

The main idea of the telemetry unit is the wireless measurement of bone strain. Once the telemetry unit is implanted in an animal, the sensor signals are multiplexed, modulated and transmitted to a remote computer by means of an integrated radio transceiver. Hence enhancing experimental studies on mobilized animals. Besides measuring strain levels the telemetry unit can also measure acceleration in 3 axes, giving further insight to the orthopedic researchers about movements.

The telemetry unit possesses multiple configurable sensor channels to sense resistance and voltage. Hence the telemetry unit can be used for other applications as well. Since the eight sensor channels are configurable, the sensors connected to the telemetry unit can be changed. Therefore sensors to measure force, temperature, light etc can be connected. Also different sensors can be connected to different channels of the telemetry unit at a time. Thus by connecting the telemetry unit with one strain gage sensor,

one temperature sensor, one force sensor, one light sensor etc. can reveal more detailed information about animal part under study.

Wireless battery charging is another important feature that was included in this design which is a key feature for surgically implanted devices. The telemetry unit discussed here is battery powered. It is important for a telemetry unit to have the feature of wireless battery charging so that the unit does not need to be surgically removed from the animal to recharge or replace the battery. Wireless battery recharging hence promises long term measurement of the bone strain once implanted.

Since the 915 MHz telemetry unit is battery powered, it is essential to design the unit as low power to avoid fast draining of the battery. Also the size of the battery used to power up the telemetry unit must be small enough so that it can go implanted in an animal. The low power consumption allows the unit to be powered by a small battery. The power consumption depends upon the individual consumption of the off-the-shelf components while in operation as well as any other strategies adopted to reduce consumption.

Even in the reduced size of the telemetry unit, the unit is expected to perform with comparable accuracy with respect to the existing system. With bone strain monitoring being the key feature of the telemetry unit, it is important for orthopedic researchers that the strain measurements are accurate. The rate of flow of data from the implanted telemetry unit is another performance criteria for adoption of the telemetry unit. A device giving accurate result very slowly and a device giving inaccurate results very fast are both not acceptable. Accurate bone strain measurements at fastest possible rate is another design goal of this telemetry unit.



The summary of the design objectives for the 915 MHz Telemetry Unit is as follows:

1. Least number of components for smallest feasible device
2. Choice of smallest feasible off-the-shelf components
3. Compact PCB routing
4. Low power consumption
5. Wireless battery recharging
6. Wireless bone strain monitoring
7. Wireless monitoring of acceleration data in 3 axes
8. Multiple configurable sensor channels to sense resistance and voltage
9. Comparable accuracy
10. Acceptable data rate

### 3.2.2 Design

The block diagram of the telemetry unit is shown in figure 35.

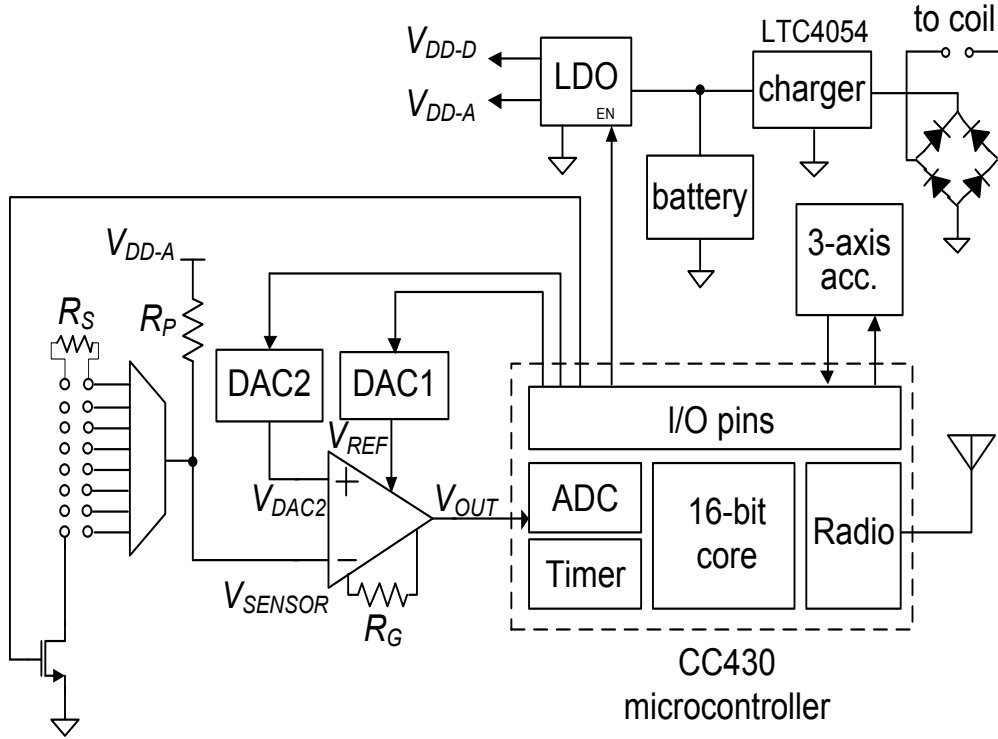


Figure 35: Block diagram of the telemetry unit

The output voltage of the instrumentation amplifier is given by (3.1):

$$V_{OUT} = G (V_{DAC2} - V_{SENSOR}) + V_{REF} \quad (3.1)$$

where  $V_{DAC2}$  is the auto-calibrated DAC2 output.  $V_{SENSOR}$  is the voltage of the branch with strain gauge and  $G$  is the gain of the amplifier.  $G$  is set by the external resistor  $R_G$  and is calculated by (3.2):

$$G = 1 + \frac{100 \text{ k}\Omega}{R_G} \quad (3.2)$$

$V_{REF}$  is the output of DAC1, programmed by the micro-controller and is the output of the amplifier when the inputs are shorted. To provide a known 'zero' for the strain signal, the micro-controller performs an auto zeroing routine. In the auto zeroing routine the micro-controller programs the  $V_{DAC2}$  such that it is equal to or very close to the  $V_{SENSOR}$ , making  $V_{OUT}$  equal to  $V_{REF}$ . Any change from this 'zero' is strain sensed by the strain gauge.

The strain gauge resistance is denoted by  $R_S$  while the the precision resistor is denoted by  $R_P$ . The nominal resistance,  $R_{S(nom)}$ , of the strain gauge is 120  $\Omega$ . The bridge is excited by  $V_{DD-A}$ . If the MOSFET switch is turned ON, the voltage  $V_{SENSOR}$  is given by (3.3):

$$V_{SENSOR} = V_{DD-A} \left( \frac{R_S}{R_S + R_P} \right) \quad (3.3)$$

The strain gauge resistance  $R_S$  changes if a strain is applied which in turn changes  $V_{SENSOR}$ . This change was however very minute for the expected range of strain values. The  $R_S$  changed by only 0.75  $\Omega$  for a strain of 3000  $\mu\epsilon$ . Hence a gain of 334 proved satisfactory and was set by choosing  $R_G$  to be 300  $\Omega$ . The amplified analog output is fed to the 12-bit on-chip ADC of the micro-controller. The digital output of the ADC will be according to (3.15):

$$D = \frac{V_{OUT}}{V_{DD-A}} 2^n \quad (3.4)$$

where  $V_{OUT}$  is the analog output of the amplifier and  $n$  is the resolution of the ADC. The on-chip timer is used to trigger the sampling by the ADC, thus setting the sampling frequency of the strain signal.

The payload of the data packet transmitted to the base station by the telemetry unit is of length 60 bytes. The first three bytes of the packet payload encodes 12 bits of  $V_{DAC2}$  value and 12 bit value of the timer period. The period of the timer determines the sampling frequency of the strain data as the timer triggers the sampling by the ADC. The next three bytes of the packet contains 12 bits of  $V_{DAC1}$  value and the activated channel information. Two 12-bit ADC samples are packed into 3 bytes. 8-bit value of acceleration in X,Y and Z gathered from the accelerometer can be packed into another 3 bytes. Only ADC samples where transmitted for comparing the telemetry unit to the data acquisition unit.

The radio transceiver data rate was set to 256 kBaud and the sampling frequency of the ADC was varied from 7.5 Hz to 160 Hz. This range was chosen since the bone was put under sinusoidal force with maximum frequency of 3 Hz.

The base station receives the radio packet and checks for CRC errors. If the CRC is passed the packet is serially send to the COM port of the PC. The GUI running on Matlab<sup>®</sup> unpacks the packets arriving at the COM port. Before plotting micro strain data the GUI first converts received digital value of  $V_{OUT}$  to analog using (3.5):

$$V_{OUT} = \frac{D}{2^n} V_{DD-A} \quad (3.5)$$

where D is the received digital value of  $V_{OUT}$  and  $n$  is the resolution of the on-chip ADC.

Next, to calculate  $V_{SENSOR}$  and the strain gauge resistance  $R_S$  from  $V_{SENSOR}$ , equations (3.6) and (3.7) are used:

$$V_{SENSOR} = V_{DAC2} + \frac{V_{OUT} - V_{REF}}{G} \quad (3.6)$$

$$R_S = \frac{R_P V_S}{V_{DD-A} - V_{SENSOR}} \quad (3.7)$$

And finally the micro strain is calculated by (3.8):

$$\mu\epsilon = \frac{R_P - R_S}{(10^6)(R_P)(GF)} \quad (3.8)$$

To remove noise an optional Butterworth digital filter is applied for a clean waveform.

### 3.2.3 Hardware Implementation

The design requirements for a strain sensing telemetry unit for *ex-vivo* and *in-vivo* settings are: light weight and miniature in size, low-power consumption for long-term and maintenance-free strain monitoring, and for implantable application must feature a wireless battery charging mechanism.

Adhering to these requirements, we present a telemetry unit designed around an ultra-low-power micro-controller CC430F5137 from Texas Instruments. The CC430F5137 integrates a Sub-1-GHz RF transceiver core with a programmable data rate of 0.6 kBaud to 500 kBaud. The micro-controller has an ultra low power consumption of  $2.0 \mu A$  during standby mode and  $12 mA$  during radio in receive mode. With wake up time from standby

mode less than  $6 \mu s$  we were able to switch to standby mode between transmissions to further reduce the power consumption. The micro-controller of 16-Bit RISC architecture with a 12-bit analog-to-digital converter and other peripherals measures only 8 mm x 8 mm.

To measure resistive-type strain gauge sensors, the most common approach is use a Wheatstone bridge and to amplify the voltage difference between the two branches of the bridge. When the branch voltages are same the output of the amplifier is equal to reference voltage  $V_{REF}$ . To change the  $V_{REF}$  of the amplifier a 12-bit digital-to-analog (DAC) converter (DAC7311) controlled by the micro-controller is employed. By precise tuning of the bridge resistors the branch voltages can be made equal making the output of the amplifier to be  $V_{REF}$ . We replaced one branch of the bridge with a another DAC7311 to avoid manual zeroing using potentiometers. By generating a ramp voltage at the output of DAC2, zeroing is performed by the micro-controller. Fig. 36 shows a block diagram for the calibration process and demonstrates how the voltages change when the calibration is being performed.

The telemetry unit employs a low power precision instrumentation amplifier INA333 from Texas Instruments. The amplifier provides very low offset voltage, high common-mode rejection and excellent offset voltage drift. Hence it operates with power supplies as low as  $1.8V$  making it ideal for battery-operated systems. A single external resistor  $R_G$  sets the gain from 1 to 1000 using (3.2) in section 3.2.2.

The unit has the capability of acquiring data from eight strain gauges at one time. The eight channels of the telemetry unit are multiplexed into the amplifier using two

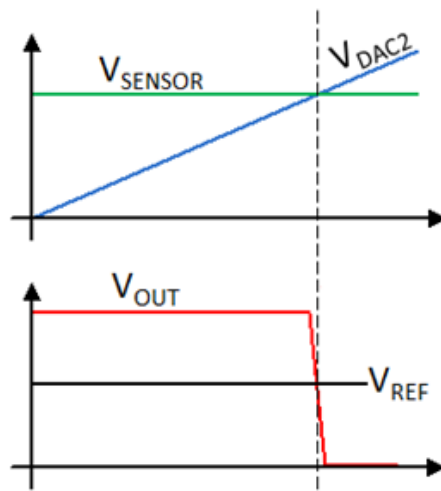
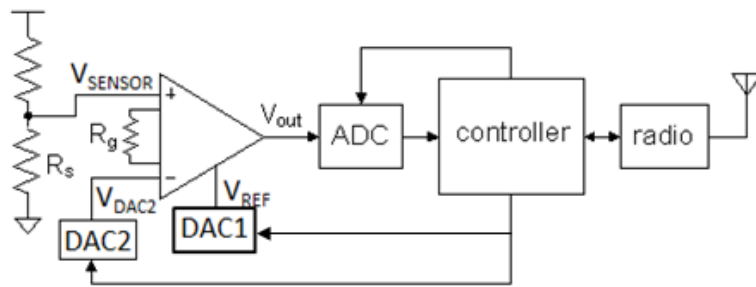


Figure 36: Ramp calibration of the wheatstone bridge by the micro-controller.  $V_{SENSOR}$  is the voltage of the branch with the strain gauge.  $V_{DAC2}$  is changed by the micro-controller and when the output of the amplifier  $V_{OUT}$  is equal to  $V_{REF}$  the ramp is stopped.

low voltage 4-channel CMOS multiplexers ADG804 from Analog Devices. To conserve power a N-channel Trench MOSFET(PMV16UN) in a small SOT23 package is used as a switch to activate and deactivate the sensors.

An antenna impedance matching network is needed for the on-chip RF transceiver of the micro-controller. An impedance matching balun from Johanson Technology (0896BM15A0001) was employed because it helps to reduce the required components and is small in size. A 915 MHz chip antenna from Johanson Technology (0915AT43A0026)

and a small 26 MHz crystal oscillator from Nihon Dempa Kogyo Co., LTD. (NX2016AB) are also needed by the RF transceiver and were included on the board.

The unit is also capable of wireless charging of the battery and thus proves suitable for implantable applications. This was done by adding a voltage linear charger (LTC4054) for single cell lithium-ion batteries. The HSMS-282P rectifier from Agilent connected to the RF coil feeds the rectified output to power up the voltage linear charger to recharge the battery.

In addition to above mentioned features, the unit can also measure the static or dynamic acceleration of the subject this unit is attached to. This is done by employing a smart low-power accelerometer MMA8453Q of 10 bits resolution. The accelerometer measuring 3 mm x 3 mm x 1 mm in QFN package is interfaced to the micro-controller via I2C protocol. The data can be collected in 10-bit or 8-bit format. The embedded interrupt functions of the accelerometer enhances the overall power savings by relieving the micro-controller from continuously polling data.

The unit operates on a 3.7 V Li-Pol battery. To provide a steady 3.0 V voltage to all the components a low-dropout (LDO) voltage regulator TLV711285 was included. This LDO has two separate outputs controlled by their respective enable pins. Output1 powers the the micro-controller and output2 is used to power the rest of the components. The micro-controller turns off output2 to conserve battery when data is not being transmitted.

All the components were integrated on a 4-layer PCB that measures 2.4 cm X 1.3 cm. Careful choosing of compact sized and low power consuming components satisfy the design challenges of the telemetry unit.



The unit was tested in an *ex-vivo* setting. The telemetry unit replaced the data acquisition unit of the existing setup. The strain gauge glued to bone was now connected to the telemetry unit. Identical force was applied to the bone to provide with a fair comparison of the two units. Results are presented in section 5.1.1.

Figure 37 depicts the *ex-vivo* testing of the telemetry unit. Figures 38 and 39 respectively show the top and bottom of the telemetry PCB.

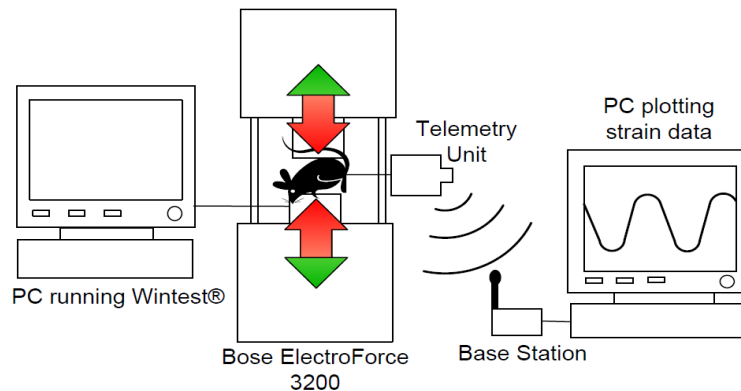


Figure 37: Bose ElectroForce 3200 load test instrument connected to the telemetry unit controlled from a dedicated PC and base station wirelessly monitoring strain data.

The software code flow diagram running in the CC430F5137 micro-controller is shown in Fig. 40. The Interrupt Service Routines for the TimerA and for the Radio are shown in Fig. 41 and Fig. 42.

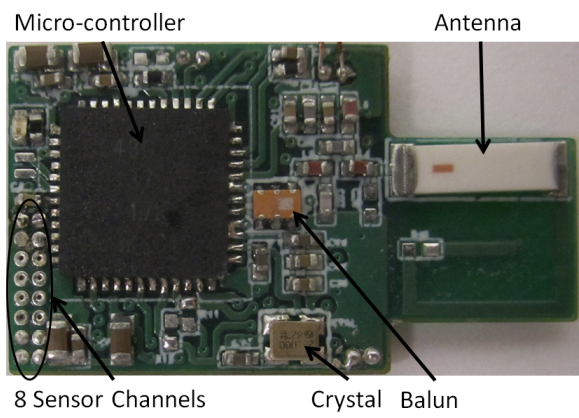


Figure 38: Top side of the telemetry unit.

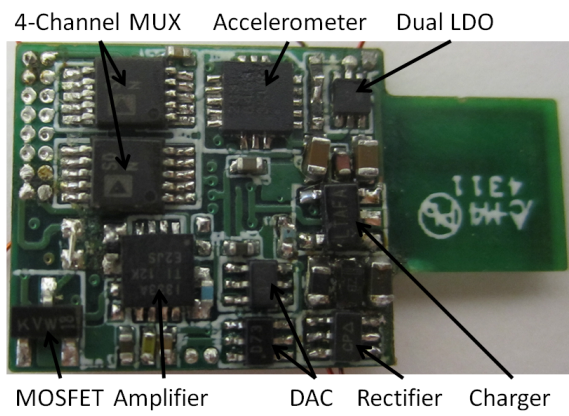


Figure 39: Bottom side of the telemetry unit.

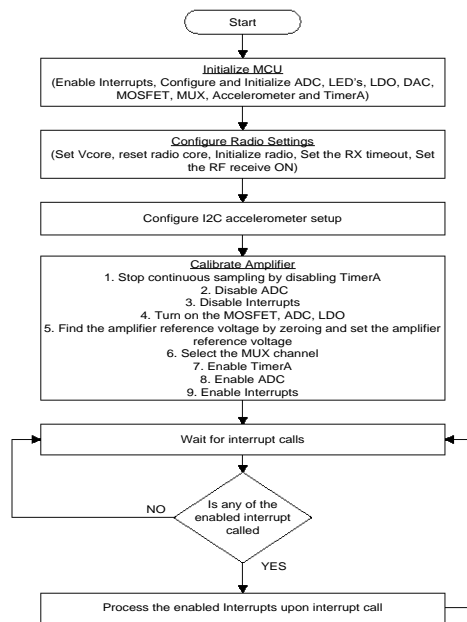


Figure 40: Flow Diagram for 915 MHz Telemetry Unit of Dimension 24 mm x 13 mm

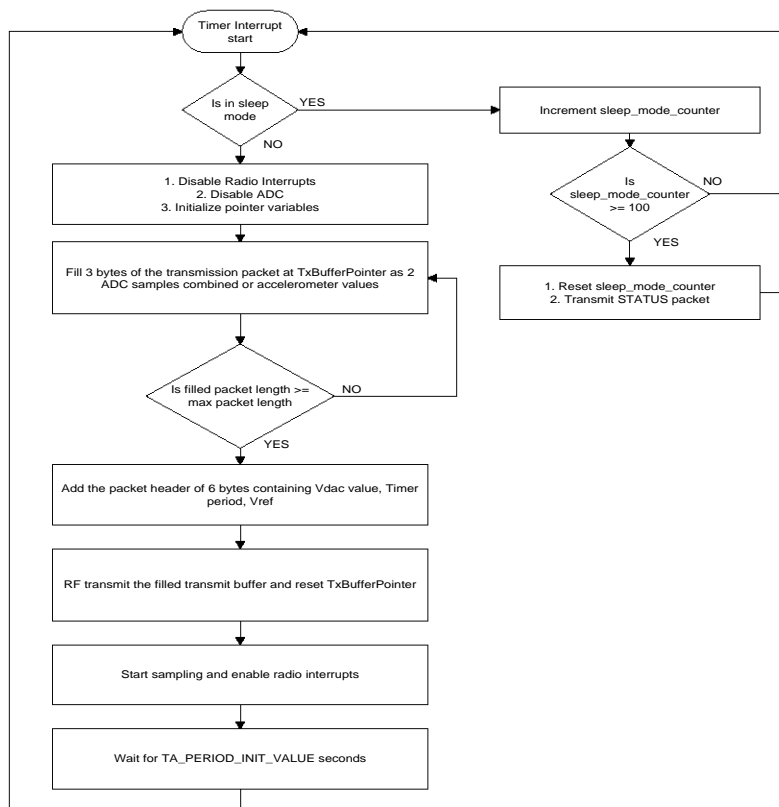


Figure 41: Flow Diagram of TimerA Interrupt Service Routine

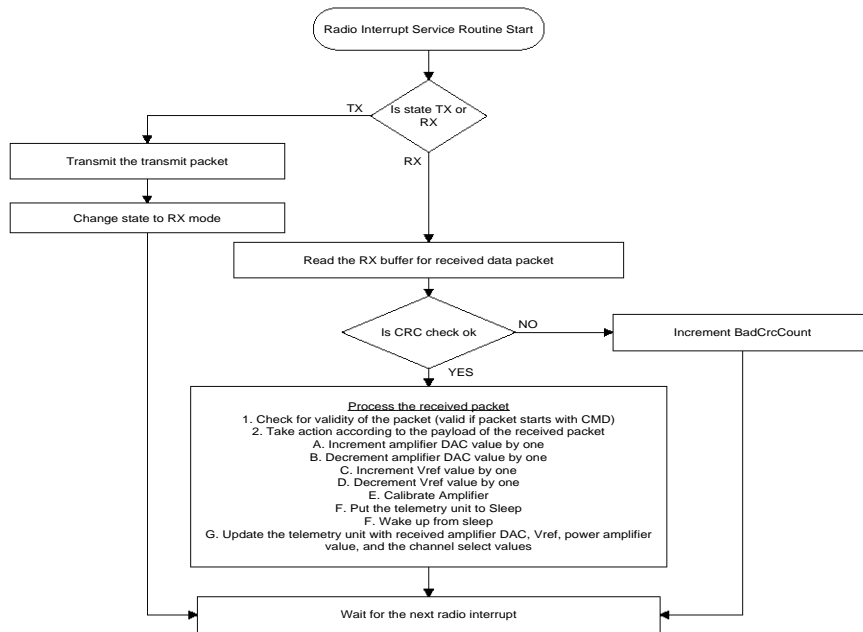


Figure 42: Flow Diagram of Radio Interrupt Service Routine

### **3.3 RFID based Telemetry Unit of Dimension 10 mm x 10 mm**

The smallest battery powered active telemetry device was still large for cranial implantation. A very promising alternative is RF power harvesting through inductive coupling offering a two way link of power gathering and data transmission. The concept is same as that of RFID, which uses inductive coupling to read an encoded identification sequence stored in the tag memory and then report the value to the interrogator. A telemetry unit with RFID interface was designed and tested. The RFID interface enables a telemetry unit of dimensions 10 mm x 10 mm. To measure bone strain in small animals such as mouse we need very tiny telemetry unit. The 915 MHz telemetry unit operates from a 3.7 V Li-Pol battery that weighs less than 3 grams. To implant the 915 MHz telemetry unit the battery as well has to go implanted in the animal. Hence it is impossible to implant the 915 MHz telemetry unit in small animals like mouse or rabbit. Therefore in addition to the advantages the 915 MHz telemetry unit had over the existing set up, the RFID based telemetry unit has a much reduced size. Since the RFID based telemetry unit is RFID powered, there is no need of a battery to be implanted in the animal to power up the board. This further reduces the size of total implant package and hence this RFID based telemetry unit is implantable in small animals like a mouse or a rabbit. The drawback of an RFID interface is its limited communication range.

### 3.3.1 Design Objectives

In addition to the design objectives of the 915 MHz telemetry unit, the prime objective of an RFID based telemetry unit was to further reduction in size. Since the unit was inductively power charged by an RFID the battery recharging components in 915 MHz telemetry could be eliminated scaling the size of the RFID based telemetry unit down. Further another trade off was made by reducing the number of sensor channels from eight to four and hence reducing the components on the telemetry unit. By efficiently placing the components and making shortest routing, the size of the RFID based telemetry unit was brought further down.

The 4 sensor channels remains configurable giving freedom to the user to change among sensors. Since this telemetry unit is inductive powered from an RFID, it is very essential to keep the telemetry unit low power. Wireless bone strain monitoring in an acceptable data rate is another objective in order to be adopted by a user.

The summary of the design objectives for an RFID based Telemetry Unit of dimension 10 mm x 10 mm is as follows:

1. Least number of components for smallest feasible device
2. Choice of smallest feasible off-the-shelf components
3. Compact PCB routing
4. Low power consumption
5. Wireless bone strain monitoring

6. Wireless monitoring of acceleration data in 3 axes
7. Multiple configurable sensor channels to sense resistance and voltage
8. Comparable accuracy
9. Acceptable data rate
10. RFID based inductive power charging

### 3.3.2 Design

The block diagram of our telemetry unit is shown in Fig. 43

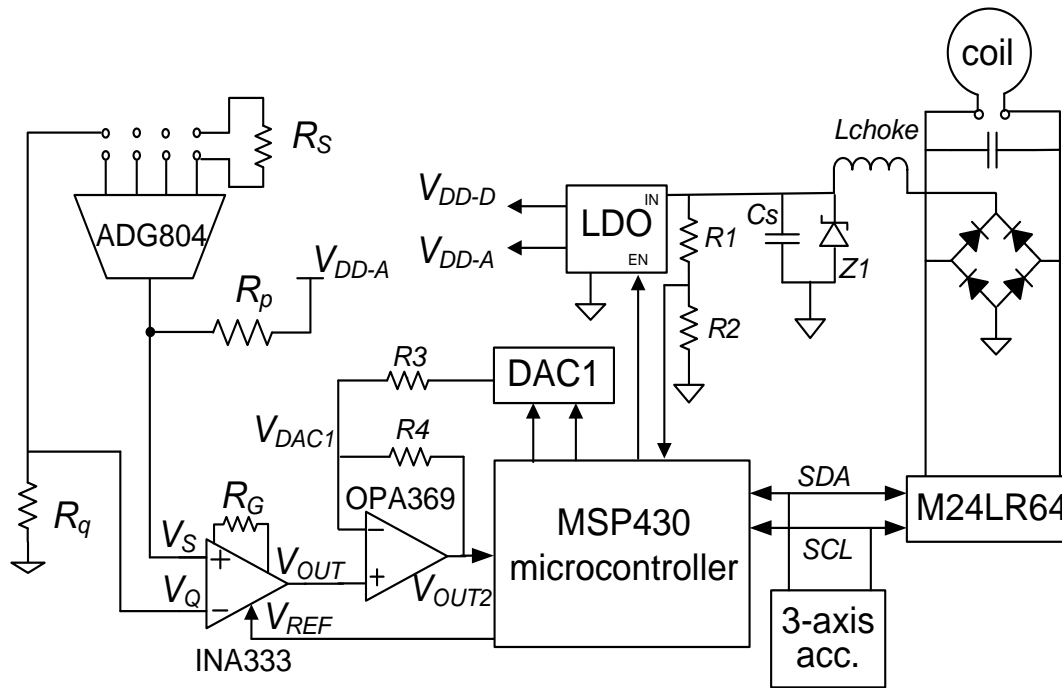


Figure 43: Block Diagram of an RFID based Telemetry Unit of dimension 10 mm x 10 mm



The output voltage  $V_{OUT}$  of the instrumentation amplifier is given by (3.9):

$$V_{OUT} = G(V_S - V_G) + V_{REF} \quad (3.9)$$

where  $V_S$  is the voltage of the branch with strain gauge,  $V_Q$  is the voltage over the resistor  $R_Q$  and  $G$  is the gain of the amplifier.  $G$  is set by the external resistor  $R_G$  and is calculated by (3.10):

$$G = 1 + \frac{100 \text{ k}\Omega}{R_G} \quad (3.10)$$

The voltage  $V_Q$  is given by the equation (3.11):

$$V_Q = V_{DD-A} \left( \frac{R_Q}{R_S + R_P + R_Q} \right) \quad (3.11)$$

where strain gage resistance is denoted by  $R_S$  while the the precision resistor is denoted by  $R_P$ . The voltage at the output of the analog mux is given by the equation (3.12)

$$V_S = V_{DD-A} \left( \frac{R_S + R_Q}{R_S + R_P + R_Q} \right) \quad (3.12)$$

The  $V_{REF}$  controlled by the micro-controller provides biasing for the sensor.  $V_{REF}$  is the output of DAC1, programmed by the micro-controller and is the output of the amplifier when the inputs are shorted. To provide a known 'zero' for the strain signal, the micro-controller performs an auto zeroing routine. In the auto zeroing routine the micro-controller programs the  $V_{DAC2}$  such that it is equal to or very close to the  $V_S$ , making  $V_{OUT}$  equal to  $V_{REF}$ . Any change from this 'zero' is strain sensed by the strain gauge.

The strain gauge resistance  $R_S$  changes if a strain is applied which in turn changes  $V_S$ . This change was however very minute for the expected range of strain values. The  $R_S$  changed by only  $0.75 \Omega$  for a strain of  $3000 \mu\epsilon$ . Hence a gain of 501 proved satisfactory and was set by choosing  $R_G$  to be  $200 \Omega$ .

To reduce noise the output of the instrumentation amplifier is further fed into an OPA369 amplifier of gain G1. The output of an OPA369 amplifier is  $V_{OUT2}$  and is given by the equation (3.13)

$$V_{OUT2} = G1 (V_{OUT} - V_{DAC1}) \quad (3.13)$$

where  $V_{OUT}$  is the output of the instrumentation amplifier and  $V_{DAC1}$  is the auto-calibrated DAC1 output. The gain G1 of an OPA369 amplifier is given by the equation (3.14)

$$G1 = 1 + \frac{R4}{R3} \quad (3.14)$$

This amplified analog output is fed to the 12-bit on-chip ADC of the micro-controller. The digital output of the ADC will be according to (3.15):

$$D = \frac{V_{OUT}}{V_{DD-A}} 2^n \quad (3.15)$$

where  $V_{OUT}$  is the analog output of the amplifier and  $n$  is the resolution of the ADC. The on-chip timer is used to trigger the sampling by the ADC, thus setting the sampling frequency of the strain signal.

The measured acceleration data is stored in the OUT\_X\_LSB (02), OUT\_Y\_LSB (04) and OUT\_Z\_LSB(06) registers of the accelerometer in 2's complement form. The

controller communicates with the accelerometer via I2C and constantly poll these registers.

### 3.3.3 Hardware Implementation

The design requirements for a strain sensing telemetry unit for *ex-vivo* and *in-vivo* settings are: light weight and miniature in size, low-power consumption for long-term and maintenance-free strain monitoring, and for implantable application must feature a wireless power charging and a wireless data communication mechanism.

Adhering to these requirements, we present a RFID based telemetry unit designed around the ultra-low-power micro-controller MSP430F2012 from Texas Instruments, the telemetry unit is inductively power charged. The controller of 16-bit RISC CPU includes a digitally controlled oscillator(DCO) which allows the wake-up from low-power modes to active mode in less than 1  $\mu$ s. The built-in communication capability of the microcontroller using synchronous protocols (SPI or I2C) facilitates interfacing with other on the board components. The architecture, combined with five low-power modes is optimized to achieve extended battery life in portable measurement applications. The controller as well comprise of 10-bit Analog-to-Digital converter and 16-bit timer and ten Input-Output pins. The main focus of this board design was an implantable sensor with a very small size and low power consumption. Due to inductive power charging of the board, the battery could of 915 MHz telemetry unit can be eliminated reducing the size of the implantable sensor. The size comparison of the RFID based telemetry unit with a penny is shown in Fig. 44.

To measure the resistive-type strain gage sensor, the voltage difference across the

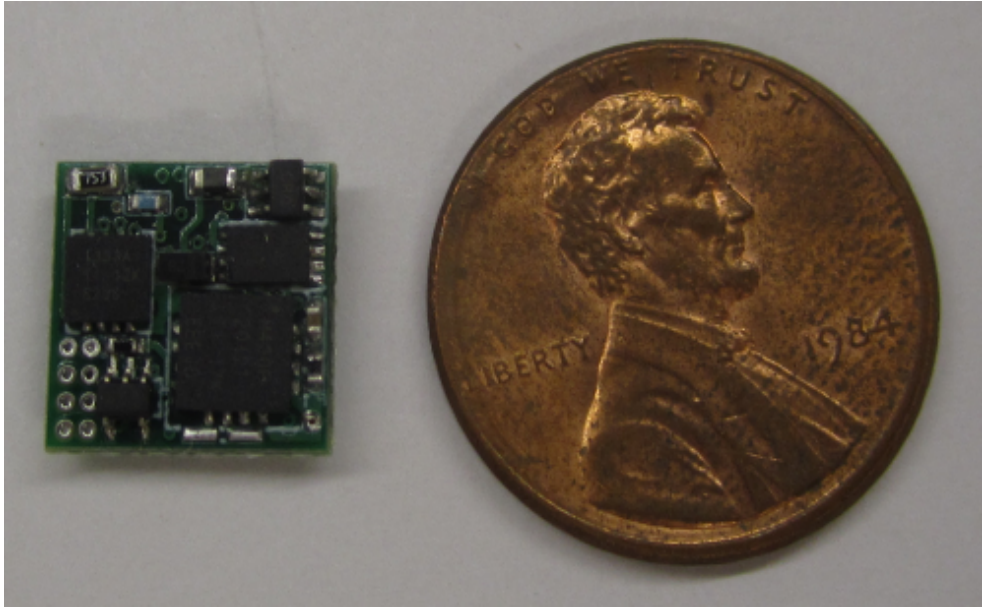


Figure 44: RFID based telemetry unit vs a penny

sensors are amplified by a low power precision instrumentation amplifier INA 333 from Texas Instruments. This amplifier provides very low offset voltage, high common-mode rejection and excellent offset voltage drift. An instrumentation amplifier is used to reject the common-mode noise. Common mode noise is present in telemetry unit at the sensor inputs due to long sensor wires and due because of the strong generated field of the RFID reader. It operates with power supplies as low as 1.8 V making it ideal for battery-operated systems. The four sensor channels of the telemetry unit are multiplexed into this amplifier using a low voltage 4-channel CMOS multiplexer ADG804 from Analog Devices. The ADG804 multiplexer was choose due to its very small size and very low  $R_{ON}$  resistance of  $0.5\Omega$ .

The output of INA333 amplifier has the problem of input crossover distortion that becomes very prominent in low voltages(below 3V), rail-to-rail input applications. For

this reason this amplifier output is further amplified using OPA369, an ultra-low-power amplifier with zero-crossover feature resolving the problem of input crossover distortion. The OPA369 comes from Texas Instruments comes in micro-size packages and with very low quiescent current and low noise of  $3.6 \mu V_{PP}$ . The amplified the voltage difference between across the sensor resistance is inputed to the micro-controller. By generating a ramp voltage at the output of the DAC, Zeroing is performed by the controller. When the output of the amplifier reaches the desired zero-level voltage the ramp is stopped.

To measure the static or dynamic acceleration forces a smart low-power accelerometer MMA8453Q of 10 bits resolution was included on the board. The accelerometer measuring 3 mm x 3 mm x 1 mm in QFN package is interfaced to the controller via I2C protocol. The embedded interrupt functions of the accelerometer enhances the overall power savings by relieving the controller from continuously polling data.

The HSMS-282P rectifier from Agilent connected to the RF coil feeds the rectified output to a voltage regulator. To provide a steady 3.3V voltage supply a low-dropout(LDO) voltage regulator TLV711285 was included. The M24LR64-R connected to the RF coil is also a contact-less memory powered by the received carrier electromagnetic wave. The memory has a dual-interface,an RFID interface and an I2C interface. In the ISO15693/ISO18000-3 mode 1 RF mode, the M24LR64-R is accessed via the 13.56 MHz carrier electromagnetic wave on which incoming data are demodulated from the received signal amplitude modulation (ASK: amplitude shift keying). Data are transferred from the M24LR64-R at 6.6 Kbit/s in low data rate mode and 26 Kbit/s high data rate mode. The M24LR64-R supports the 53 Kbit/s in high data rate mode in one subcarrier

frequency at 423 kHz. In the memory I2C mode of operation the controller writes into the memory the data that it needs to send to the base station using I2C protocol. Hence the memory is connected to RF coil as well as the SDA and SCL lines of the controller.

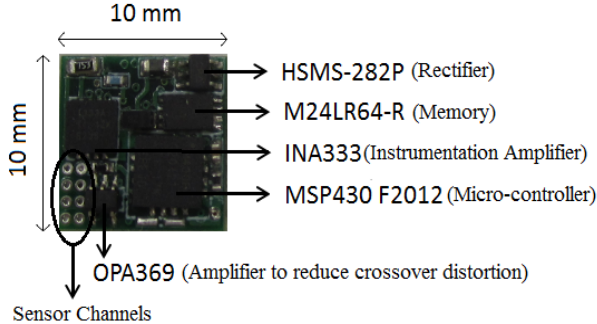


Figure 45: Top side of an RFID based telemetry unit

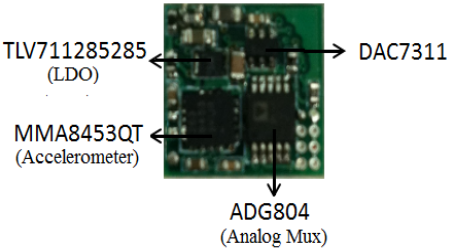


Figure 46: Bottom side of an RFID based telemetry unit

### 3.4 User Interface and Base Station

A graphical user interface(GUI) was designed in Matlab<sup>®</sup> to remotely change telemetry unit settings such as sampling rate, transmission power, select sensor channel,  $V_{REF}$  of the amplifier and the zero level by changing  $V_{DAC}$  of the amplifier. The auto-zeroing routine can also be triggered from the GUI. The development board for CC430F5137 is used as the base station which is connected to the PC via FTDI serial-to-USB cable. The GUI connects to the base station via a COM port. The incoming data is plotted in this GUI along with options to start and stop readings and to save data into a file. The flow diagram of the code executed by the GUI is as shown in Fig. 48.

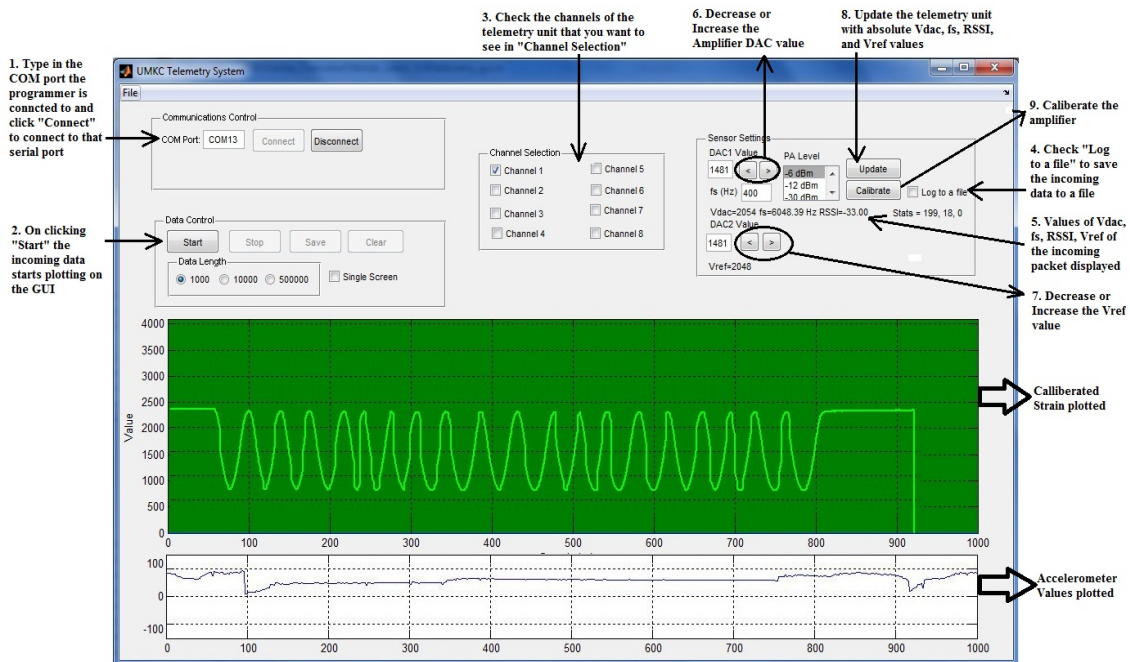


Figure 47: Matlab<sup>®</sup> GUI plotting strain values and accelerometer values

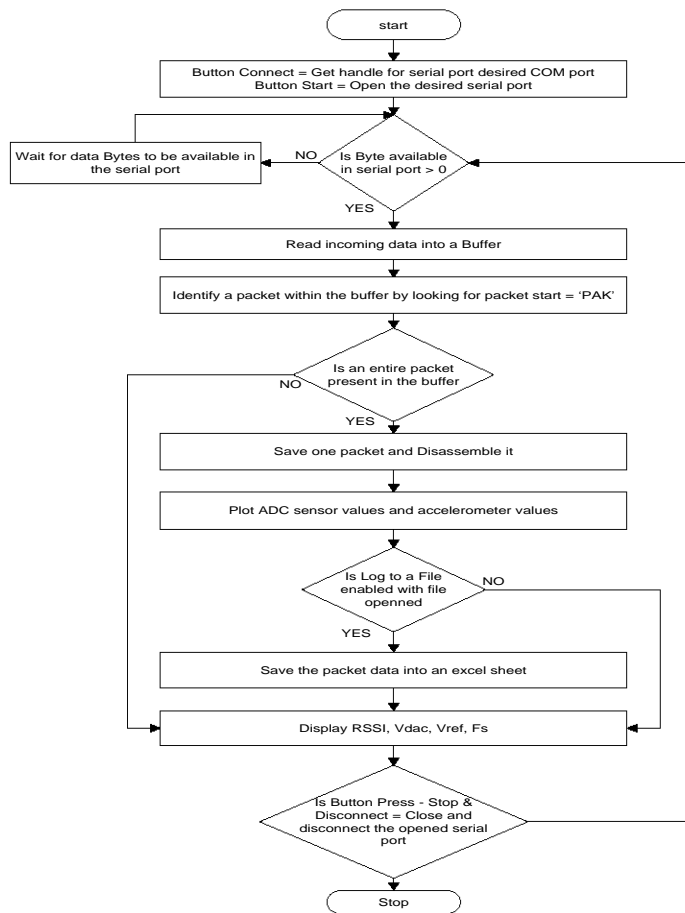


Figure 48: Flow Diagram of Code Executed by the GUI



## CHAPTER 4

### ZIGBEE WIRELESS NETWORK FOR HOME AUTOMATION

Home automation can be described as the introduction of technology within a home environment to improve the life quality of its occupants by providing services such as multimedia entertainment, tele-health and energy conservation. A rapid introduction of network enabled with digital technology in the home environment was seen in recent past. This increased the connectivity between devices within the home environment. Smart home using wireless communication also replaces the messy wired system which was difficult to setup. With rapid expansion of Internet, the potential for the monitoring and for remote controlling of such network enabled devices was possible.

#### **4.1 Existing Home Automation Technologies**

The oldest standard identified was the X10 industry standard developed in 1975 [30] which was about the communication between the electronic devices. Through the home power lines this could provide limited control over household devices.

A Java based home automation system [31] where an embedded board connected physically all the home automation devices and by integrating with a personal computer (PC) based web server could provide remote access to the system. Built-in network security featured a secure solution by incorporating the use of Java. However, the system requires an expensive and intrusive wiring installation as well as a high end PC.

A Bluetooth based home automation system [32] was introduced in which includes a primary controller and multiple Bluetooth sub-controllers. Each home device was connected physically to a Bluetooth sub-controller. By wireless communication all sub-controllers sends information to the primary controller. Hence each home device has a dedicated Bluetooth module. Since these Bluetooth modules are expensive, they are sometimes shared among several devices. This design reduces physical wiring and thus the intrusiveness of installation. The sharing of the Bluetooth module has the drawback of an access delay. Hence each dedicated wireless module has to be made more cheaper.

An alternative approach of a phone based remote controller for home automation is presented in [33]. All communications happen over a fixed telephone line rather than over the Internet. This system could be accessed by using any telephone which can supports dual tone multiple frequency(DTMF). The disadvantages of this system are that there was no graphical user interface for the user and hence users have to remember an access code and also they have to remember the sequence of buttons to press for the controlling connected devices.

## **4.2 Design Goals**

Upon doing a literature survey on the existing technologies the major drawbacks of the existing system were analyzed and are as follows:

- Wired Connections
- Complex and expensive architecture

- Intrusive installation
- Lack of network interoperability
- Control and monitoring interface inflexibility
- No Security
- Limited range of coverage

Currently, various wireless technologies are available such as Infrared (IR), Bluetooth, ZigBee, Radio Frequency (RF) and etc. 10 years ago for short-range communication the Bluetooth wireless technology was introduced. It was developed for usage in Personal Area Network (PAN) network to support low power communication between devices such as personal computers (PC), phones, Personal Digital Assistance (PDA) and etc. The Bluetooth wireless device can have ranges up to 10 meters and with 2.5 mW (4dBm) power consumption. Operating in Industrial Scientific-Medical (ISM) band at 2.4 GHz Bluetooth has the capability of frequency hopping and only star topology is supported. A Radio frequency (RF) module works on either 413 MHz or 315 MHz frequency. This module do not follow any protocol rather just broadcast the signal without any security. The wireless range can be upto 100 meters and a star topology is supported. RF only supports star topology and the wireless range can cover up to 100 meters.

The existing wireless smart home systems however, can only cover up to a certain area range which is limited by the wireless module range being used. A multi-hop communication capability for data transfer offered by ZigBee provides unlimited range of communication for the system since there are intermediate nodes which can pass the data

from one node to another till it reaches the destination. Developed based on Open System Interconnection (OSI) layer model Zigbee builds on IEEE standard 802.15.4. Zigbee supports all three types of typologies such as star topology, mesh topology and tree topology. Zigbee wireless device can operate with very-low power consumption that makes it the most attractive wireless device to use in Wireless Sensor Network (WSN). ZigBee is a low-rate and lowcost wireless standard as well.

A Home Automation system based on CC2530ZDK-ZNP-MINI kit was designed with the following design goals:

- Wireless connections between the central control unit and the end-devices
- Cheap architecture
- Simple installation
- Standardized ZigBee protocol adaptation
- Flexible Interface for controlling and monitoring
- Security achieved through encryption
- Extended coverage range by using routers

The hardware and software implementation of a Home Automation System designed around CC2530ZDK-ZNP-MINI kit from Texas Instruments are detailed in the chapter. Through experiment this ZigBee wireless network system was proved feasible and practical.

### 4.3 Hardware

Designed around CC2530ZDK-ZNP-MINI kit from Texas Instruments, the hardware unit as well includes a HB404PWA AC Power/Wattage Meter from Annex Depot Inc. A simplified block diagram of the telemetry unit for home automation is shown in Fig. 49.

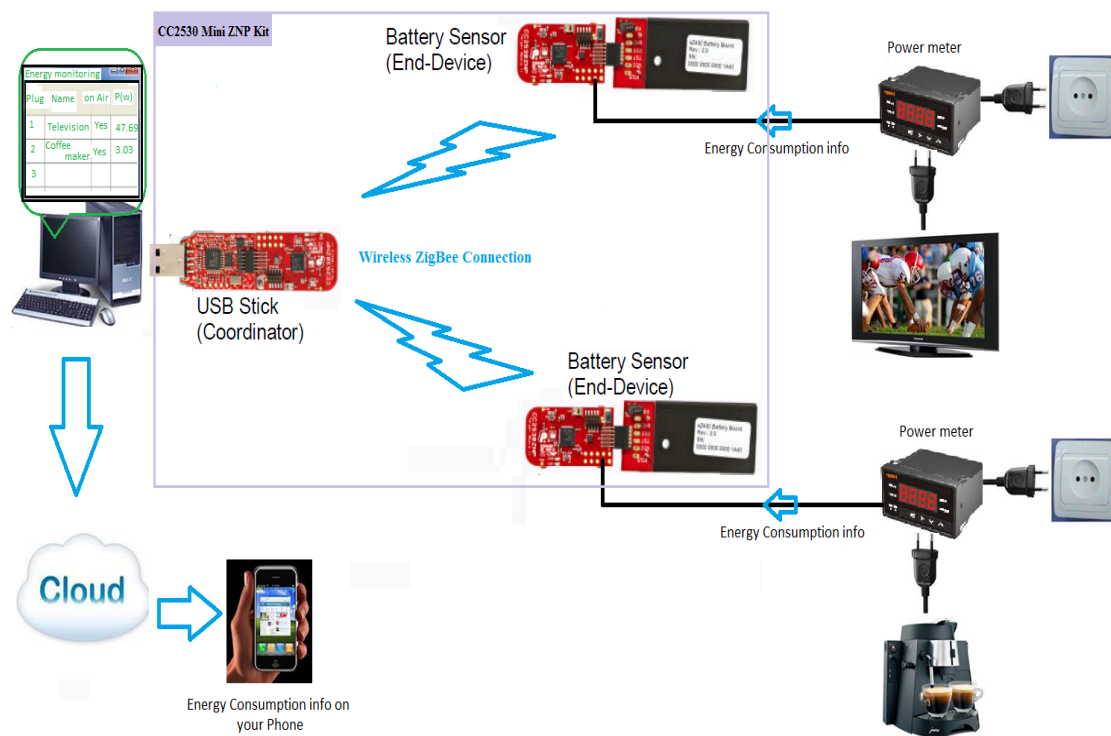


Figure 49: Data Flow Diagram

#### 4.3.1 End-Device Setup

The hardware and software setup details of CC2530ZDK-ZNP-MINI kit is explained in Chapter 2. The hardware of CC2530ZDK-ZNP-MINI kit includes an MSP430F2274

micro-controller that controls the ZigBee device and a CC2530 ZigBee device preprogrammed with ZigBee software. It can be seen from the Fig. 49 that there is a dedicated battery sensor or end-device connected to each home appliance. The home appliance is not connected directly to the end-device rather is connected to a HB404PWA AC Power/Wattage Meter. HB404PWA AC Power/Wattage Meter displays the power consumption of the connected device as well as gives an analog output of the measure of power consumption. Hence the battery sensor acquires the analog measure of power consumption in any device connected to HB404PWA AC Power/Wattage Meter through this analog output port of HB404PWA AC Power/Wattage Meter. The port P2.3(A6) of MSP430F2274 micro-controller is programmed as analog input to which the analog output of the HB404PWA AC Power/Wattage Meter is connected. The port P2.3 is an analog input(A6), which means the analog input at this port is routed to an in-built 12 bit ADC which converts the analog input into digital form.

The MSP430F2274 microcontroller has an inbuilt temperature sensor. The microcontroller was programmed to measure temperature in Fahrenheit. The CC2530ZDK-ZNP-MINI kit is designed such that the MSP430F2274 micro-controller is interfaced with an external light sensor and accelerometer as shown in Fig. 24. The battery powered sensors or end-devices periodically report their key data such as temperature, light, energy consumption, and movement sensor data(accelerometer) to the coordinator in the packet format as shown in Fig. 59. These devices can also be programmed as routers that are typically used to extend the ZigBee network by routing messages from other end-devices. The hardware for coordinator, router and end-device are identical. Each target board can

be programmed as coordinator, router or end-device.

### 4.3.2 Coordinator Setup

The target board connected to the USB stick programmer is programmed with a coordinator application. This USB stick serves both as a debugger or programmer and as virtual serial port interface. This means that the USB stick should be connected to the coordinator target board during normal operation. The coordinator sets up the ZigBee network and configures the ZigBee network parameters which is the central control unit of the network. A ZigBee system can only have one coordinator.

Using a virtual USB serial port the ZigBee coordinator on the USB stick connects to the PC. Through a Hyperterminal program or through Matlab, the serial port interface can be accessed. The Windows default terminal interface can be found on the Windows Start menu/Accessories/Communication/Hyperterminal and the setup is explained in section Hardware of Chapter - 2. On activation of the end-device, it is programmed to send information to the coordinato periodically. This message includes network information as well as sensor data as in the packet format shown in Fig. 59. A RX-message from the end-device will appear in the coordinator terminal.

### 4.3.3 HB404PWA AC Power/Wattage Meter from Annex Depot Inc

To measure energy consumption of any home appliance we used a HB404PWA AC Power/Wattage Meter from Annex Depot Inc shown in Fig. 30. The meter has an AC voltage input range of 0 to 400V with a 0 to 20 mA analog data output. To create a power socket plug-in and a plug-out the wire ups on the back plate of the meter was done as

shown in Fig. 50. However, without an external current transformer, the power meter only supports 5A max Fig. 32. To measure over 5A, an external current transformer is required. Since most home appliances consumer more than 5A an external current transformer was used. The wire up with a current transformer is shown in Fig. 51. The 9th and 10th pin in the back plate gives the ground and analog measurement of the energy consumed by any device via the HB404PWA power meter. This analog output is connected to port P2.3(A6) which is programmed as analog input to the MSP430F2274 microcontroller.

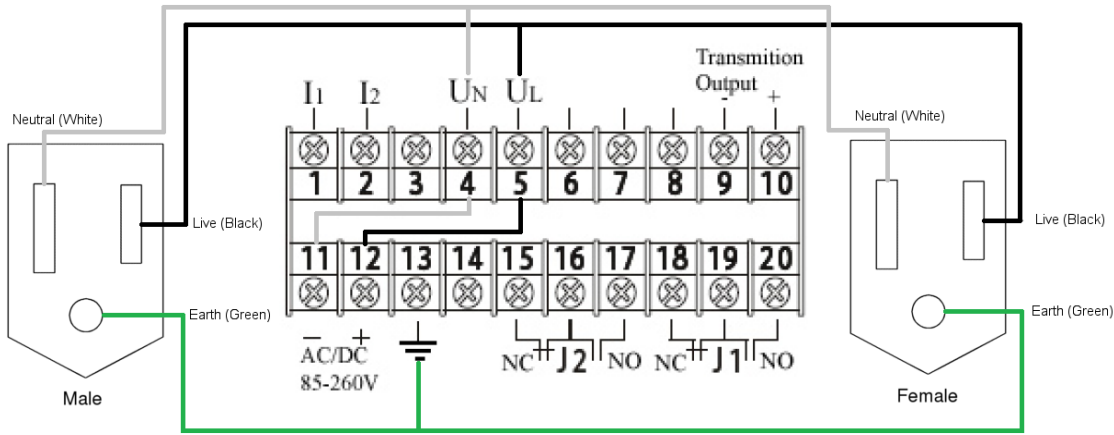


Figure 50: Wire-Up in the Back Plate of HB404PWA AC Power/Wattage Meter from Annex Depot Inc.



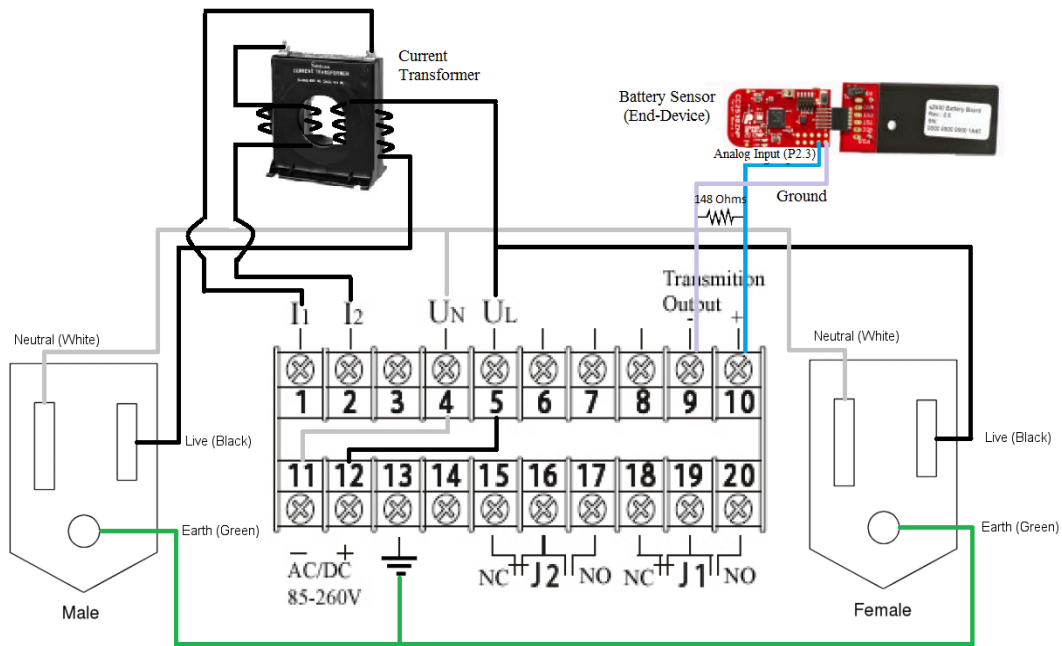


Figure 51: Wire-Up in the Back Plate of HB404PWA AC Power/Wattage Meter with Current Transformer

To control the appliance connected via a relay circuit is as shown in Fig. 52. This circuit was wired up on breadboard as shown in Fig. 53. The port P4.4 is programmed as an output port to turn on or off the MOSFET transistor. On receiving the command to turn on or off the connected appliance from the central control unit (coordinator), the end-device controls the digital output port P4.4 to go to logic '1' or '0'. The whole hardware setup is as shown in Fig. 53.

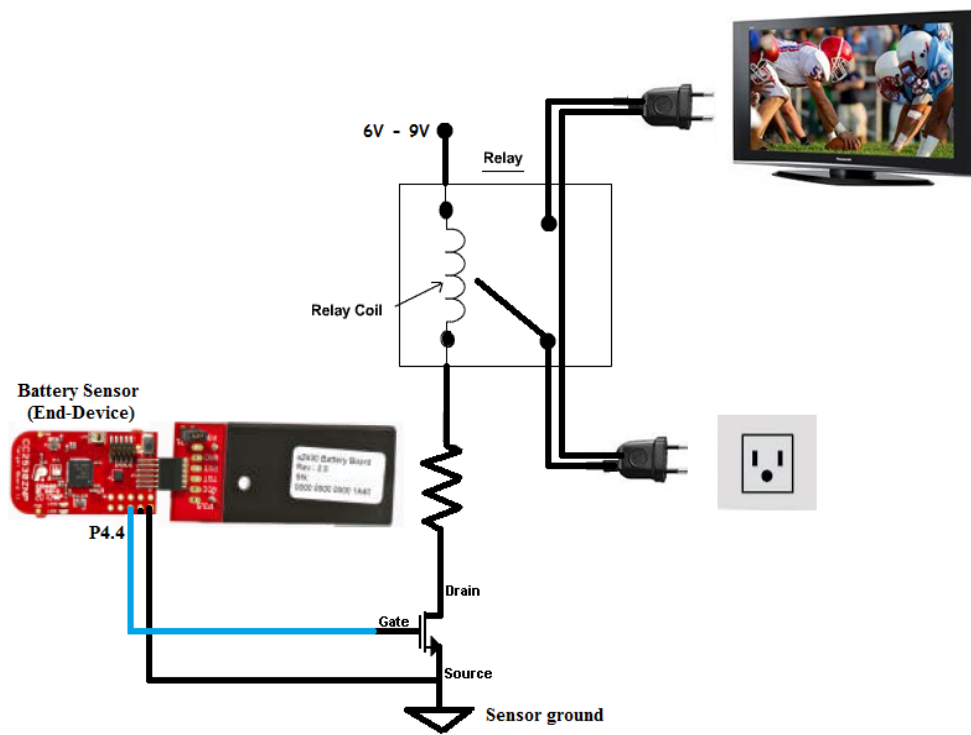


Figure 52: The Relay Circuit for Controlling ON or OFF Status of an Appliance

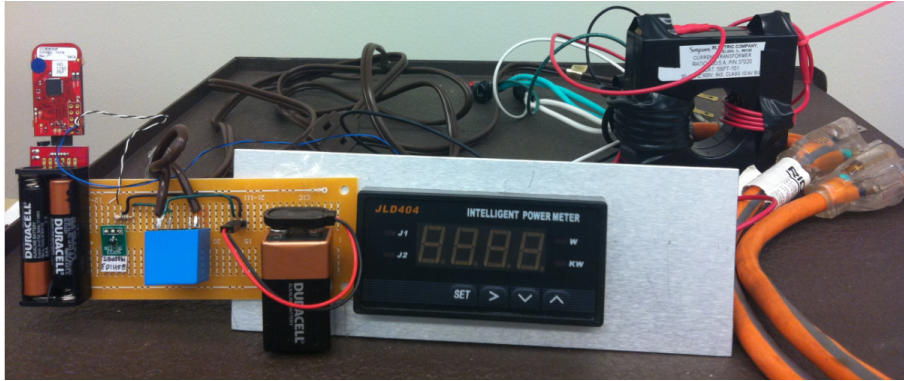


Figure 53: The Whole Wiring Set-Up of the End-Device

## 4.4 Software

### 4.4.1 Coordinator

Along with the CC2530ZDK-ZNP-MINI kit Texas Instruments provides ZNP library methods. The execution flow of the programs for the coordinator and end-device are discussed here. The Coordinator displays messages that arrive from the end-device. This time, the coordinator checks if an info message is received, and if so it displays the parsed message. To send a message from coordinator to the end-device we should know the short address (or long address) of the device which you wish to send the message to. This is out of the scope of the Zigbee protocol and is typically set during network commissioning or using binding. Here a broadcast message was send with a data payload of the device type. All end-devices receives this broadcast message and acts only if it belongs to themselves. To receive messages the application waits for SRDY to be asserted. Once this happens, it polls for pending message and then if there is a pending message it displays the header information and payload. Once this information is displayed the

controller is again waiting for the next message.

We have used the generic ZNP startup sequence for coordinator programming as follows:

1. Initialize the hardware
2. Reset the ZNP
3. Set Startup Options (STARTOPT\_CLEAR\_CONFIG + STARTOPT\_CLEAR\_STATE)  
- upon reset this will restore the ZNP to a blank configuration
4. Set the Zigbee Device Type as COORDINATOR, ROUTER, or END\_DEVICE
5. Turn on callbacks
6. Register the application
7. Start the application
8. LED indication that the device has started successfully.

A detailed flow chart of the coordinator program is shown in Fig. 55 and Fig. 55.

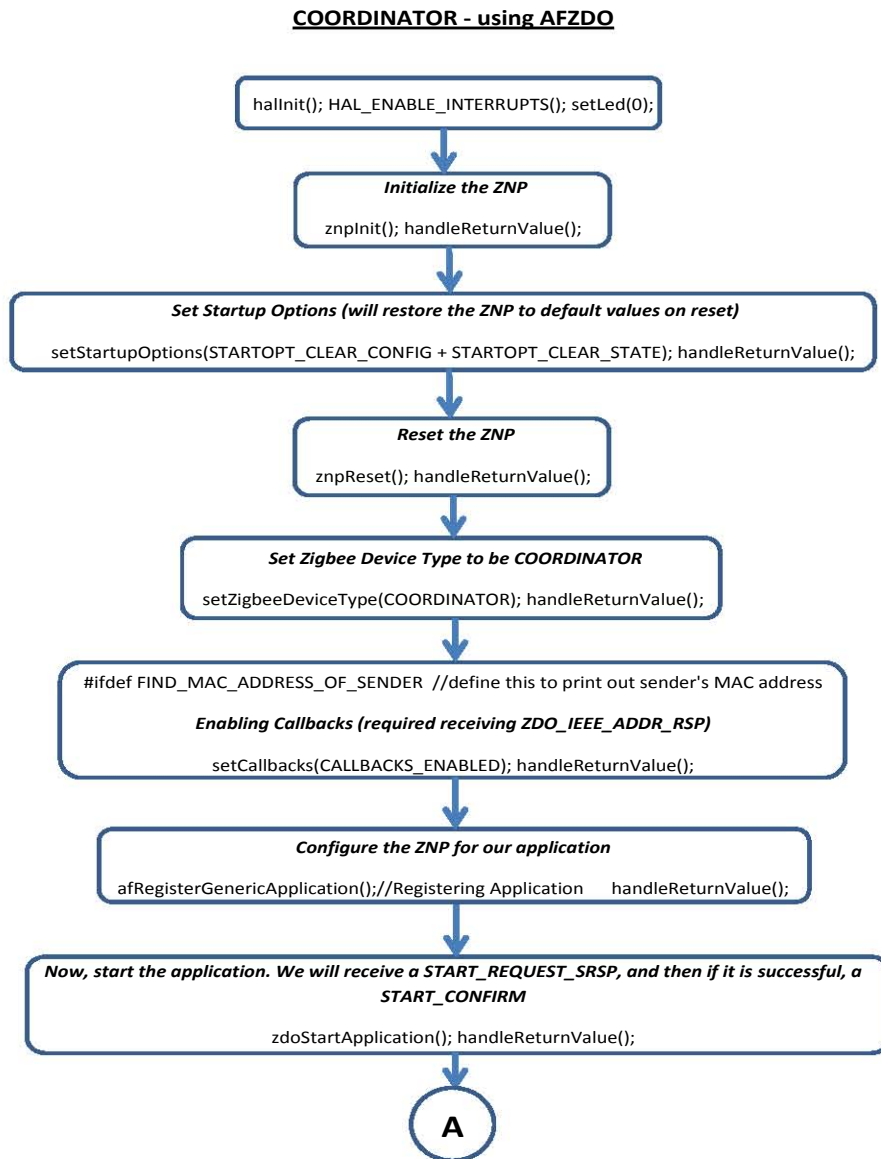


Figure 54: Flow Chart of Coordinator Node

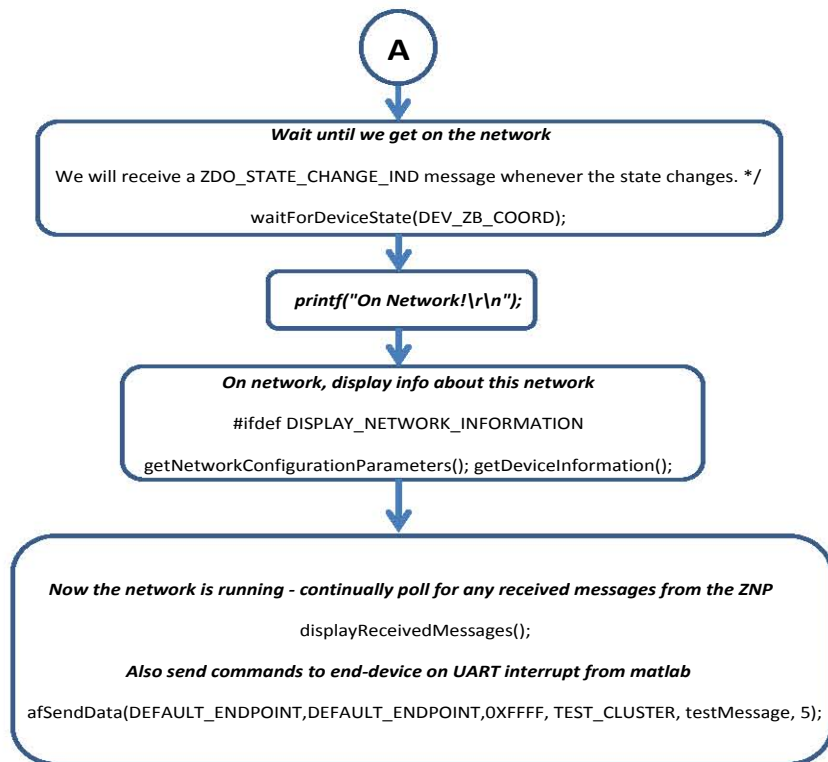


Figure 55: Flow Chart of Coordinator Node (continued..)

#### 4.4.2 End-Device

The ZigBee end-device periodically send sensor data on start up with a sleep in between transmissions. The accelerometer is configured such that the ZigBee end-device can send message upon motion interrupt. The SPI port has to be initialized every time we wish to use it since it is shared between the Accelerometer and the ZNP. The Analog-to-Digital(ADC) converters has to be also enabled and disabled every time we use it for temperature sensing or for energy consumption monitoring. A detailed flow chart of the end-device program is shown in Fig. 56, Fig. 57 and Fig. 58.

**END DEVICE - using AFZDO**

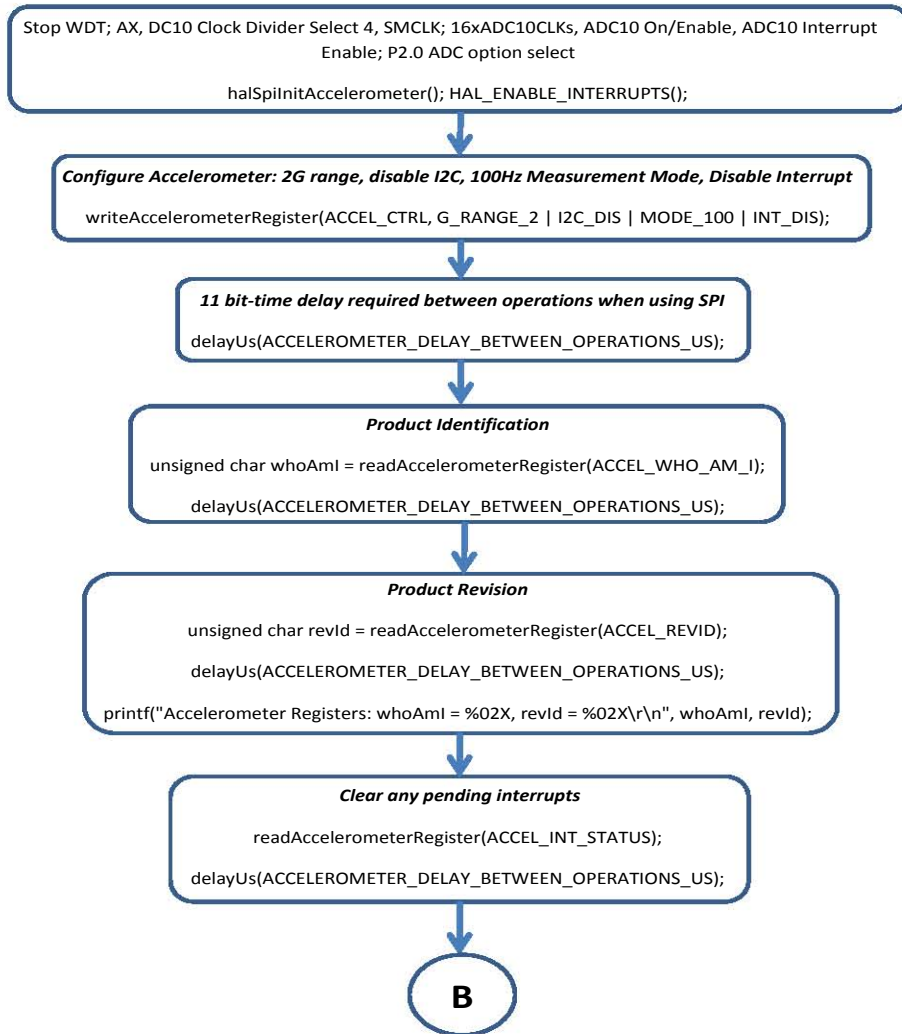


Figure 56: Flow Chart of End Device Node



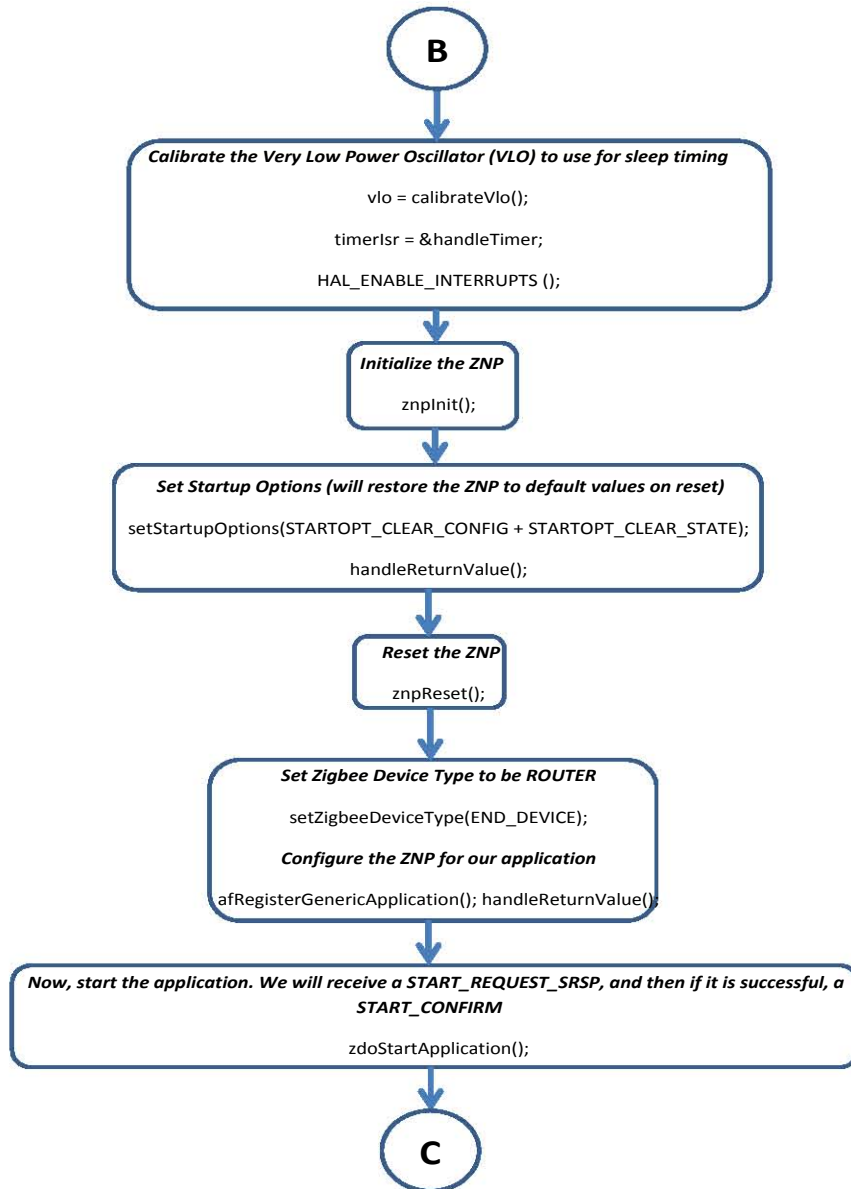


Figure 57: Flow Chart of End Device Node (continued..)

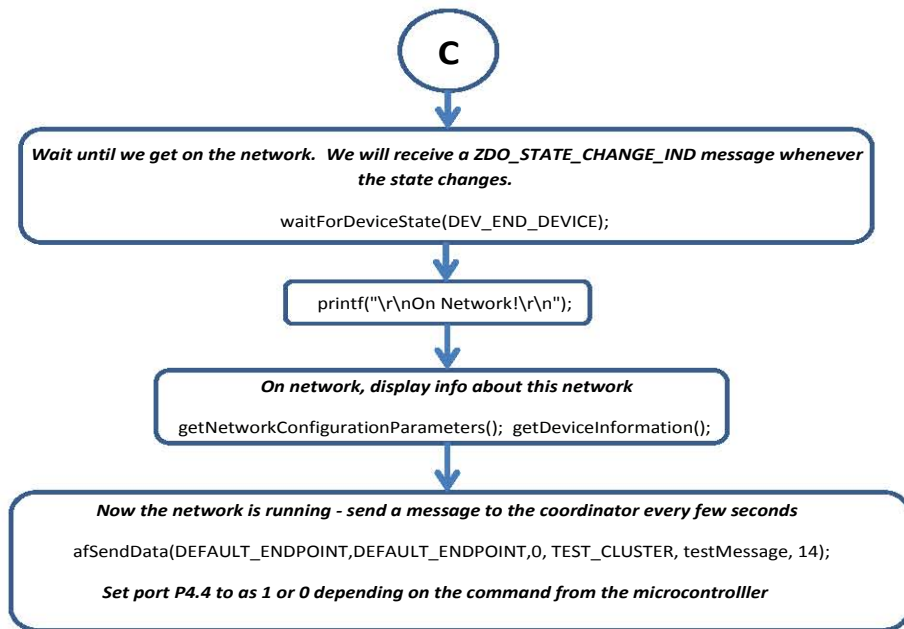


Figure 58: Flow Chart of End Device Node (continued..)

The format of the packets send from end-device to coordinator is as shown in Fig. 59. Each packet has a message header, which includes sender’s MAC Address, device-type information, protocol version, flags and sequence numbers. All operations however to implement this ZigBee home automation system was done only by manipulating the payload of the packet.

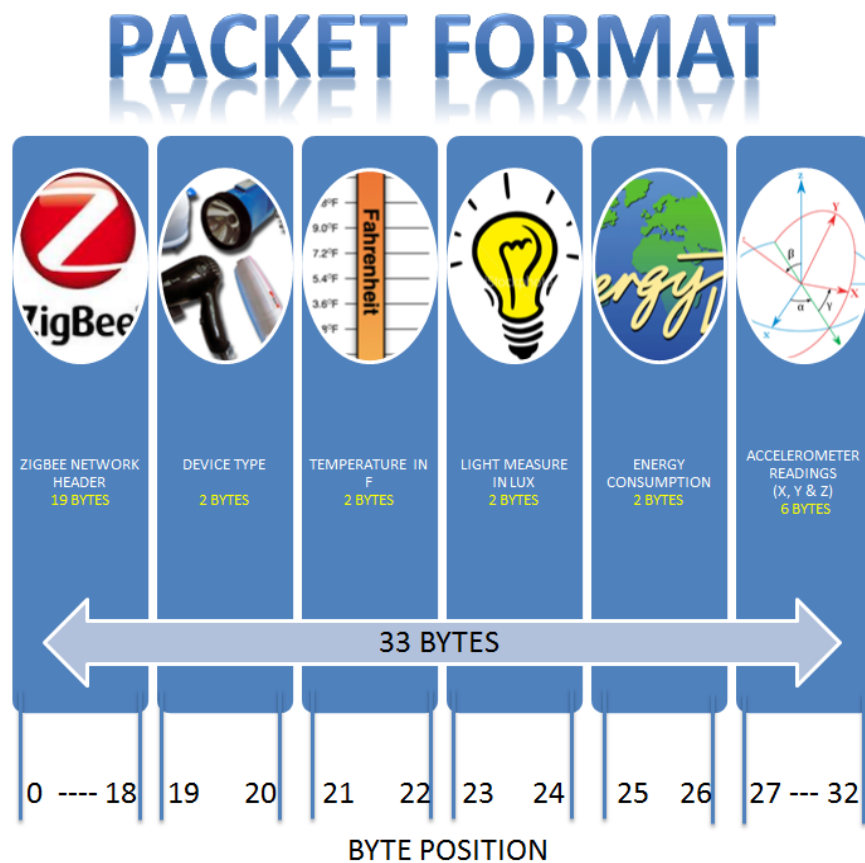
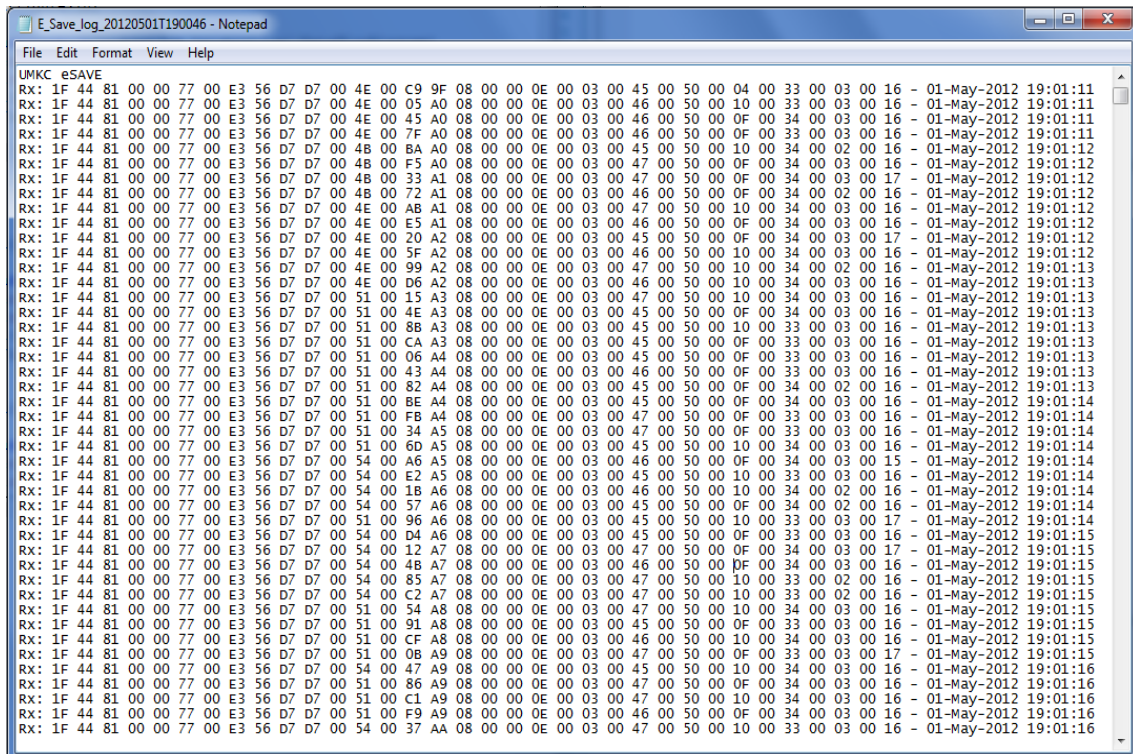


Figure 59: Packet Format

## 4.5 User Interface

The graphical user interface(GUI) was designed in Matlab<sup>®</sup> to read the serial data from the end-device. On connecting to the COM port that target board is plugged in, and by starting the GUI data starts flowing in. The packet data field of energy consumption was plotted in matlab. All the incoming data can also be saved into a text file as shown in Fig. 68 in the format E\_Save\_log\_yyyymmddTHHMMSS.txt(eg: E\_Save\_log\_20120306T130234.txt). Every hour a new file is created for the convenience of the software implemented to push these data into the database. A new line is appended into the file whenever a packet is received by the coordinator.



```
File Edit Format View Help
UMKC eSAVE
Rx: 1F 44 81 00 00 77 00 E3 56 D7 D7 00 4E 00 C9 9F 08 00 00 0E 00 03 00 45 00 50 00 04 00 33 00 03 00 16 - 01-May-2012 19:01:11
Rx: 1F 44 81 00 00 77 00 E3 56 D7 D7 00 4E 00 05 A0 08 00 00 0E 00 03 00 46 00 50 00 10 00 33 00 03 00 16 - 01-May-2012 19:01:11
Rx: 1F 44 81 00 00 77 00 E3 56 D7 D7 00 4E 00 45 A0 08 00 00 0E 00 03 00 46 00 50 00 0F 00 34 00 03 00 16 - 01-May-2012 19:01:11
Rx: 1F 44 81 00 00 77 00 E3 56 D7 D7 00 4E 00 7F A0 08 00 00 0E 00 03 00 46 00 50 00 0F 00 33 00 03 00 16 - 01-May-2012 19:01:11
Rx: 1F 44 81 00 00 77 00 E3 56 D7 D7 00 4B 00 BA A0 08 00 00 0E 00 03 00 45 00 50 00 10 00 34 00 02 00 16 - 01-May-2012 19:01:12
Rx: 1F 44 81 00 00 77 00 E3 56 D7 D7 00 4B 00 F5 A0 08 00 00 0E 00 03 00 47 00 50 00 0F 00 34 00 03 00 16 - 01-May-2012 19:01:12
Rx: 1F 44 81 00 00 77 00 E3 56 D7 D7 00 4B 00 33 A1 08 00 00 0E 00 03 00 47 00 50 00 0F 00 34 00 03 00 17 - 01-May-2012 19:01:12
Rx: 1F 44 81 00 00 77 00 E3 56 D7 D7 00 4B 00 72 A1 08 00 00 0E 00 03 00 46 00 50 00 0F 00 34 00 02 00 16 - 01-May-2012 19:01:12
Rx: 1F 44 81 00 00 77 00 E3 56 D7 D7 00 4E 00 AB A1 08 00 00 0E 00 03 00 47 00 50 00 10 00 34 00 03 00 16 - 01-May-2012 19:01:12
Rx: 1F 44 81 00 00 77 00 E3 56 D7 D7 00 4E 00 E5 A1 08 00 00 0E 00 03 00 46 00 50 00 0F 00 34 00 03 00 16 - 01-May-2012 19:01:12
Rx: 1F 44 81 00 00 77 00 E3 56 D7 D7 00 4E 00 20 A2 08 00 00 0E 00 03 00 45 00 50 00 0F 00 34 00 03 00 17 - 01-May-2012 19:01:12
Rx: 1F 44 81 00 00 77 00 E3 56 D7 D7 00 4E 00 5F A2 08 00 00 0E 00 03 00 46 00 50 00 10 00 34 00 03 00 16 - 01-May-2012 19:01:12
Rx: 1F 44 81 00 00 77 00 E3 56 D7 D7 00 4E 00 99 A2 08 00 00 0E 00 03 00 47 00 50 00 10 00 34 00 02 00 16 - 01-May-2012 19:01:13
Rx: 1F 44 81 00 00 77 00 E3 56 D7 D7 00 4E 00 D6 A2 08 00 00 0E 00 03 00 46 00 50 00 10 00 34 00 03 00 16 - 01-May-2012 19:01:13
Rx: 1F 44 81 00 00 77 00 E3 56 D7 D7 00 51 00 15 A3 08 00 00 0E 00 03 00 47 00 50 00 10 00 34 00 03 00 16 - 01-May-2012 19:01:13
Rx: 1F 44 81 00 00 77 00 E3 56 D7 D7 00 51 00 4E A3 08 00 00 0E 00 03 00 45 00 50 00 0F 00 34 00 03 00 16 - 01-May-2012 19:01:13
Rx: 1F 44 81 00 00 77 00 E3 56 D7 D7 00 51 00 8B A3 08 00 00 0E 00 03 00 45 00 50 00 10 00 33 00 03 00 16 - 01-May-2012 19:01:13
Rx: 1F 44 81 00 00 77 00 E3 56 D7 D7 00 51 00 CA A3 08 00 00 0E 00 03 00 45 00 50 00 0F 00 33 00 03 00 16 - 01-May-2012 19:01:13
Rx: 1F 44 81 00 00 77 00 E3 56 D7 D7 00 51 00 06 A4 08 00 00 0E 00 03 00 45 00 50 00 0F 00 33 00 03 00 16 - 01-May-2012 19:01:13
Rx: 1F 44 81 00 00 77 00 E3 56 D7 D7 00 51 00 43 A4 08 00 00 0E 00 03 00 46 00 50 00 0F 00 33 00 03 00 16 - 01-May-2012 19:01:13
Rx: 1F 44 81 00 00 77 00 E3 56 D7 D7 00 51 00 82 A4 08 00 00 0E 00 03 00 45 00 50 00 0F 00 34 00 02 00 16 - 01-May-2012 19:01:13
Rx: 1F 44 81 00 00 77 00 E3 56 D7 D7 00 51 00 BE A4 08 00 00 0E 00 03 00 45 00 50 00 0F 00 34 00 03 00 16 - 01-May-2012 19:01:14
Rx: 1F 44 81 00 00 77 00 E3 56 D7 D7 00 51 00 FB A4 08 00 00 0E 00 03 00 47 00 50 00 0F 00 33 00 03 00 16 - 01-May-2012 19:01:14
Rx: 1F 44 81 00 00 77 00 E3 56 D7 D7 00 51 00 34 A5 08 00 00 0E 00 03 00 47 00 50 00 0F 00 33 00 03 00 16 - 01-May-2012 19:01:14
Rx: 1F 44 81 00 00 77 00 E3 56 D7 D7 00 51 00 6D A5 08 00 00 0E 00 03 00 45 00 50 00 10 00 34 00 03 00 16 - 01-May-2012 19:01:14
Rx: 1F 44 81 00 00 77 00 E3 56 D7 D7 00 54 00 A6 A5 08 00 00 0E 00 03 00 46 00 50 00 0F 00 34 00 03 00 15 - 01-May-2012 19:01:14
Rx: 1F 44 81 00 00 77 00 E3 56 D7 D7 00 54 00 E2 A5 08 00 00 0E 00 03 00 45 00 50 00 10 00 33 00 03 00 16 - 01-May-2012 19:01:14
Rx: 1F 44 81 00 00 77 00 E3 56 D7 D7 00 54 00 1B A6 08 00 00 0E 00 03 00 46 00 50 00 10 00 34 00 02 00 16 - 01-May-2012 19:01:14
Rx: 1F 44 81 00 00 77 00 E3 56 D7 D7 00 54 00 57 A6 08 00 00 0E 00 03 00 45 00 50 00 0F 00 34 00 02 00 16 - 01-May-2012 19:01:14
Rx: 1F 44 81 00 00 77 00 E3 56 D7 D7 00 54 00 96 A6 08 00 00 0E 00 03 00 45 00 50 00 10 00 33 00 03 00 17 - 01-May-2012 19:01:14
Rx: 1F 44 81 00 00 77 00 E3 56 D7 D7 00 54 00 D4 A6 08 00 00 0E 00 03 00 45 00 50 00 0F 00 33 00 03 00 16 - 01-May-2012 19:01:15
Rx: 1F 44 81 00 00 77 00 E3 56 D7 D7 00 54 00 12 A7 08 00 00 0E 00 03 00 47 00 50 00 0F 00 34 00 03 00 17 - 01-May-2012 19:01:15
Rx: 1F 44 81 00 00 77 00 E3 56 D7 D7 00 54 00 4B A7 08 00 00 0E 00 03 00 46 00 50 00 0F 00 34 00 03 00 16 - 01-May-2012 19:01:15
Rx: 1F 44 81 00 00 77 00 E3 56 D7 D7 00 54 00 85 A7 08 00 00 0E 00 03 00 47 00 50 00 10 00 33 00 02 00 16 - 01-May-2012 19:01:15
Rx: 1F 44 81 00 00 77 00 E3 56 D7 D7 00 54 00 C2 A7 08 00 00 0E 00 03 00 47 00 50 00 10 00 33 00 02 00 16 - 01-May-2012 19:01:15
Rx: 1F 44 81 00 00 77 00 E3 56 D7 D7 00 51 00 54 A8 08 00 00 0E 00 03 00 47 00 50 00 10 00 34 00 03 00 16 - 01-May-2012 19:01:15
Rx: 1F 44 81 00 00 77 00 E3 56 D7 D7 00 51 00 91 A8 08 00 00 0E 00 03 00 45 00 50 00 0F 00 33 00 03 00 16 - 01-May-2012 19:01:15
Rx: 1F 44 81 00 00 77 00 E3 56 D7 D7 00 51 00 CF A8 08 00 00 0E 00 03 00 46 00 50 00 10 00 34 00 03 00 16 - 01-May-2012 19:01:15
Rx: 1F 44 81 00 00 77 00 E3 56 D7 D7 00 51 00 0B A9 08 00 00 0E 00 03 00 47 00 50 00 0F 00 33 00 03 00 17 - 01-May-2012 19:01:15
Rx: 1F 44 81 00 00 77 00 E3 56 D7 D7 00 54 00 47 A9 08 00 00 0E 00 03 00 45 00 50 00 10 00 34 00 03 00 16 - 01-May-2012 19:01:16
Rx: 1F 44 81 00 00 77 00 E3 56 D7 D7 00 51 00 86 A9 08 00 00 0E 00 03 00 47 00 50 00 0F 00 34 00 03 00 16 - 01-May-2012 19:01:16
Rx: 1F 44 81 00 00 77 00 E3 56 D7 D7 00 51 00 C1 A9 08 00 00 0E 00 03 00 47 00 50 00 10 00 34 00 03 00 16 - 01-May-2012 19:01:16
Rx: 1F 44 81 00 00 77 00 E3 56 D7 D7 00 51 00 F9 A9 08 00 00 0E 00 03 00 46 00 50 00 0F 00 34 00 03 00 16 - 01-May-2012 19:01:16
Rx: 1F 44 81 00 00 77 00 E3 56 D7 D7 00 54 00 37 AA 08 00 00 0E 00 03 00 47 00 50 00 10 00 33 00 03 00 16 - 01-May-2012 19:01:16
```

Figure 60: Data Collected

## 4.6 Bidirectional Communication

To communicate from coordinator to end device communication for control the end-devices the intended action was written into the text file 'E\_Save\_log\_EndDevice \_Commands.txt'. The format of this command is CMD(DeviceID)(ON/OFF action) (Delay x seconds). For example CMD0006ON DELAY8. The matlab keeps polling this file for any new line command. Fig. 61 shows these interfaces.

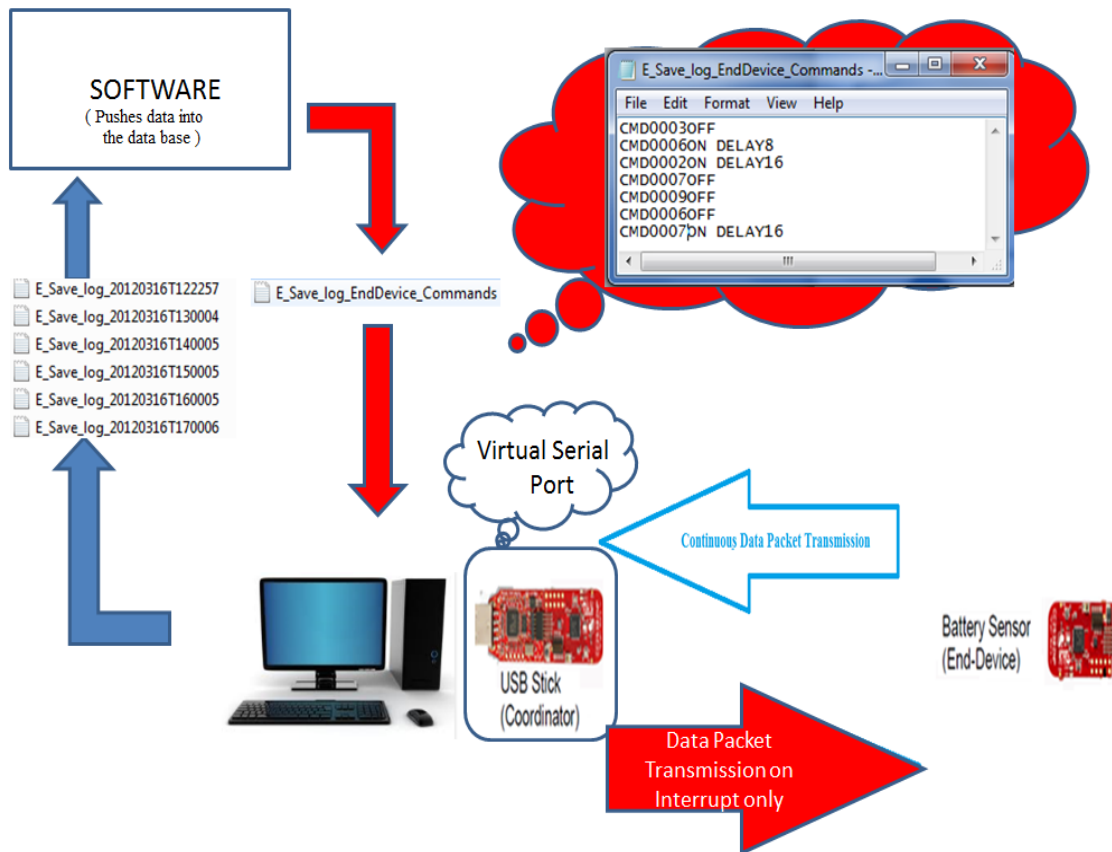


Figure 61: Bidirectional Communication Data Flow Diagram

## CHAPTER 5

### DATA COLLECTION AND RESULTS

#### 5.1 915 MHz Telemetry Unit of Dimension 24 mm x 13 mm

In this section we present a plot showing the acquired micro strain data by both the acquisition unit and our telemetry unit. We discuss the current consumption and the battery charging mechanism of the telemetry unit.

##### 5.1.1 Acquired Micro-Strain Data

The telemetry unit was tested on *ex-vivo* settings. For *ex-vivo* testing a surgically removed bone of a mouse was glued with a  $120\Omega$  strain gauge (Vishay, EA-06-015DJ-120) and placed on Bose ElectroForce 3200 Fig. 62. The adhesive used was M-bond 2000 from Vishay-Micro-Measurements.

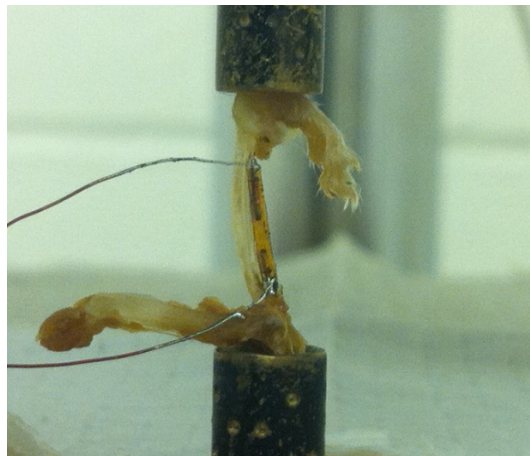


Figure 62: Strain gage glued to the dissected ulna of a mouse

The readings were first taken from the existing bench top set up. The strain gauge connected to the data acquisition system was loaded with a sinusoidal force with varying magnitude and frequencies. The strain data plotted on StrainSmart<sup>®</sup> was recorded into a text file. The strain gauge was then disconnected from the data acquisition system and connected to the telemetry unit. The same sinusoidal force was reapplied to the bone of the mouse. The strain data transmitted by the telemetry unit received at the base station was digitally filtered. Figure 63 shows readings from both the units on one plot. Four cycles of one reading with peak-to-peak force 0.5 Hz and 2 N peak-to-peak is shown. For both units, the recorded strain ranged from -1500 to 0  $\mu\epsilon$  making the telemetry unit a successful replacement of the bulky bench top setup.

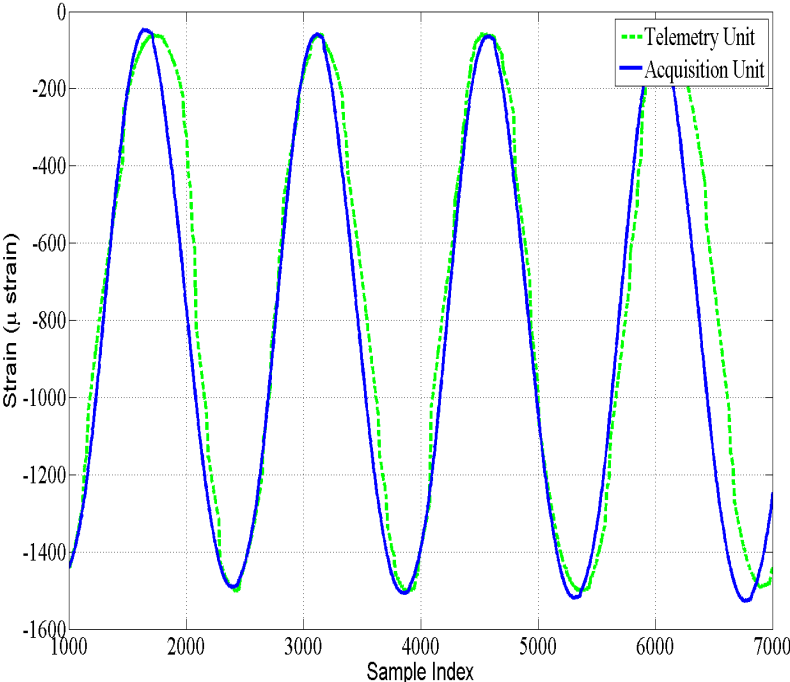


Figure 63: Telemetry unit readings vs StrainSmart<sup>®</sup> readings.

Table 2: Features of the 915 MHz Telemetry Unit of Dimension 24 mm x 13 mm.

Dimensions	24 mm x 13 mm
Frequency band	915 MHz
Current consumption while trans-receiving at 7.5 Hz sampling	1.75 mA
Current consumption on sleep	0.5 mA

### 5.1.2 Current Consumption

The on-chip timer of the micro-controller triggers the analog-to-digital conversion of the strain data. Varying the period of the timer sets the sampling frequency of the strain data. We varied the sampling frequency from 7.5 Hz to 160 Hz. Figure 64 shows that at 7.5 Hz, current consumed by the telemetry unit is only 1.75 mA which increases to 4 mA for sampling frequency of 160 Hz. The figure also shows that during sleep the unit consumes only 0.4 mA of current. During sleep the micro-controller puts the radio core into power down mode, turns off the MOSFET switch, and disables the LDO output powering the amplifier, the two DACs, the two MUXs and the accelerometer. Since the current consumption during sleep is low compared to the current consumption during trans-reception, the telemetry unit was made to sleep in between transmissions. By adopting this strategy we were able to reduce the the current consumption while trans-reception to 1.75 mA.



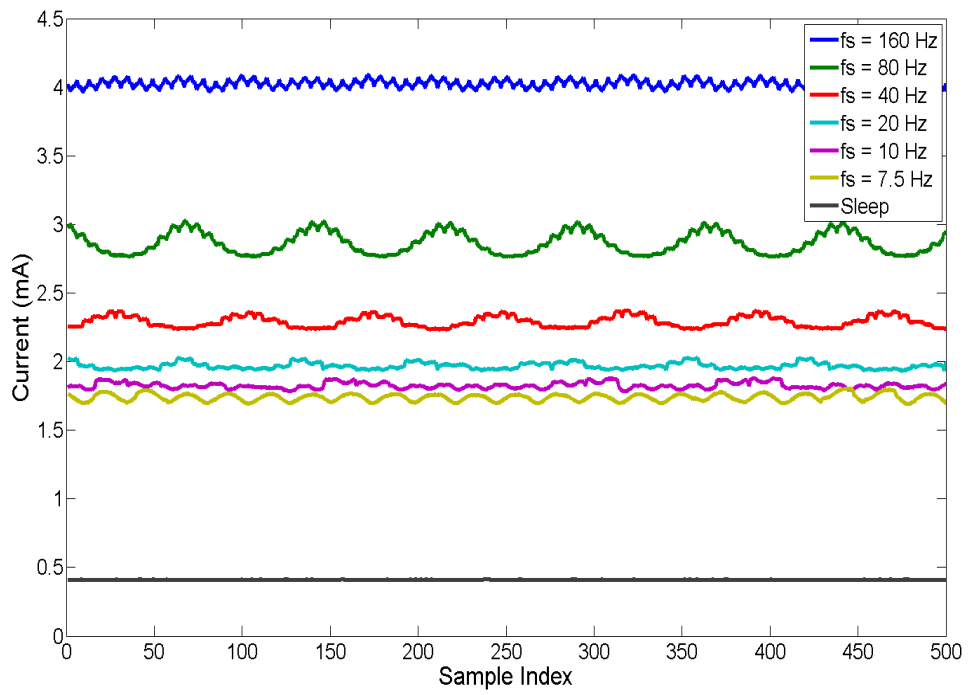


Figure 64: Telemetry unit current consumption.

### 5.1.3 Battery Charging Mechanism

The telemetry unit is equipped with a battery charger for a single Li-Ion battery. A full wave rectifier is also included for wireless charging. A coil designed to couple with external RF reader connects to the rectifier and the rectified signal turns on the charger. Voltage of the battery is monitored by the micro-controller through one of the ADC channels. A LED is used to indicate that the voltage of the battery is fallen below 2.9 V and charging is required. A 45 mAh Li-Ion battery was used power up the unit. From section ?? we see that for sampling frequency of 160 Hz, the telemetry unit consumes 4 mA of current. For continuous data collection at 160 Hz sampling frequency it was seen that the battery needed charging after 11 hours. When put to charge, this same battery was fully-charged after 4 hours. Figure 65 shows the charging of the battery over time.

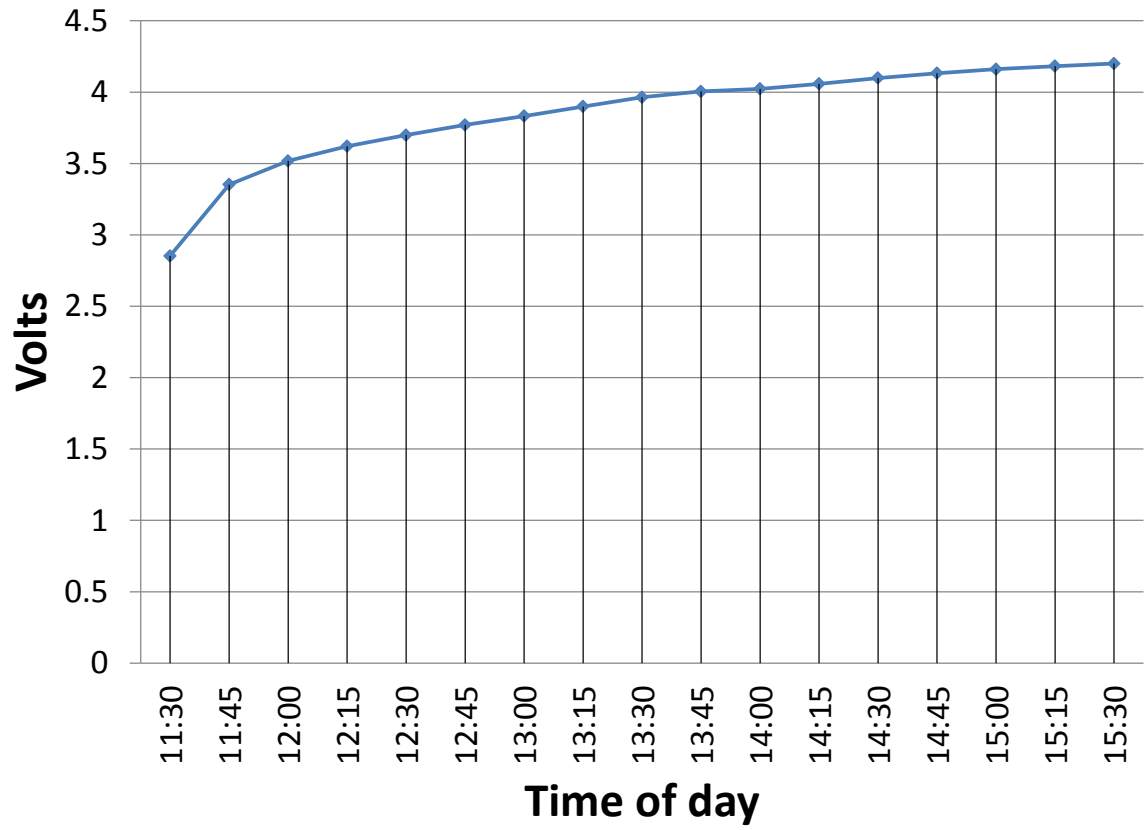


Figure 65: Time taken by battery to charge.

Table 3: Cost of a 915 MHz Telemetry Unit

COMPONENT	COST
CC430F5137	\$6.75
Crystal	\$1.89
DAC7311	\$2.47
INA333	\$5.17
HSMS-282P	\$0.01
Johanson Antenna	\$22
Johanson Balun	\$27
LTC4054-4.2	\$3.6
MMA8453QT	\$1.49
PMV16UN	\$0.23
TLV711285285	\$0.66
ADG804	\$1.26
<b>TOTAL OFF-THE-SHELF COMPONENT COST</b>	<b>\$73.53</b>

#### 5.1.4 Cost of a 915 MHz Telemetry Unit

The individual cost of each off-self-component used in the 915 MHz telemetry unit is tabulated in Table. 3. However the total cost of the board turns out to be \$278.53.

TOTAL COST PER BOARD = \$73.53 +

\$5(Cost of passive components) +

\$200(Fabrication cost)

## **5.2 RFID based Telemetry Unit of Dimension 10 mm x 10 mm**

Resistance Temperature Detectors (RTDs) are sensors which are used to measure temperature by correlating temperature with the resistance of the RTD element. A thin film platinum resistance temperature detector(Pt-RTD) PPG102C1 from U.S. Sensor was connected to one of the four channels of the RFID based telemetry unit. A thin film Pt-RTD was chosen for their low cost while having a tolerance of 24 % and high accuracy. A varying temperature was applied on the RTD sensor connected to the telemetry unit powered by an RFID reader. The temperature sensor data was multiplexed, amplified and transmitted. An received temperature sensor data as read by an RFID reader is shown in Fig. 66. The telemetry unit also measures acceleration in 3 axes. An received acceleration sensor data as read by an RFID reader is shown in Fig. 67.

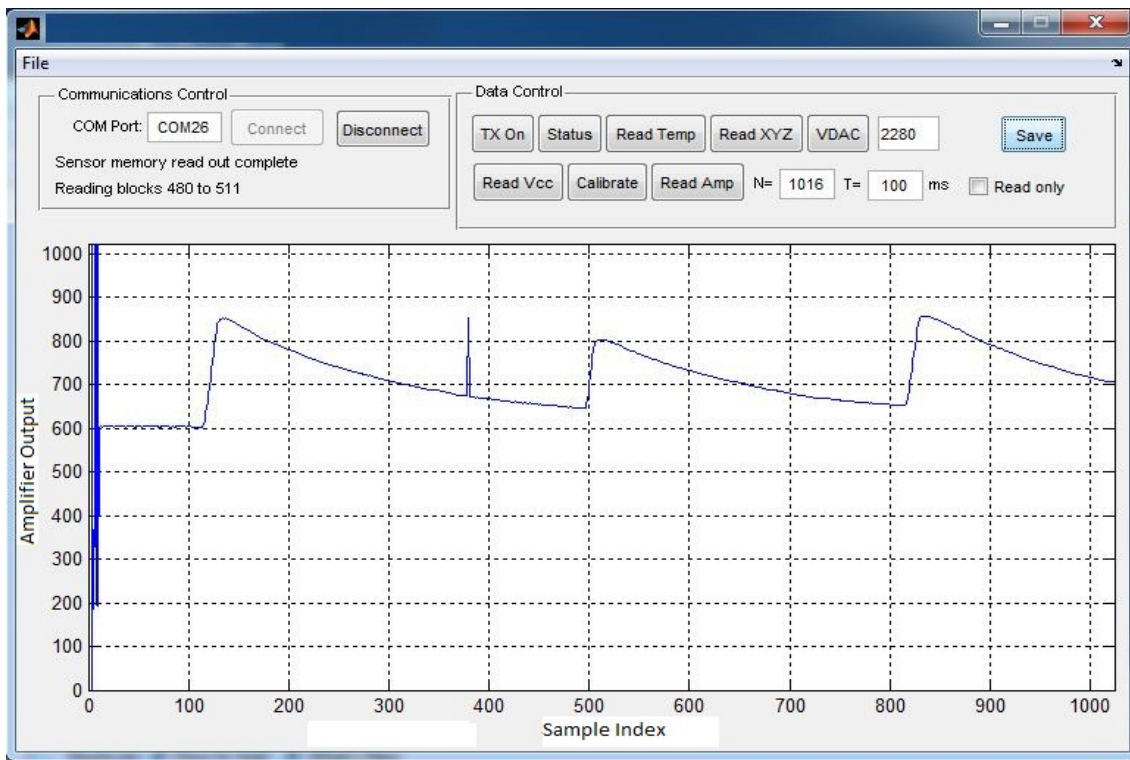


Figure 66: Un-calibrated Temperature Sensor Data

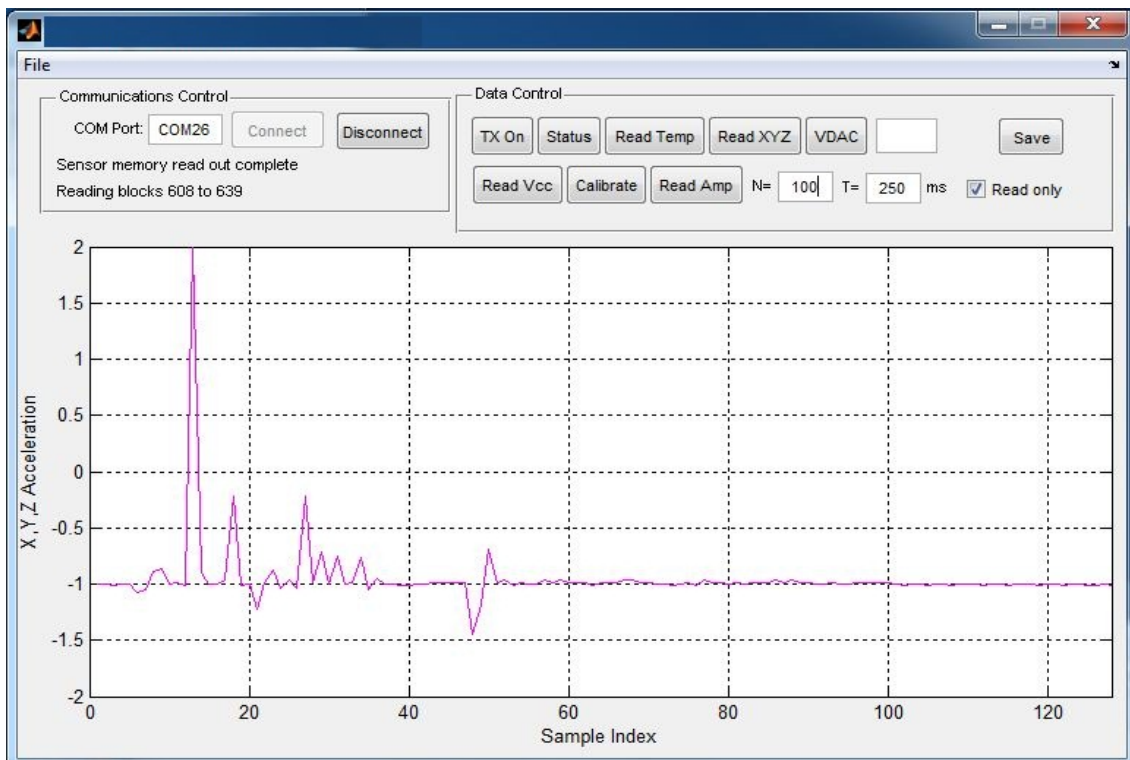


Figure 67: Accelerometer Values

Table 4: Cost of an RFID based Telemetry Unit

COMPONENT	COST
MSP430F2012	\$2.44
M24LR64-R	\$0.89
DAC7311	\$2.47
INA333	\$5.17
HSMS-282P	\$0.01
MMA8453QT	\$1.49
TLV711285285	\$0.66
ADG804	\$1.26
OPA369	\$2.49
TOTAL OFF-THE-SHELF COMPONENT COST	\$16.88

#### 5.2.1 Cost of an RFID based Telemetry Unit

The individual cost of each off-the-shelf-component used in the RFID based telemetry unit is tabulated in Table. 4. However the total cost of the board turns out to be 119.16\$.

$$\begin{aligned}
 \text{TOTAL COST PER BOARD} &= \$16.88 + \\
 &\quad \$2.28(\text{Cost of passive components}) + \\
 &\quad \$100(\text{Fabrication cost})
 \end{aligned}$$



### 5.3 ZigBee Wireless Network for Home Automation

The graphical user interface(GUI) was designed in Matlab<sup>®</sup> to read the serial data from the end-device. On connecting to the COM port that target board is plugged in, and by starting the GUI data starts flowing in. The packet data field of energy consumption was plotted in matlab. All the incoming data can also be saved into a text file as shown in Fig. 68 in the format E\_Save\_log\_yyyymmddTHHMMSS.txt(eg: E\_Save\_log\_20120306T130234.txt). Every hour a new file is created for the convenience of the software implemented to push these data into the database. A new line is appended into the file whenever a packet is received by the coordinator.

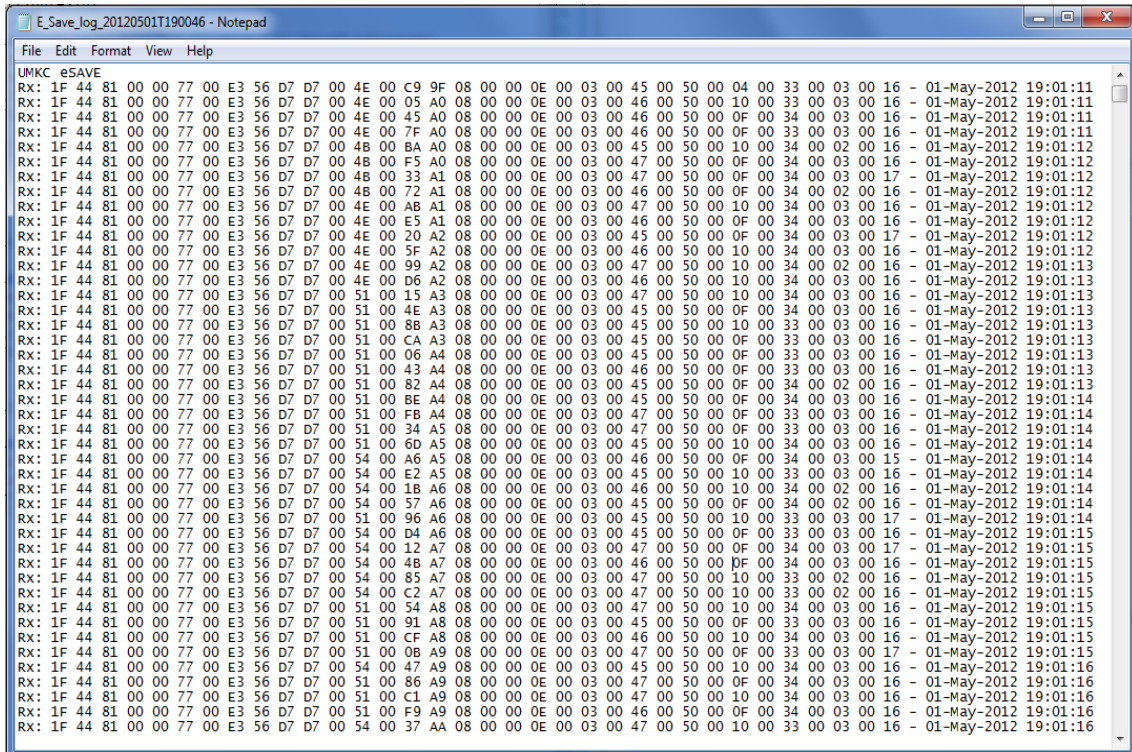


Figure 68: Data Collected

The incoming serial data can also be viewed by using a Hyperterminal as shown in Fig. 69. The information about the ZNP and the device is initially displayed on the connected Hyperterminal indicating that the coordinator is now ready to connect to other devices on the network. The RX messages from the active end-device are displayed on this coordinator HyperTerminal as could be seen in Fig. 69.

```

COM 11 - HyperTerminal
File Edit View Call Transfer Help
*****
Basic Communications Example - COORDINATOR - using AFZ00
Initializing the ZNP Success
Setting StartupOptions Success
Reset the ZNP Success
Setting Zigbee Device Type Success
Enabling Callbacks Success
Registering Application Success
Starting the Application Success
Rx: 01 45 C0 09
On Network!
ZNP Configuration Parameters
ZCD_NV_PANID          FFFF

ZCD_NV_CHANLIST      00 08 00 00
ZCD_NV_SECURITY_MODE 00
ZCD_NV_PRECFGKEYS_ENABLE 00
Device Information Properties (MSB first)
Device State:        DEV_ZB_COORD (9)
MAC Address:         00 12 4B 00 01 CA 8B 9A
Short Address:       0000
Parent Short Address: 0000
Parent MAC Address:  00 00 00 00 00 00 00
Device Channel:      11
PAN ID:              AF51
Extended PAN ID:     00 12 4B 00 01 CA 8B 9A
Rx: 0D 45 C1 DF 22 DF 22 04 E9 64 01 00 4B 12 00 00
Rx: 1F 44 81 00 00 77 00 DF 22 D7 D7 00 05 00 D0 B7 00 00 00 0E 00 03 00 48 01 F
4 03 69 00 06 00 30 FF F3
Rx: 1F 44 81 00 00 77 00 DF 22 D7 D7 00 2F 00 AA F6 00 00 00 0E 00 03 00 4A 01 F
4 00 01 00 06 00 30 FF F3
Rx: 1F 44 81 00 00 77 00 DF 22 D7 D7 00 3D 00 B7 27 01 00 00 0E 00 03 00 49 01 F
4 00 01 00 06 00 30 FF F3
Rx: 1F 44 81 00 00 77 00 DF 22 D7 D7 00 1E 00 CD 58 01 00 00 0E 00 03 00 49 01 F
4 00 01 00 06 00 30 FF F3
Rx: 1F 44 81 00 00 77 00 DF 22 D7 D7 00 35 00 DF 89 01 00 00 0E 00 03 00 4B 01 9
0 00 01 00 06 00 30 FF F3
-
Connected 0:01:29  Auto detect  9600 8-N-1  SCROLL  CAPS  NUM  Capture  Print echo

```

Figure 69: The Coordinator Hyper-terminal

## CHAPTER 6

### CONCLUSION AND FUTURE WORK

A multichannel strain gage telemetry unit using off-the-shelf components is presented. The unit of size 24 mm x 13 mm operates in 915 MHz ISM band. The off-the-shelf components were chosen with two design challenges: minimum size and low power consumption. The board was made best compact by optimum placement of components, minimal routing and with four layered PCB. By turning the radio off in between transmissions, the power consumption of the telemetry unit was reduced to the best. With wake up time from standby mode less than 6  $\mu s$  and with low data transmission rate, we could afford the extra time that takes to turn the radio on. We have demonstrated that our battery operated telemetry unit in comparison to existing bench-top system is cost-effective, tiny and accurate. The ex-vivo and in-vivo testing depicts the suitability of our unit as an implantable sensors in bio-medical studies. By changing the sensors on the multiple channels this device can find wide applications such as environmental monitoring, gunshot detection, monitoring volcanic eruptions, glacier monitoring, forest fire detection, emergency medical care and disaster response, home automation, neuromotor disease assessment and urban scale monitoring. These wireless telemetry sensors could be perceived as microscopes to observe the world at high spatial resolutions continuously in digital form.

A ZigBee wireless sensor network prototype which monitors and controls home

appliances was designed and successfully tested. Appliance specific sensor data such as light, temperature, accelerometer and energy consumption values was periodically report to the central control unit from each appliance. A home appliance of less than 10 Amps present in the ZigBee network could be turned on or off from the central control unit. With bidirectional communication achieved between the central control unit and the end-device, we were able to achieve a home automation system. However the sensors used for deployment in smart home do not require high-speed communication capacities rather more focus should be on a limited delay in communication and a low energy consumption. The end-devices were kept on sleep state in between transmission to reduce power consumption. Since the end-devices are powered by batteries it is important to design the end-devices as low-power-consuming. The ZigBee network technology is emerging as a wireless communication standard which is capable of satisfying such such requirements. Hence exploring the various potentials of ZigBee network standard for home automation application gave highly rewarding results.

## APPENDIX A

## APPENDIX A

### A.1 Four Layer PCB Layout of the Eight Channel Telemetry Unit

Fig. 77 shows the four layer PCB layout of the eight channeled telemetry unit. Each layer of the eight channeled telemetry unit is shown in Fig. 71, Fig. 72, Fig. 73 and Fig. 74. The components placed in the top and bottom layers are marked and are shown in Fig. 75, Fig. 76 and Fig. 77

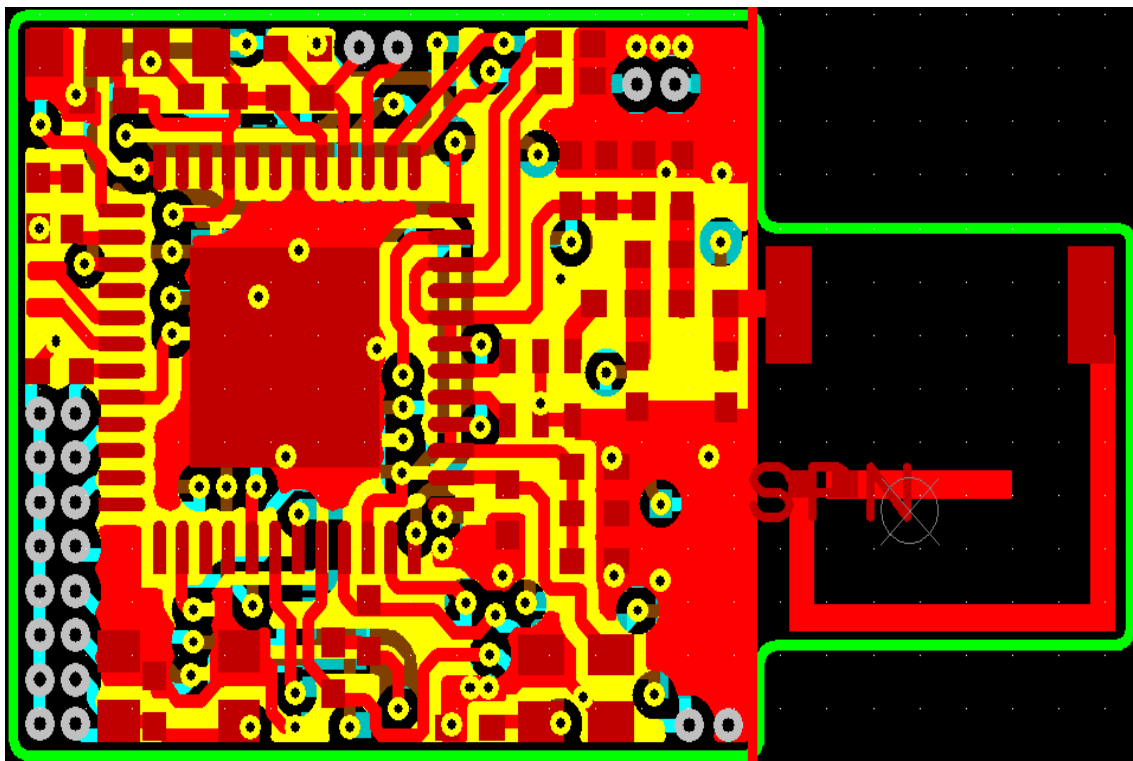


Figure 70: Four Layer PCB Layout of the eight channeled telemetry unit of dimension 24 mm x 13 mm

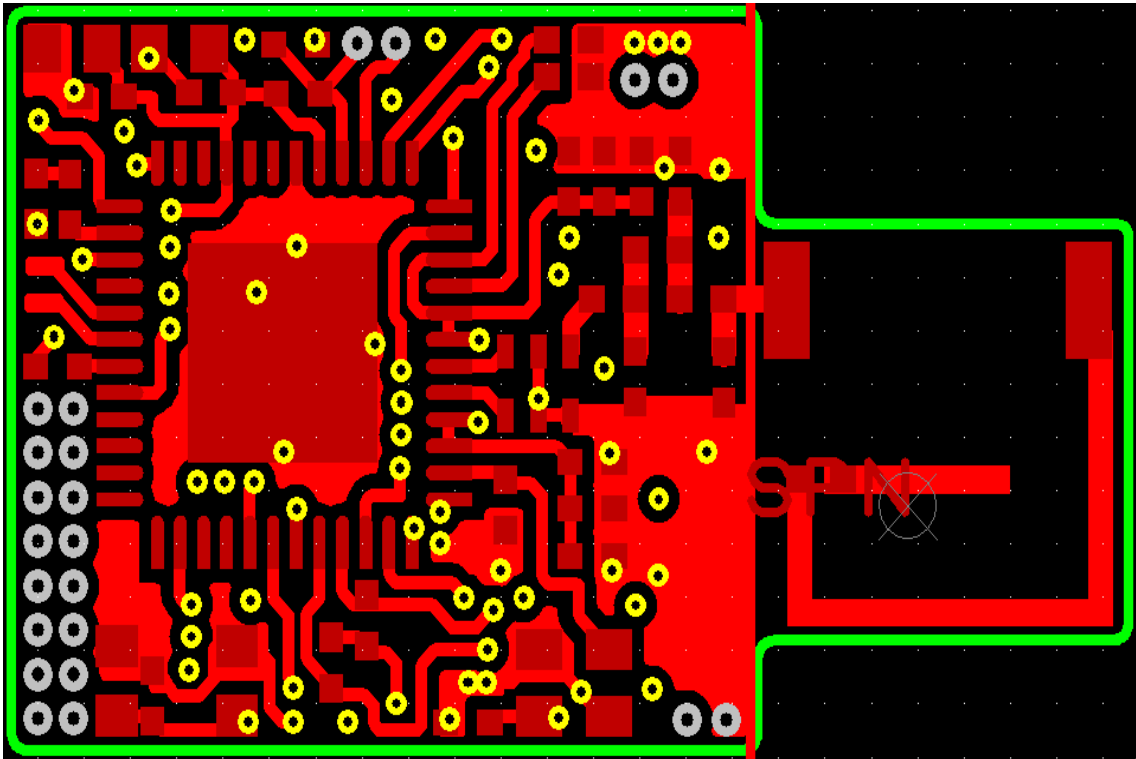


Figure 71: Top Layer PCB Layout of the eight channeled telemetry unit of dimension 24 mm x 13 mm

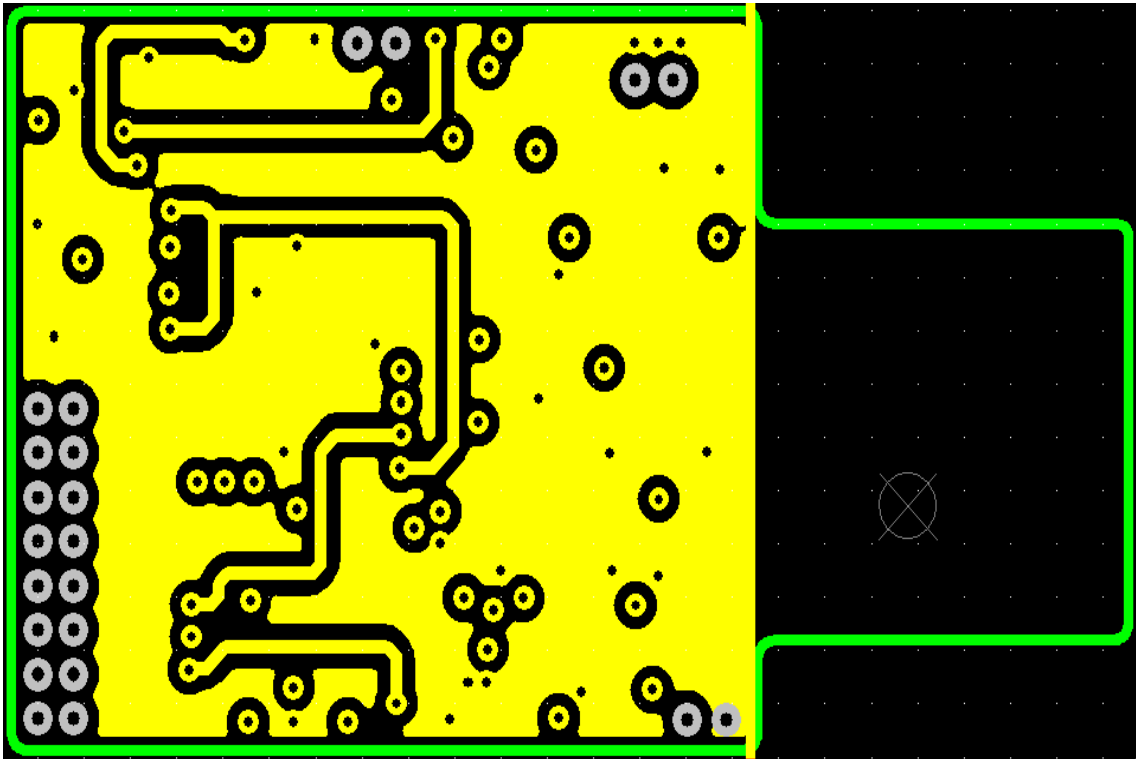


Figure 72: Second Layer PCB Layout of the eight channeled telemetry unit of dimension 24 mm x 13 mm

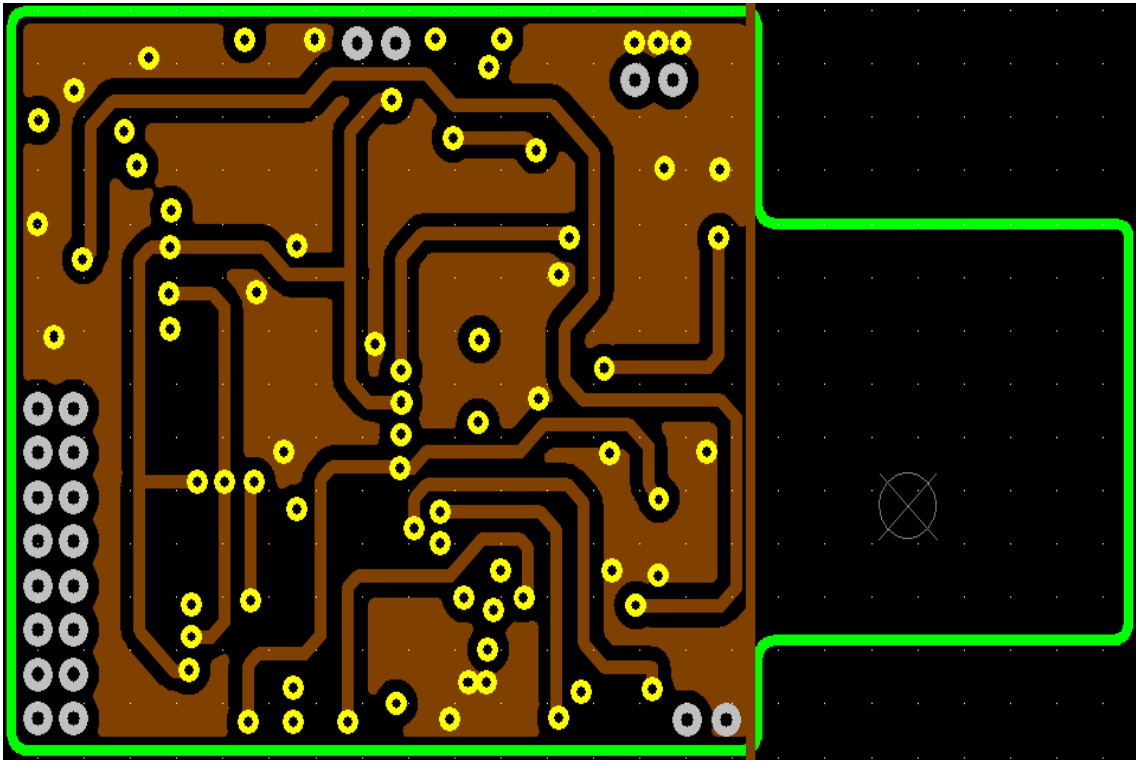


Figure 73: Third Layer PCB Layout of the eight channeled telemetry unit of dimension 24 mm x 13 mm



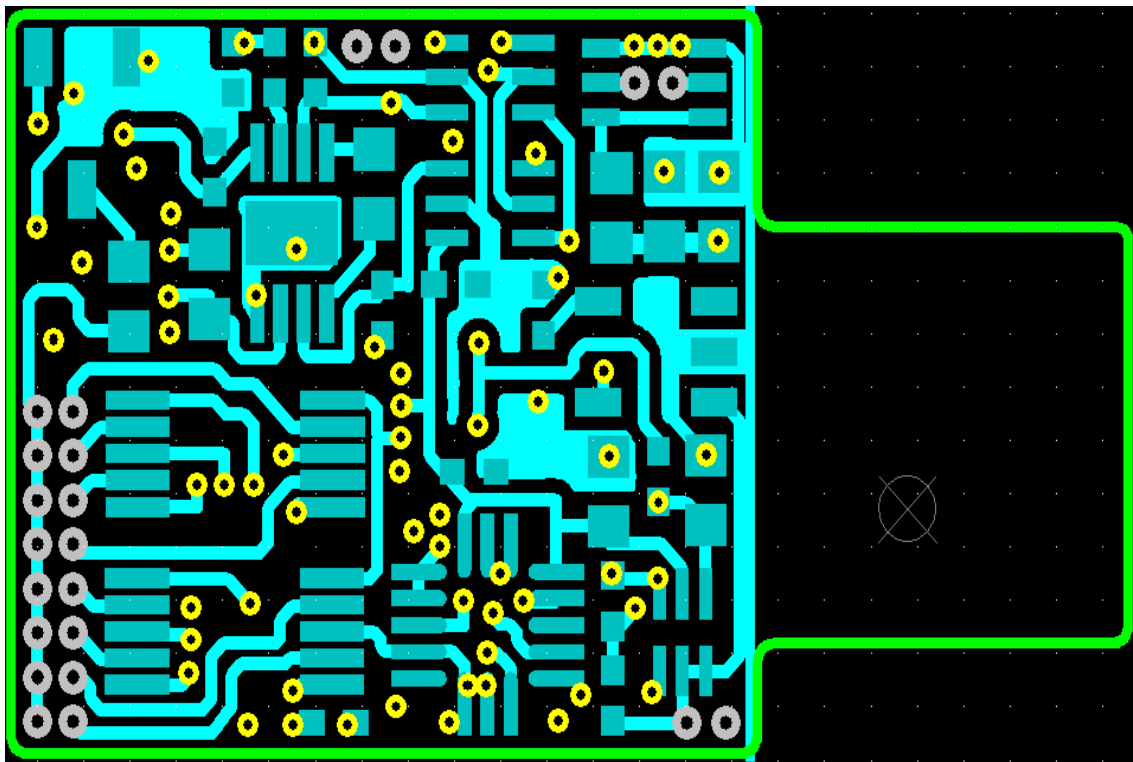


Figure 74: Bottom Layer PCB Layout of the eight channeled telemetry unit of dimension 24 mm x 13 mm

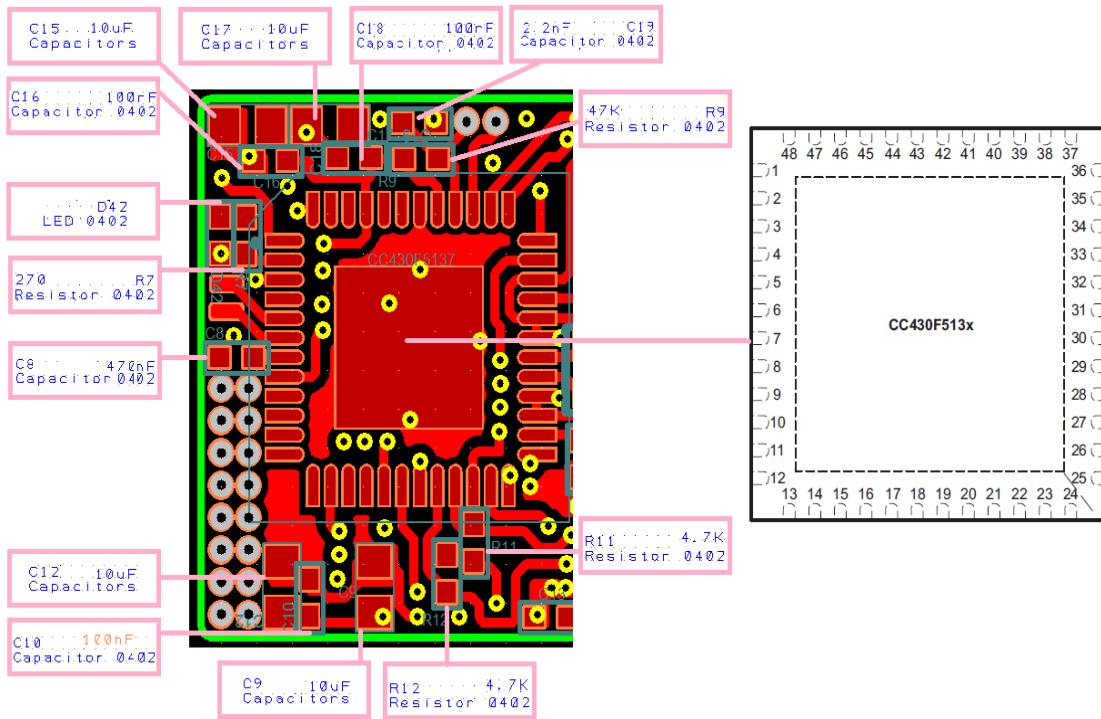


Figure 75: Components placed in the top layer of the eight channelled telemetry unit of dimension 24 mm x 13 mm

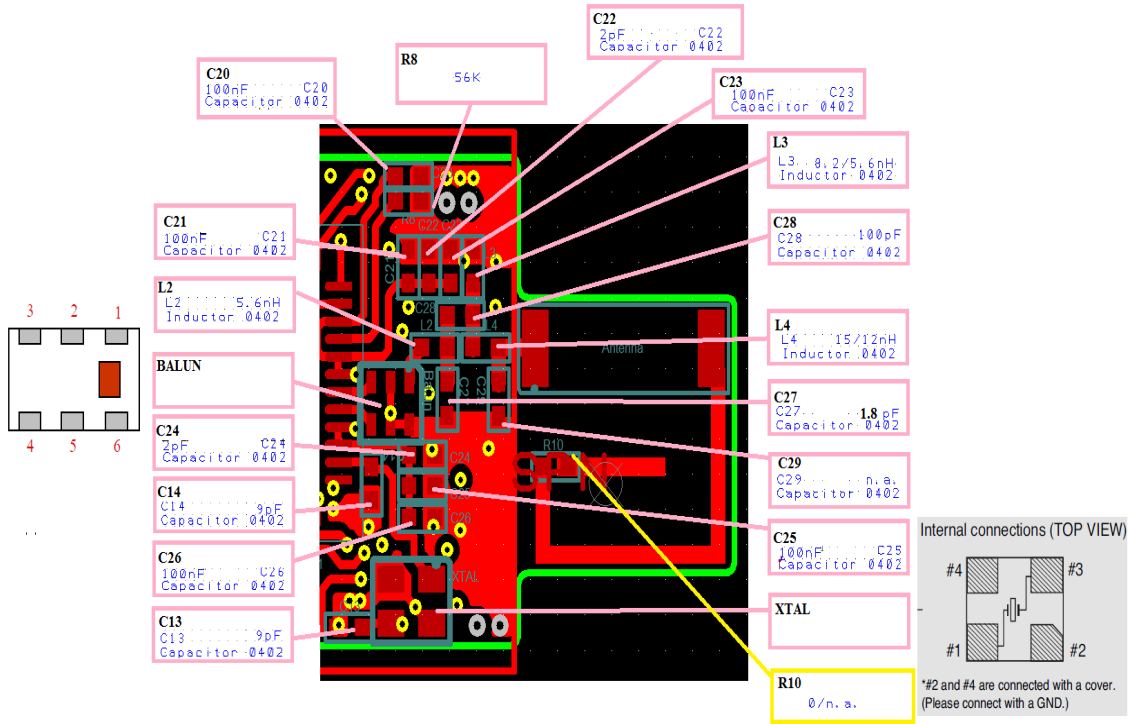


Figure 76: Radio components placed in the top layer of the eight channelled telemetry unit of dimension 24 mm x 13 mm

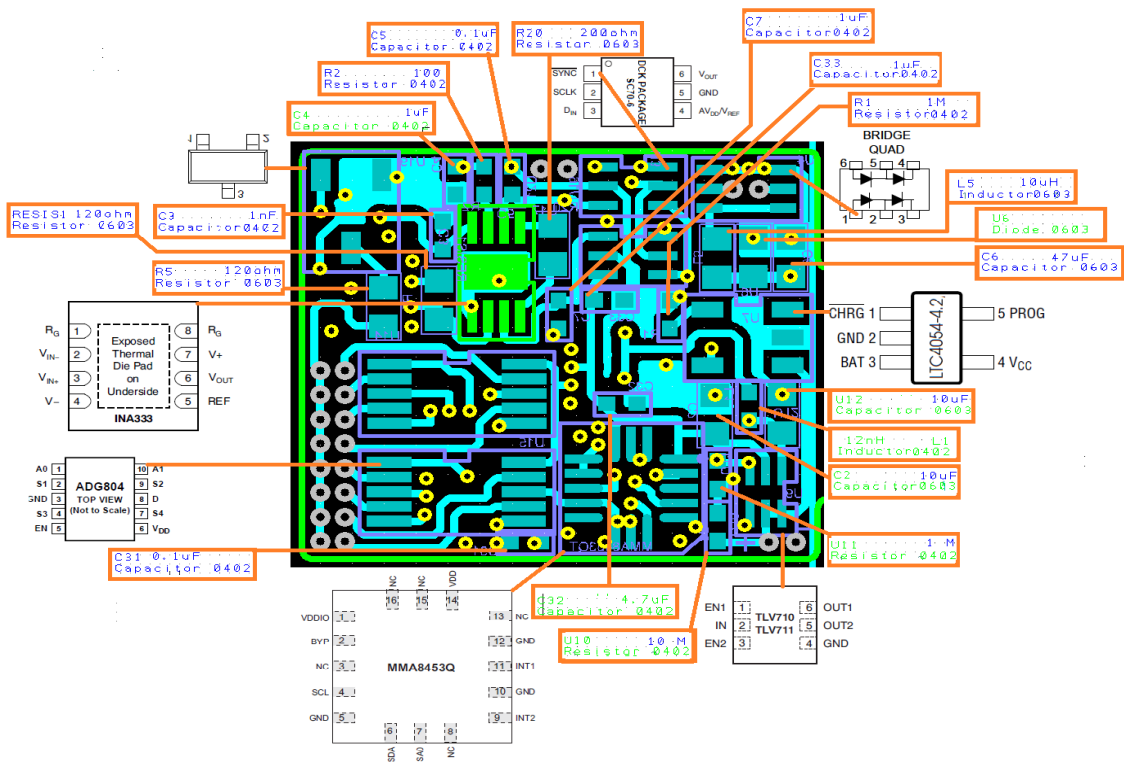


Figure 77: Components placed in the bottom layer of the eight channelled telemetry unit of dimension 24 mm x 13 mm

## A.2 Four Layer PCB Layout of the Four Channel Telemetry Unit

The PCB for this telemetry unit was designed and fabricated in four layers for compactness. Fig. 78 shows the four layer PCB layout of the telemetry unit. Each layer of the four channeled telemetry unit is shown in Fig. Fig. 79, Fig. 80, Fig. 81 and Fig. 82. The components placed in the top and bottom layers are marked and are shown in Fig. 83, and Fig. 84.

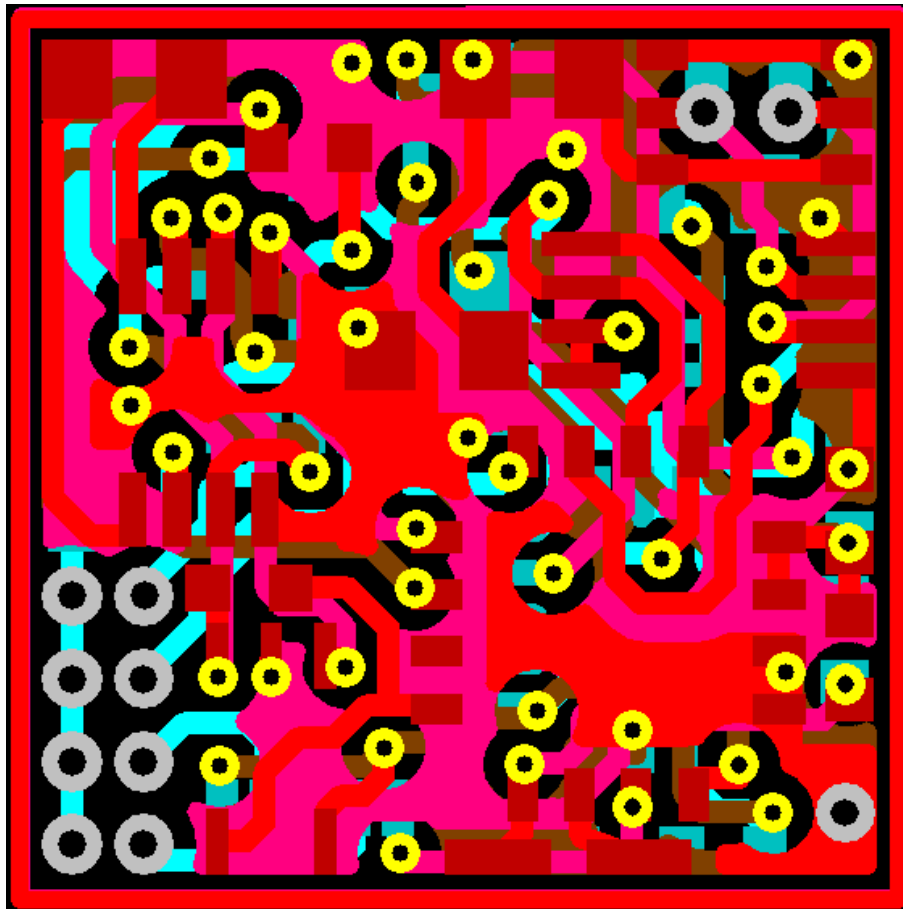


Figure 78: Four Layer PCB Layout of four channeled telemetry unit of the dimension 10 mm x 10 mm

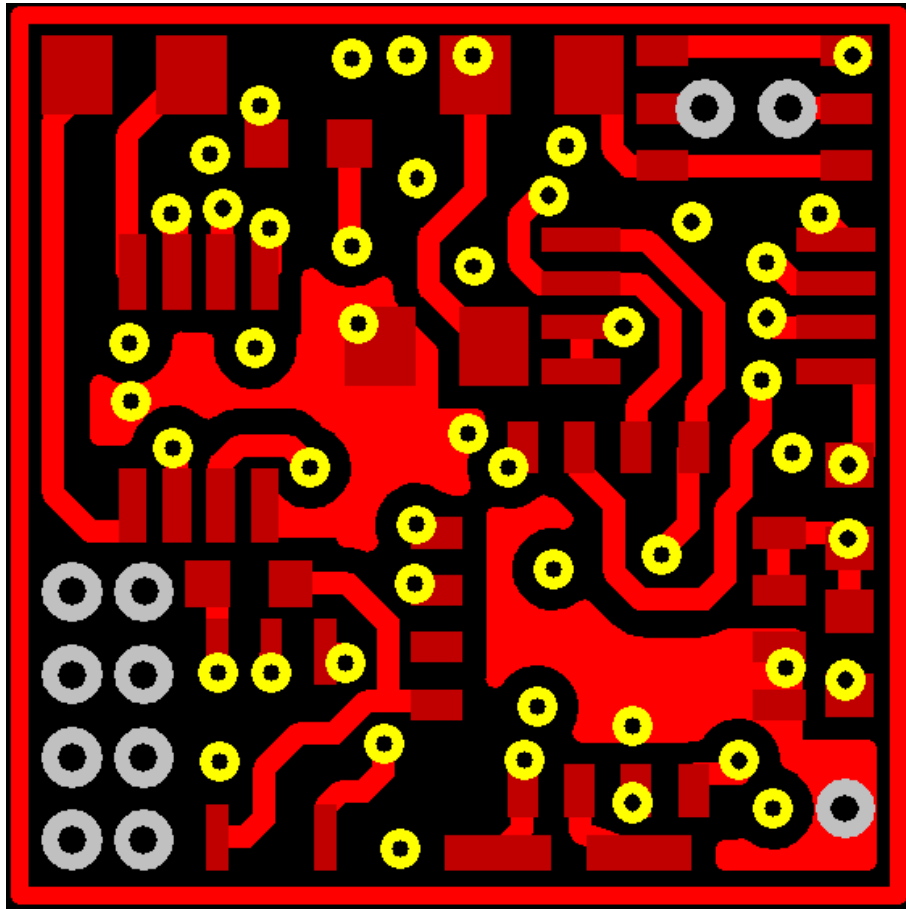


Figure 79: Top Layer PCB Layout of four channeled telemetry unit of the dimension 10 mm x 10 mm

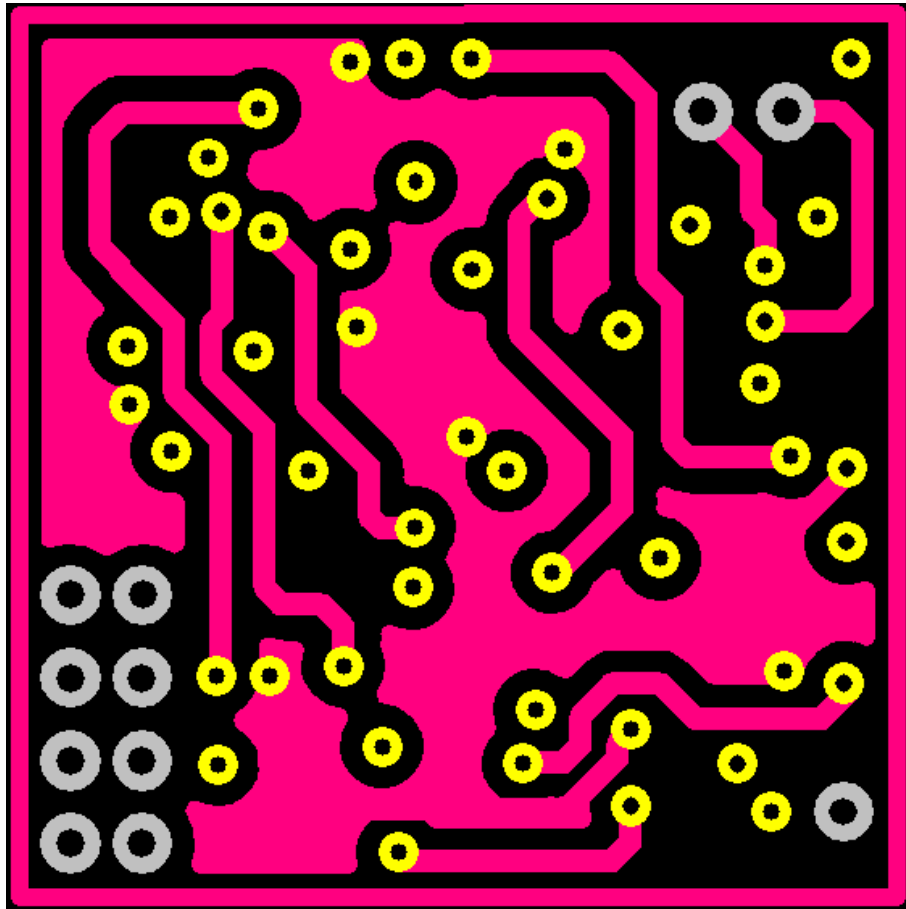


Figure 80: Second Layer PCB Layout of four channeled telemetry unit of the dimension 10 mm x 10 mm

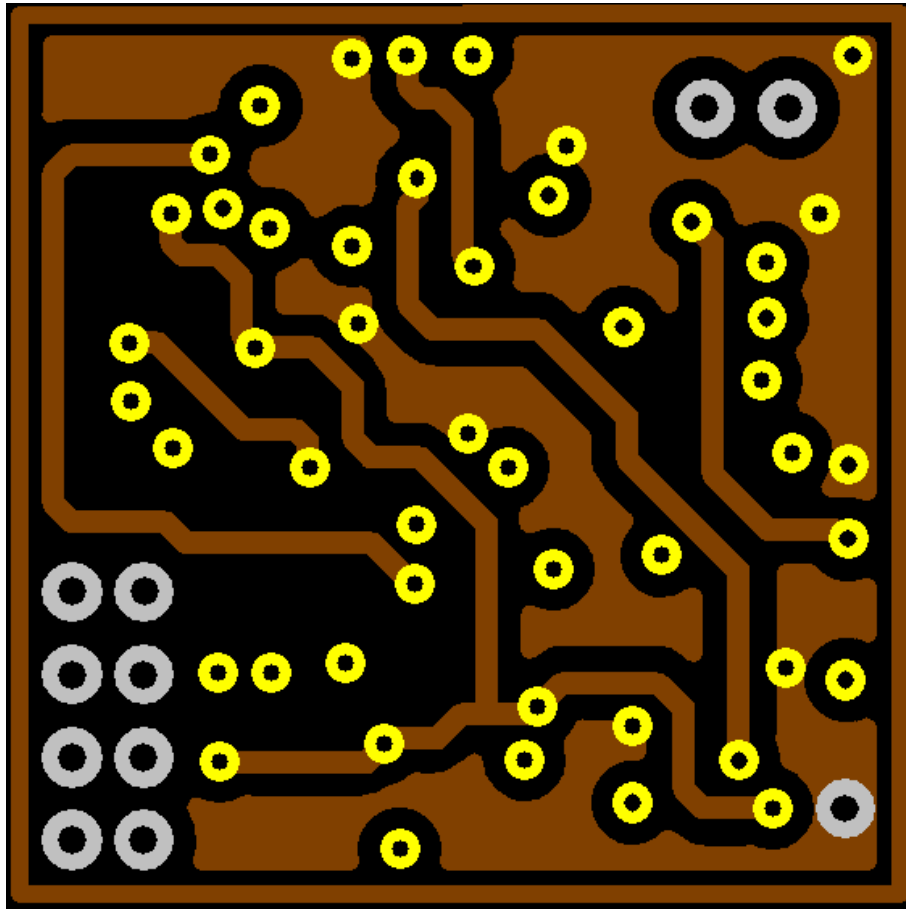


Figure 81: Third Layer PCB Layout of four channeled telemetry unit of the dimension 10 mm x 10 mm



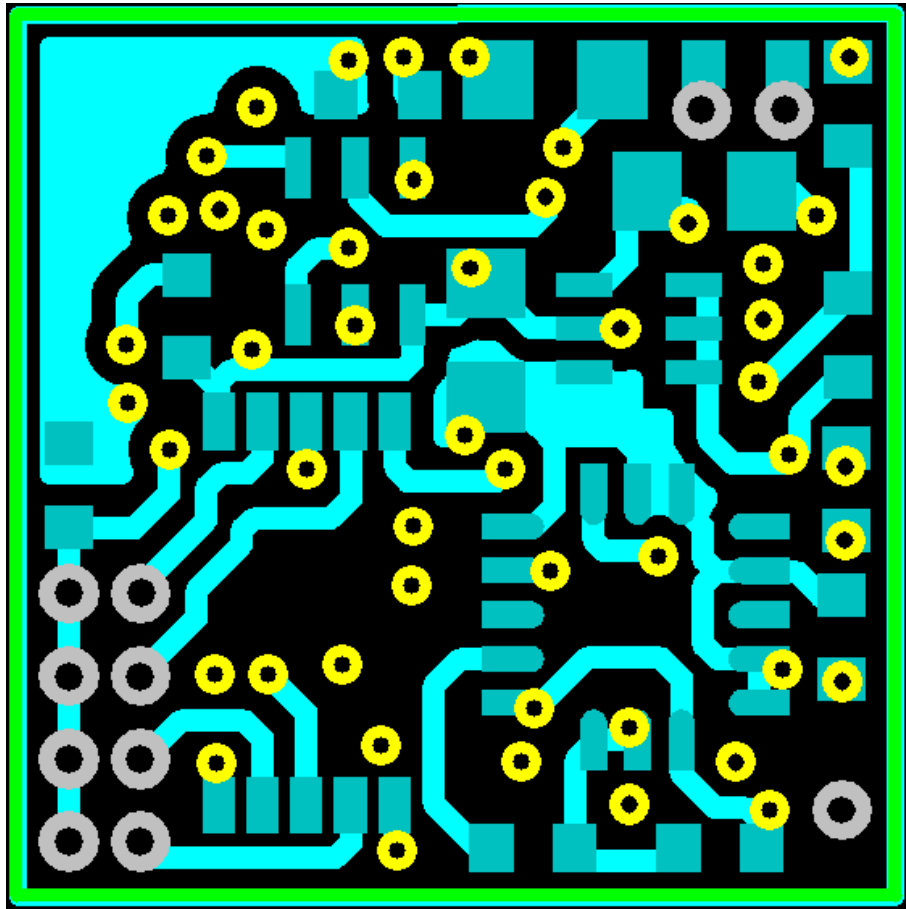


Figure 82: Bottom Layer PCB Layout of four channeled telemetry unit of the dimension 10 mm x 10 mm

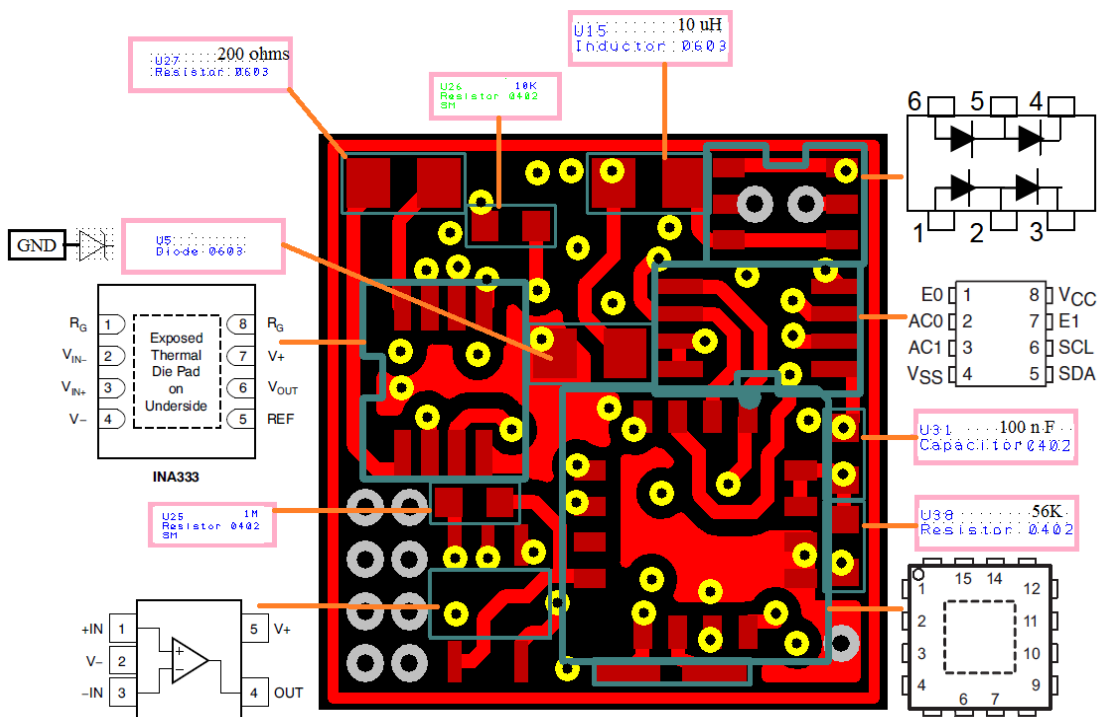


Figure 83: Components placed in the Top Layer PCB Layout of the four channeled telemetry unit of dimension 10 mm x 10 mm

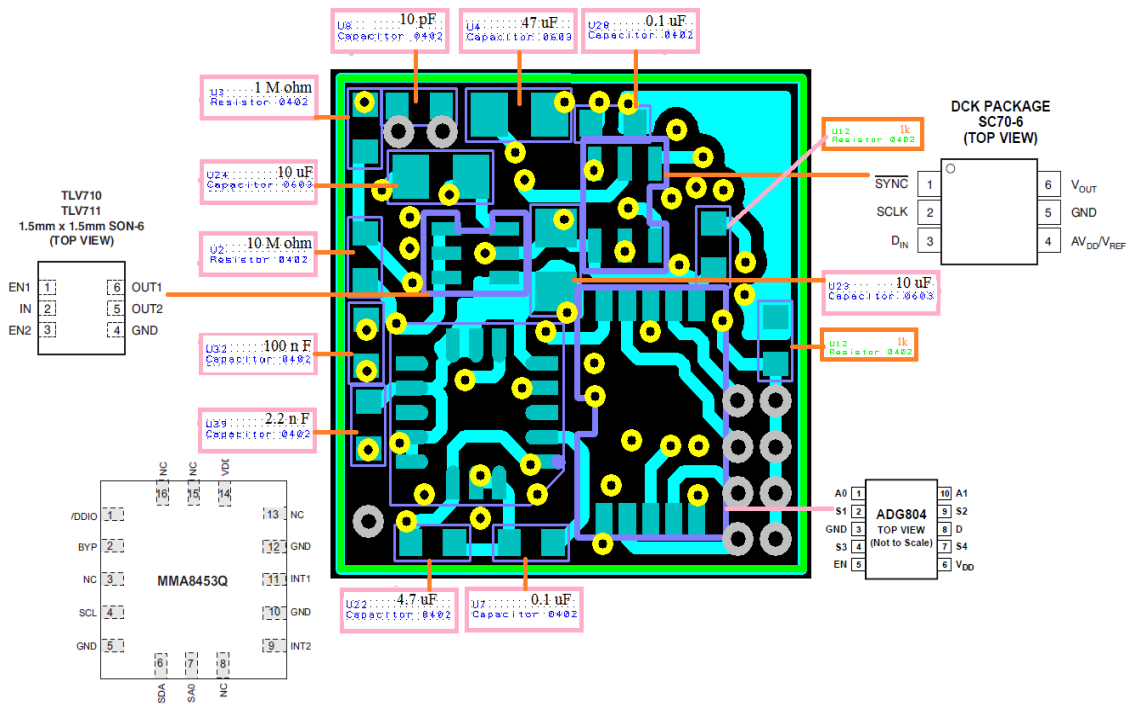


Figure 84: Components placed in the Bottom Layer PCB Layout of the four channeled telemetry unit of dimension 10 mm x 10 mm

## REFERENCE LIST

- [1] Burny, F., Donkerwolcke, M., and Bourgois, R. Monitoring of the deformation of internal implants. In *Biomaterials and biomechanics 1983: proceedings of the Fourth European Conference on Biomaterials, Leuven, Belgium, August 31-September 2, 1983* (1984), vol. 5, Elsevier Publishing Company, p. 183.
- [2] Puers, B., Sansen, W., VEREECKEN, R., Folens, G., and HENDRICKX, M. A bladder pressure telemetry device for long term monitoring. *H. Kimmich and M. Neuman, Braunschweig, BRD* (1987), 155–158.
- [3] Van Schuylenbergh, K., Puers, R., Rodes, F., Bumy, F., Donkerwolcke, M., and Moulart, F. Monitoring orthopaedic implants using active telemetry. In *Engineering in Medicine and Biology Society, 1992 14th Annual International Conference of the IEEE* (1992), vol. 6, IEEE, pp. 2672–2673.
- [4] Bergmann, G., Graichen, F., Siraky, J., Jendrzynski, H., and Rohlmann, A. Multi-channel strain gauge telemetry for orthopaedic implants. *Journal of Biomechanics* 21, 2 (1988), 169–176.
- [5] Belayev, A., Saul, I., Liu, Y., Zhao, W., Ginsberg, M., Valdes, M., Busto, R., and Belayev, L. Enriched environment delays the onset of hippocampal damage after global cerebral ischemia in rats. *Brain research* 964, 1 (2003), 121–127.

- [6] Sauer, C., Stanacevic, M., Cauwenberghs, G., and Thakor, N. Power harvesting and telemetry in CMOS for implanted devices. *Circuits and Systems I: Regular Papers, IEEE Transactions on* 52, 12 (2005), 2605–2613.
- [7] Graichen, F., Arnold, R., Rohlmann, A., and Bergmann, G. Implantable 9-channel telemetry system for in vivo load measurements with orthopedic implants. *Biomedical Engineering, IEEE Transactions on* 54, 2 (2007), 253–261.
- [8] Huang, Q., and Oberle, M. A 0.5-mW passive telemetry IC for biomedical applications. *Solid-State Circuits, IEEE Journal of* 33, 7 (1998), 937–946.
- [9] Valdastri, P., Menciassi, A., Arena, A., Caccamo, C., and Dario, P. An implantable telemetry platform system for in vivo monitoring of physiological parameters. *Information Technology in Biomedicine, IEEE Transactions on* 8, 3 (2004), 271–278.
- [10] Burny, F., Donkerwolcke, M., Moulart, F., Bourgois, R., Puers, R., Van Schuylenbergh, K., Barbosa, M., Paiva, O., Rodes, F., Bégueret, J., et al. Concept, design and fabrication of smart orthopedic implants. *Medical engineering & physics* 22, 7 (2000), 469–479.
- [11] Hanson, M., Powell, H., Barth, A., Ringgenberg, K., Calhoun, B., Aylor, J., and Lach, J. Body area sensor networks: Challenges and opportunities. *Computer* 42, 1 (2009), 58–65.

- [12] Klaus Finkenzeller, *RFID Handbook: Fundamentals and Applications in Contactless Smart Cards and Identification, Second Edition*, Copyright 2003 John Wiley and Sons, Ltd. ISBN: 0470844027
- [13] <http://www.wikipedia.org/>
- [14] <http://www.ti.com/tool/cc2530zdk-znp-mini?DCMP=CC2530ZNP&HQS=Other%252bOT%252bCC2530ZNP>
- [15] CC2530ZNP wiki page: <http://processors.wiki.ti.com/index.php/CC2530ZDK-ZNP-MINI>
- [16] [http://www.ti.com/lstds/ti/microcontroller/16-bit\\_msp430/overview.page](http://www.ti.com/lstds/ti/microcontroller/16-bit_msp430/overview.page)
- [17] <http://www.ti.com/product/cc430f5137>
- [18] Chang Liu, *Foundations of MEMS*, Pearson Prentice Hall, 2006 ISBN: 0131472860
- [19] <https://sites.google.com/site/umkcsmartenergy/home>
- [20] <http://www.greenimpactzone.org/>
- [21] <http://www.ti.com/cc2530znp>
- [22] CC2530 product web page [www.ti.com/cc2530](http://www.ti.com/cc2530)
- [23] ZigBee training material: [http://processors.wiki.ti.com/index.php/Low\\_Power\\_RF\\_Solutions\\_Workshop](http://processors.wiki.ti.com/index.php/Low_Power_RF_Solutions_Workshop)

- [24] <http://www.lightobject.com/Programmable-Digital-AC-Single-Phase-Power-Watt-Meter-Blue-LED-w-Control-20mA-P547.aspx>
- [25] <http://www.ti.com/iarkickstart>
- [26] [http://processors.wiki.ti.com/index.php/Simple\\_Applications\\_Examples](http://processors.wiki.ti.com/index.php/Simple_Applications_Examples)
- [27] <http://www.ti.com/lit/an/swra215e/swra215e.pdf>
- [28] [http://www.eng.yale.edu/enalab/courses/eeng460a/homeworks/hw1\\_results/zigbee.html](http://www.eng.yale.edu/enalab/courses/eeng460a/homeworks/hw1_results/zigbee.html)
- [29] Walter D. Leon-Salas Technical Report: ELEC-NPDN-200708-02 Networking Engineering *University of Nebraska-Lincoln Department of Electrical Engineering*.
- [30] Bromley, K., Perry, M. and Webb, G. Trends in Smart Home Systems, Connectivity and Services, 2003 newblock *Medical engineering & physics* 22, 7 (2000), 469–479.
- [31] Al-Ali, A.R. and Al-Rousan, M. Java-based home automation system *IEEE Transactions on Consumer Electronics*, IEEE Vol. 50, 2 (2004), 498–504.
- [32] Sriskanthan, N. and Tan, F. and Karande, A. Bluetooth based home automation system, *Microprocessors and Microsystems*, Elsevier Vol. 26, 6 (2002), 281–289.

- [33] Coskun, I. and Ardam, H. A remote controller for home and office appliances by telephone, *IEEE Transactions on Consumer Electronics*, IEEE Vol. 44, 4 (1998), 1291–1297.



## VITA

Sharika Krishna Kumar was born on April 11, 1987 in Kottayam, Kerala, India. She was educated in local private schools under Central Board of Secondary Education and graduated High School in 2004. She attended Cochin University of Science and Technology, Chengannur Engineering College, from which she graduated in 2008. Her degree was a Bachelor of Technology in Electronics and Communication Engineering. During her undergraduate studies she had actively served as Chairperson of WIE (Women In Engineering), an Affinity group of IEEE (2006-07), Vice Chairperson of College SENATE, College of Engineering, Chengannur (2006-07) and Vice Chairperson of WIE (Women In Engineering), an Affinity group of IEEE (2005-06).

Mrs. Sharika Kumar worked two years as product design and development engineer for digital television and multimedia solutions (DTV-n-MMS), Tata Elxsi Limited, Trivandrum, India. She worked in low level designs for a high end cross media station and an android based set top box. To pursue her graduate studies Mrs. Sharika Kumar came to United States.

She began work toward her master's program in Electrical Engineering at the University of Missouri-Kansas City in the spring of 2011. Due to her academic excellence she was awarded "CSEE Instructional Support Award", "Graduate Teaching Assistant School of Computing and Engineering Non-Resident Award" and "Graduate Research Assistant School of Computing and Engineering Non-Resident Award". While pursuing her graduate studies, Mrs. Sharika Kumar received job offer from Cummins Inc. Currently she is

pursuing her career as an Heavy Duty Diesel(HDD) Engine Controls Engineer at Cummins Inc, Columbus, Indiana.